Matrin 3 Regulation in Physiology and Neurodegenerative Disease

by

Ahmed M. Malik

A dissertation submitted in partial fulfillment
of the requirements for the degree of
Doctor of Philosophy
(Neuroscience)
in the University of Michigan
2021

Doctoral Committee:

Associate Professor Sami J. Barmada, Chair
Professor Anthony Antonellis
Assistant Professor Kristin S. Koutmou
Professor Andrew P. Lieberman
Professor Michael D. Uhler

Ahmed M. Malik

ahmalik@umich.edu

ORCID iD: 0000-0002-2625-7483

Acknowledgements

I would first like to thank Sami for his mentorship over the past five years—I could not imagine having had a better environment for my PhD training. He truly gave me the opportunity to pursue those questions that I thought were most interesting and was ever-ready to offer advice and perspective. There were so many parts of graduate school inside and outside of the lab that I enjoyed, but our weekly meetings swapping ideas and riffing off one another's what-ifs and but-then-agains will always have a unique place in my memory of this time. I would also like to acknowledge my thesis committee—Drs. Tony Antonellis, Kristin Koutmou, Andy Lieberman, and Mike Uhler. I never found committee meetings to be the dreaded inquisitorial affairs that some graduate students do and instead could see them as opportunities to hear from insightful, supportive investigators who wanted to help me make my science better.

A large thanks goes to Elizabeth, who is such a big part of the team that makes our lab the unique place it is. Culture is inculcated from the top-down, and Elizabeth and Sami have created a great lab culture. Speaking of the lab, there are so many people to acknowledge who enriched my last five years. I always said (rather annoyingly, I admit) that I have the good fortune of working with my best friends, and I meant it. The old guard who welcomed me—Brittany, Kate, Nate, Xingli, Roberto, Hilary-—have their special place, and the new guard—Sumin, Mike, Nico, Jason, Gen—have contributed to our lab in their own weird, unique, fun ways. An especially large thanks goes to Nate,

who has been a mentor to me in research and in my personal life. Discussing papers with him was half the fun of reading them, and as soon as I started in the lab he got me aboard his philosophy that in our line of work, reading the literature isn't broccoli to be reluctantly chewed; it's candy. I'd also like to acknowledge Niki, Christie, and Quinn, undergraduate and post-bac students I've had the luck to work with over the years. Learning science alongside them has been endlessly satisfying, and they have all helped clarify and refine my own thinking in many ways.

The last few years would have been so empty without my friends. All of those in NGP and beyond have been such a great source of companionship over the years and have helped make this dynamic, sometimes erratic, time in our lives feel grounded. A special thanks to Tony, whose even-keeled perspective and omnivorous curiosity have provided such personal and intellectual nourishment over the past decade. Thanks also to Fred—MSTP is a long road, and it is so helpful to have a close friend and sounding board who understands and is willing to hone ideas, both personal and scientific.

Lastly, I would like to thank my family members who made so much possible for me. From my grandparents born into a different world who worked towards a better future for their children to my parents who left the country they knew to bring me to an unfamiliar one, there have been so many countless efforts and sacrifices made over the generations from which I now benefit. An especially sincere thanks to my parents who instilled in me from childhood not only curiosity and love of learning but also an appreciation of just how much I have and how I am obligated to take advantage of that privilege. *Dušman zer, sajjan dher*.

I am more grateful for the people named here than I can say.

Table of Contents

List of Tables

List of Figures

Abstract

RNA-binding proteins (RBPs) are critical for the regulation of RNA splicing, transport, and translation. Over the previous decade, clinical, genetic, and histopathological evidence has accumulated linking RBP dysfunction to the pathogenesis of amyotrophic lateral sclerosis (ALS) and frontotemporal dementia (FTD) spectrum disorders, with mutations in the genes encoding many RBPs resulting in inherited disease and RBP pathology observed even in sporadic disease. Mutations in the gene encoding Matrin 3 (MATR3), a poorly understood DNA- and RNA-binding protein, have been linked to ALS, ALS/FTD, and a form of distal myopathy, and MATR3 pathology is also present in the motor neurons of individuals with sporadic ALS. Despite this, little is known about MATR3 function and physiological regulation or about the pathophysiological processes underlying MATR3-mediated neuromuscular disease.

In this dissertation, I present findings on basic MATR3 biology, including determinants of its localization and abundance in neurons, as well as hints towards possible pathological mechanisms, especially as they relate to pathogenic MATR3 mutants. Chapter 1 reviews the state of the literature on MATR3, beginning with a discussion of its functions and regulation, moving on to its implication in neurological disorders, and ending with insights gleaned from disease models. In chapter 2, I detail our work studying how MATR3 domains and localization alter its toxicity in a primary cortical neuron model and how select disease-associations mutations alter the

biophysical properties of MATR3. Chapter 3 dissects the activity-dependent, Ca^{2+}-mediated regulation of MATR3 abundance and RNA-binding functionality in neurons, with an exploration of how these themes may apply to many other ALS/FTD-linked RBPs as well. In chapter 4, I discuss the key open questions regarding MATR3's nucleic acid binding, physiological regulation, and involvement in both familial and sporadic disease. Appendix A details ChIP-sequencing experiments and briefly explores how these negative data may shed light on the cell type-specific spectrum of DNA and RNA binding by MATR3.

In summary, the work presented in this dissertation offers a foundation for understanding not only the fundamental biology of MATR3 in neurons but also the pathological mechanisms underlying MATR3-mediated disorders. It is my hope that the findings presented here on neuronal regulation of MATR3 will inform future studies on activity-dependent RBP homeostasis and will further our knowledge of human disease linked to RBP dysfunction.

Chapter 1: Introduction[1]

1.1 Overview

Amyotrophic lateral sclerosis (ALS) is a neurodegenerative disease characterized by the loss of upper and lower motor neurons, resulting in weakness and paralysis. In contrast, frontotemporal dementia (FTD) involves behavioral and speech changes due to degeneration of neurons in the frontal and temporal lobes[1]. Despite affecting disparate parts of the nervous system and manifesting in different symptoms, ALS and FTD share several clinical, genetic, and pathological features. In particular, RNA-binding proteins (RBPs) are integral players in both ALS and FTD pathogenesis, with mutations in a number of RBP-encoding genes causing familial ALS, FTD, or both. Even in individuals with sporadic disease with no known underlying mutation or family history—accounting for the majority of ALS and FTD—RBP mislocalization in affected nervous system regions is a signature pathological event[2-4]. For many of these genes, the spectrum of affected tissues extends beyond neurons to skeletal muscle, manifesting as myopathies. One such gene encodes the highly conserved nuclear protein Matrin 3 (MATR3), which possesses both DNA- and RNA-binding capacity. *MATR3* mutations were originally associated with inherited vocal cord and pharyngeal

[1] This chapter is adapted from the following publication: Malik A.M. and Barmada S.J. Matrin 3 in neuromuscular disease: physiology and pathophysiology. 2021. *JCI Insight*. 6(1):e143948. doi: 10.1172/jci.insight.143948.

distal myopathy (VCPDM) and later recognized in patients with familial ALS and FTD. This introductory chapter will discuss basic MATR3 biology and its functions in nucleic acid processing in the nervous system, clinical evidence tying MATR3 to neuromuscular disease, and insights into MATR3-mediated pathogenesis from model systems and human post-mortem tissue.

1.2 MATR3 function

1.2.1 MATR3 as a DNA-binding protein

MATR3 was initially identified as a major component of the nuclear matrix, the proteinaceous network responsible for organizing and maintaining nuclear architecture[5,6]. Consistent with this, a nuclear protein eventually recognized as MATR3 was found in association with repetitive DNA sequences[7-9]. MATR3 possesses not only zinc finger (ZF) domains but also tandem RNA recognition motifs (RRMs), and the remainder of the protein consists of two large intrinsically disordered regions (IDRs), with the C-terminal IDR being highly acidic (Fig. 1.1). The importance of MATR3 functional and regulatory domains in overexpression toxicity and localization will be examined in further detail in chapter 2 of this dissertation.

MATR3's two ZF domains are of the C2H2 variety, which bind DNA but can also recognize RNA and mediate protein-protein interactions[10,11]. MATR3's DNA substrates and the functional consequences of its DNA binding, however, remain poorly understood. Early work demonstrated that MATR3 recognizes repetitive, AT-rich fragments isolated from rat liver DNA and that the recognition of these sequences is ZF dependent, as deletion of individual ZFs reduces binding measured by electromobility

shift assays (EMSAs). Deletion of both ZFs abolishes binding completely[12], suggesting that these domains function in an additive or cooperative fashion to bind DNA. AT-rich DNA sequences make up canonical scaffold/matrix attachment regions (S/MARs)[13,14], sections of chromosomal DNA that serve as contact points between chromatin and the nuclear matrix. Protein components of the nuclear matrix can modulate gene expression by binding to S/MARs adjacent to genes or regulatory elements, thereby changing their accessibility to transcriptional and replication machinery[15-19]. Imaging-based approaches have detected MATR3 in close proximity to functional genomic areas, such as transcriptional start and DNA replication sites[20,21], supporting a possible role in tuning DNA availability.

Even so, the specific consequences of MATR3 DNA binding for gene expression are less clear. Using a luciferase reporter fused to a MATR3 DNA target, Hibino and colleagues demonstrated that luciferase activity is progressively inhibited by DNA methylation, which blocks MATR3 binding to the reporter, suggesting a potential role for MATR3 in transcriptional regulation[22]. MATR3 phosphorylation greatly enhances its DNA-binding ability, indicating a physiological mechanism for regulating MATR3's interaction with DNA[7]. However, reporter methylation in these studies may have affected the binding of other transcription factors independent of MATR3, and it is unclear if the changes in reporter expression were truly mediated by MATR3.

Additional evidence supports a potential function for MATR3 in cell type-specific gene regulation. Using chromatin immunoprecipitation-sequencing (ChIP-seq) in a rat pituitary cell line, Skowronska-Krawczyk and coworkers found that MATR3 binding is concentrated in non-coding areas of the genome and significantly overlaps with

enhancer signals[23]. The association of MATR3 with many of these sequences, as well as gene expression from these loci, appears to be indirect and is instead dependent on the pituitary-specific transcription factor Pit1. Similarly, MATR3 was identified as a DNA-binding protein capable of recognizing chromatin insulator sequences, but this interaction is also indirect and dependent on the transcription factor CTCF[24], and in muscle cells, association of MATR3 with chromatin was wholly dependent on the long noncoding RNA (lncRNA) *pCharme*[25]. Therefore, although MATR3 is capable of binding to chromatin *in vitro* via its ZF domains, it is currently unclear how or if MATR3 regulates gene expression or chromatin accessibility by direct association with DNA. More likely, MATR3 affects gene expression indirectly by acting in concert with tissue- and cell-specific transcription factors.

In addition to transcriptional control, MATR3 functions in DNA repair, as indicated by the abnormal accumulation and impaired disassembly of non-homologous end joining repair factors at sites of DNA damage upon MATR3 knockdown in U2OS cells[26]. MATR3 also binds to and stabilizes mRNA encoding Rad51, a key factor involved in homologous recombination, resulting in increased Rad51 levels and function[27]. Under different circumstances, however, double-stranded DNA damage triggers the formation of a complex including MATR3, p53, and lncRNA that drives the expression of genes responsible for cell cycle arrest and modulation of apoptosis[28].

1.2.2 MATR3 as an RBP

MATR3 has two tandem RRMs capable of binding RNA sequences *in vitro* and *in vivo*, and a number of studies have offered insights into the contributions of MATR3 to

RNA metabolism. The first evidence of RNA binding came from Hibino and coworkers, who identified an albumin-encoding mRNA sequence bound by MATR3 and, via EMSAs, showed that deletion of RRM1 and RRM2 impairs recognition by MATR3[12]. Since then, accruing data link MATR3 to multiple points in the RNA lifecycle. In U2OS cells, a C-terminally truncated MATR3 isoform localizes to cytoplasmic processing bodies (P-bodies), where it presumably functions as part of the RNA-induced silencing complex to degrade targeted RNAs[29]. Consistent with this notion, proteomic analyses previously identified MATR3 as a component of argonaute-rich RNA-silencing complexes[30].

In other contexts, RNA immunoprecipitation followed by sequencing uncovered several MATR3 substrate RNAs that were stabilized by MATR3 binding, in agreement with a large-scale study of RBPs suggesting that MATR3 binding increases luciferase reporter levels[31,32]. While MATR3 variants lacking RRM1 pull down many of the same RNA-dependent protein targets as full-length MATR3, deletion of RRM2 prevents this, indicating that—as with other tandem RRM-harboring RBPs—one RRM may dominate in RNA binding[33-35]. Furthermore, ZF domain deletion enhances MATR3 splicing activity, implying that MATR3's DNA- and RNA- binding functions may compete and/or interfere with one another[36]. Supporting this, ZF1 deletion promotes interaction of MATR3 with miR138-5p, and RRM removal interrupts this association[37]. These data suggest that MATR3's DNA-binding activity may antagonize its functions in RNA splicing and metabolism. Arguing against a clean functional division between ZF and RRM domains, however, deletion of ZF2 reduces MATR3 association with miR138-5p, indicating potential overlap in nucleic acid binding between the two types of domains.

A large-scale *in vitro* study of RBP motifs determined that MATR3 recognizes a consensus AUCUU sequence in substrate RNA[38]. This result was subsequently corroborated in human neuroblastoma (SH-SY5Y) cells using photoactivatable ribonucleoside-enhanced CLIP (PAR-CLIP). In these investigations, the majority of MATR3 sites were located in introns, and *MATR3* knockdown resulted in significant changes in exon cassette usage, suggesting that MATR3 functions as a splicing factor[39]. Approximately equal numbers of novel exon skipping and inclusion events were noted upon MATR3 knockdown, but exons adjacent to introns with MATR3 binding sites were disproportionately included in the absence of MATR3. These observations suggest that MATR3 normally functions as an intronic splicing suppressor. In support of this conclusion, MATR3 represses exon inclusion in ~2/3 of differentially spliced genes in HeLa cells, implying that MATR3 represses splicing of most but not all of its substrate pre-mRNAs[36,40]. As with the DNA regulatory functions of MATR3, however, it remains unclear whether MATR3 directly or indirectly contributes to RNA splicing. For example, MATR3 and polypyrimidine tract binding protein 1 (PTBP1) share many substrates, physically interact with one another via the PTB RRM2 interacting (PRI) motif in MATR3, and act cooperatively to repress retrotransposons[41,42]. In addition to PTBP1, a number of protein-protein interaction screens and proteomics experiments have identified MATR3 in association with many other distinct RBPs and ribonuclear complexes, suggesting cooperative functions and broader roles in RNA metabolism beyond those uncovered to date[20,43-51].

As with other RBPs, MATR3 demonstrates prominent self-association that is antagonized by RNA binding. Deletion of RRM2—either in isolation or in combination

with RRM1—results in spherical droplet formation through liquid-liquid phase separation (LLPS). This phenomenon likely arises due to uninhibited interaction between MATR3's IDRs, particularly the N-terminal IDR[52,53]. Importantly, RNA- binding deficient TDP-43 and FUS variants also undergo LLPS[54-56]. These data suggest that RBPs demix and form liquid-like droplets under low RNA conditions or when RNA binding is impaired via unchecked interactions between IDRs.

Somewhat surprisingly in light of its DNA- and RNA-binding capacity, MATR3 overexpression or knockdown results in relatively few detectable changes in gene expression. MATR3-YFP overexpression affects only a handful of genes in H4 neuroglioma cells compared to YFP alone[52], and *MATR3* knockdown in SH-SY5Y and HeLa cells results in expression changes for only a few dozen genes, despite affecting hundreds of alternative splicing events[36,39]. Nevertheless, the true magnitude or consequences of MATR3 loss may be cell type dependent. In myoblasts, for instance, MATR3 binds to and regulates several genes important for muscle differentiation and maturity, and MATR3 knockdown impairs the differentiation of these cells into mature myotubules[57]. Interestingly, MATR3 exhibits dynamic changes in subcellular distribution as myoblasts mature into myotubes—while it is localized diffusely in the myoblast nucleoplasm, MATR3 rims the inner face of the nuclear envelope in myotubes, suggesting specialized roles for MATR3 in muscle development[58]. One possibility is that this change reflects a shift in the function of MATR3 at each stage of differentiation, from DNA-mediated transcriptional regulation to RNA-mediated splicing activity or vice-versa. Additional work is needed, however, to determine whether changes in MATR3

localization predict its function at the DNA or RNA levels, and if MATR3 may serve similar roles in other cell types.

1.3 MATR3 regulation

Immature *MATR3* pre-mRNA undergoes alternative splicing, generating several unique transcripts that encode at least three district protein-coding variants. To date, only the full-length, 847 amino acid isoform has been studied. The two other species, 509 amino acids and 559 amino acids, lack the N-terminal IDR and ZF1. Rajgor and coworkers proposed the existence of a novel, C-terminally truncated isoform in U2OS cells, though this was not detectable by 3' rapid amplification of cDNA ends (RACE)[29]. The regulatory mechanisms that coordinate alternative *MATR3* splicing are unknown, as are the potential functions of N-terminally or C-terminally truncated MATR3 variants.

The *MATR3* transcript is also alternatively polyadenylated in a tissue-specific manner. Sequencing data demonstrate two different polyA signals within the *MATR3* 3' UTR. While the proximal polyA site is overrepresented in adult human cardiac and skeletal muscle cells[59], all other cell types, including neurons and lymphoblasts, use the distal site almost exclusively. Unexpectedly, lymphoblasts from a patient with a balanced translocation interrupting the distal polyA site displayed a massive upregulation of the proximal polyA species and MATR3 protein levels. These results suggest that the proximal polyA signal may increase the stability and/or efficiency of *MATR3* mRNA translation. Abnormal intron retention, as observed in hepatocellular carcinoma, also results in increased *MATR3* mRNA abundance, further supporting the

effects of alternative splicing on *MATR3* transcript stability[60] while implicating additional, as yet unknown mechanisms in MATR3 regulation at the RNA level.

MATR3 levels are tightly regulated during development and in a cell type-specific fashion. In mice, MATR3 protein expression appears to be highest during fetal development but declines and ultimately stabilizes after birth[61]. MATR3 levels vary considerably across cell types and are lowest in skeletal muscle and in the nervous system; such cell type-specific regulation may be particularly pertinent given that muscle and neurons are the two tissues most affected by MATR3-mediated disease.

On a more granular level, MATR3 expression within the brain varies considerably among individual neurons, as adjacent neurons of the same type located in the same brain region display varying MATR3 immunostaining intensities. A possible explanation for this heterogeneity may lie in the activity-dependent regulation of MATR3 abundance, and this is explored in detail in chapter 3 of this dissertation. In cerebellar neurons, N-methyl-D-aspartate (NMDA) receptor activation results in PKA-mediated MATR3 phosphorylation and subsequent degradation[62]. Additionally, MATR3 is tightly bound by activated calmodulin, a major factor responsible for calcium-mediated signal transduction in response to neuronal depolarization[63]. Differences in NMDA receptor activity between neurons may therefore account for the varying intensities of MATR3 staining observed in brain sections. Furthermore, given that expression of NMDA receptor subunits is developmentally regulated[64], an analogous mechanism may explain differences in MATR3 expression over development.

Subcellular MATR3 distribution and abundance are regulated by several factors, including primary sequence, functional domains, and post-translational modifications

(PTMs). Nuclear localization signals (NLSs) effectively concentrate MATR3 within the nucleus but appear to be differentially utilized by distinct cell types. In chicken lymphoma cells, for example, both arms of a bipartite NLS[65] are necessary for targeting MATR3 to the nucleus, while in rat Ac2F cells[12], a separate stretch of positively charged amino acids in the middle of the C-terminal IDR drives MATR3 nuclear localization. In NLS-mutant-expressing cells, cytoplasmic MATR3 forms discrete granules. Given the propensity for MATR3 to form liquid droplets in the absence of functional RNA binding, and the relatively low RNA concentrations in the cytoplasm compared to the nucleus, it is probable these structures represent phase-separated MATR3 droplets[53,66]. The primary sequence determinants of MATR3 distribution in neurons are further examined in chapter 2 of this dissertation.

PTMs may also regulate MATR3 nucleocytoplasmic shuttling and function. While alpha herpesviruses infection does not change host MATR3 localization in human fibroblasts, transduction with viral variants lacking a homologous serine/threonine kinase results in a striking redistribution of MATR3 to the cytoplasm[67]. These results suggest that phosphorylation of MATR3 or another target upon infection with WT viruses maintains nuclear MATR3 localization. In agreement, application of a broad-spectrum kinase inhibitor resulted in the accumulation of cytoplasmic MATR3 in NIH3T3 cells, indicating an endogenous phosphorylation pathway in mammalian cells responsible for nuclear MATR3 enrichment[65]. Additional investigations suggested that MATR3 phosphorylation at Ser208 promotes nuclear localization, as expression of the phosphorylation-null Ser208Ala variant in fibroblasts leads to MATR3 nuclear clearance[68]. Of note, ATM phosphorylates Ser208 in response to DNA damage, an

event that is necessary for MATR3 function in at least certain arms of the DNA damage response[26].

PTMs also affect the ability of MATR3 to recognize nucleic acids. Although the specific phosphoresidues are unknown, phosphorylation enhances MATR3 binding to AT-rich DNA[7] as well as RNA sequences[69]. These effects may be closely related to MATR3 subcellular localization, as nuclear MATR3 is more heavily phosphorylated than cytoplasmic MATR3[12]. Where these PTMs are located and how they alter substrate recognition, however, remain unexplored.

1.4 MATR3 in neuromuscular disease

1.4.1 Spectrum of MATR3-mediated disease

As described above, MATR3 was first implicated in human disease in an American family with an autosomal dominant form of distal myopathy with vocal cord and pharyngeal weakness (VCPDM)[70]. The causative gene was localized to chromosome 5q31, and subsequent investigations of a Bulgarian family with VCPDM revealed a Ser85Cys mutation in *MATR3* affecting a highly conserved amino acid within the N-terminal IDR that segregated with disease[71]. Several additional families with MATR3(Ser85Cys)-linked VCPDM have since been described. These individuals are weak due to atrophy of distal limb muscles as well as proximal muscles of the pharynx and diaphragm[72]. Microscopically, affected muscles exhibit atrophic fibers with rimmed vacuoles, internalized nuclei, and, at end stage, fatty replacement[73-75]. Immunostaining reveals cytoplasmic MATR3 in dystrophic muscle[76] in addition to myofiber inclusions rich in TDP-43, p62/SQSTM1, and ubiquitin[77,78]. Electromyography (EMG)

demonstrates a myopathic pattern similar to related myopathies[79,80] with variable degrees of neurogenic changes, consistent with a primarily myogenic form of disease[70,73,77]. Biochemical analysis of MATR3 protein from patient samples shows no difference in abundance[76] but instead the accumulation of detergent-insoluble MATR3 that is more resistant to extraction[71].

Exome sequencing identified several novel *MATR3* mutations in patients with familial ALS or combined ALS/FTD. Four missense mutations, including Ser85Cys, located in MATR3's IDRs were associated with ALS with or without cognitive deficits[77]. Since then, a number of exome sequencing studies have reported ALS- associated missense mutations concentrated within the disordered regions of the protein[81-85]. The vast majority of these were identified in patients with ALS, though the Ser707Leu mutant was implicated in combined ALS/FTD. Moreover, two splice site mutations were found in ALS patients, one in the 5' UTR and the other predicted to add 24 new residues to the N-terminus of the 559 residue MATR3 isoform[83]. In addition, one individual heterozygous for the Leu145Phe *SOD1* variant and a novel Arg841Cys *MATR3* mutation exhibited a pseudopolyneuritic form of ALS. Conclusions regarding the pathogenicity of this *MATR3* mutation are complicated by the presence of another ALS-causing gene variant, however[86].

Despite accumulating genetic evidence that testifies to the relationship between *MATR3* mutations and human disease, the consequences and tissue specificity of the Ser85Cys mutation remain controversial. This point mutation, first identified in families with VCPDM displaying myogenic and neurogenic EMG features[70,71], was later associated with slowly progressive ALS and upper motor neuron involvement based on

the presence of brisk reflexes in some patients[77]. Similar neurogenic features have since been identified in a number of patients with the Ser85Cys mutation by ante-mortem (clinical examination, EMG) and post-mortem (pathological) studies[73,74,78,87]. Taken together, these data suggest that the Ser85Cys mutation can cause myopathy or motor neuron disease, perhaps depending on unrecognized genetic or environmental modifiers. Further phenotyping in addition to detailed genetic analyses are needed to fully understand the spectrum of disease related to the MATR3(Ser85Cys) mutation.

The degree of dementia also appears to vary considerably in individuals with disease-associated *MATR3* mutations. The initial study linking *MATR3* mutations to ALS identified a Phe115Cys mutation in a patient with cognitive deficits, though this was reported only as dementia without detailed characterization[77]. More recently, however, the Ser707Leu mutation was found in Italian patients displaying cognitive and behavioral symptoms consistent with FTD[84]. To date, these two reports are the only evidence linking *MATR3* mutations to cognitive symptoms. Additional genetic studies coupled with detailed clinical descriptions are necessary to determine the extent to which different neuron subtypes and regions of the CNS are affected by MATR3-linked disease.

1.4.2 MATR3 histopathology

In normal neurons, MATR3 adopts a granular nuclear localization. Individuals with familial ALS due to the highly prevalent *C9orf72* hexanucleotide repeat expansion show diffuse cytoplasmic MATR3 staining as well as cytoplasmic MATR3-positive inclusions in spinal motor neurons[77,88]. An identical pattern was observed in a patient

with the MATR3(Phe115Cys) mutation[77], and cytoplasmic MATR3 aggregates are also found in patients with *FUS* mutation-linked ALS[88], suggesting a conserved pattern of MATR3 mislocalization in disease similar to that displayed by TDP-43. Importantly, these studies also highlighted MATR3 mislocalization in sporadic ALS (sALS), which accounts for more than 80% of incident ALS cases. Spinal cord samples from patients with sALS display strong nuclear MATR3 staining as well as cytoplasmic MATR3 localization, indicating abnormalities not only in MATR3 distribution but also abundance. Similarly, RNA sequencing of post-mortem patient tissue indicates that *MATR3* expression increases in mild and moderate disease stages before dropping in late stages[89], supporting dysregulation of MATR3 expression as well as localization in ALS.

Subsequent investigations confirmed the presence of MATR3 pathology in spinal motor neurons of ALS patients but failed to replicate changes in MATR3 abundance with disease[90]. In some motor neurons, MATR3 appears to be diffusely distributed in the cytoplasm, while in others MATR3 takes on a granular pattern or accumulates within large inclusions that co-stained for TDP-43. Although all MATR3-positive inclusions contain TDP-43, not all TDP-43-positive inclusions stain for MATR3, and TDP-43-positive inclusions are substantially more numerous than MATR3-positive deposits.

These observations suggest that, while both RBPs can undergo redistribution from the nucleus to the cytoplasm in disease, TDP-43 mislocalization may precede MATR3 pathology. Even so, the precise nature of the relationship between MATR3 and other ALS proteins requires further study, as does the discrepancy in reports of MATR3 overabundance in sALS cases.

MATR3 pathology can also be found in neurodegenerative conditions outside of ALS and FTD. Cytoplasmic MATR3 was recently detected in subiculum from patients with Alzheimer's disease (AD) but not age-matched controls. Of note, these authors described not only increased MATR3 levels and diffusely cytoplasmic MATR3 immunostaining in affected neurons, but also ringed MATR3 deposits surrounding granulovacuolar degenerative bodies in AD neurons[91]. In cultured cells, amyloid-β species drive MATR3 phosphorylation, but it is unknown whether this is the mechanism responsible for the MATR3 deposition noted in AD patients[92].

1.5 Dysregulation in disease models

1.5.1 Cell and non-mammalian models

A number of investigators have attempted to recapitulate MATR3-mediated disease using both cellular and animal models. Pathogenic MATR3 mutants show no clear differences in nucleocytoplasmic localization or protein levels in comparison to MATR3(WT) in myoblasts[93]. Proteomic studies of MATR3 binding partners in a mouse spinal neuron/neuroblastoma hybrid cell line identified a distinct set of nuclear transport factors that differentially interact with pathogenic MATR3 variants. These factors, including components of the transcription and export (TREX) complex, were not confirmed in similar experiments conducted in HEK293T cells, suggesting that pathogenic MATR3 mutants may selectively associate with TREX complex members in neuronal cells[51,52], thereby impairing nuclear mRNA export in a cell type-specific manner.

Among the disease-associated MATR3 mutations investigated in model systems, the Ser85Cys variant displays several unique properties. Unlike MATR3(WT), MATR3(S85C) was nearly absent from the soluble nuclear fraction of patient lymphoblasts but was instead concentrated in the insoluble fraction[71]. Even MATR3(WT) becomes markedly insoluble under conditions of thermal or proteotoxic stress, suggesting that the Ser85Cys mutation may lower the threshold for this behavior, rather than introducing novel properties per se[94,95]. Furthermore, in MATR3 variants that are unable to bind RNA and undergo LLPS, the Ser85Cys mutation dramatically affects the internal dynamics of MATR3 within liquid-like droplets. RNA binding-deficient MATR3(Ser85Cys) forms irregular, fibrillar structures instead of spheres in C2C12 myoblasts[52]. Perhaps related to these biophysical phenotypes, the formation of liquid droplet-like cytoplasmic stress granules is impaired in fibroblasts from Ser85Cys patients compared to those from healthy controls, and Ser85Cys but not WT protein enhances the aggregation of cytoplasmically targeted TDP-43 when overexpressed[96]. Whether and how these features explain the distinctive clinical picture of VCPDM-associated selectively with the Ser85Cys mutation remains unknown.

Insights into MATR3-mediated disease have also emerged from *in vivo* modeling in *Drosophila*, which lack a MATR3 homologue. Two independent groups found that MATR3 expression in *Drosophila* results in shortened lifespan and motor deficits, with disease-associated mutants exhibiting increased toxicity over MATR3(WT)[97,98]. Notably, both studies found that Ser85Cys is uniquely insoluble in flies, recapitulating findings from patient cells. Robust wing defects caused by muscle-specific MATR3 expression were accentuated by pathogenic mutations, particularly Ser85Cys; this phenotype

formed the basis for an RNAi screen that uncovered genes related to axonal transport as enhancers of toxicity, suggesting that alterations in intracellular trafficking may be involved in MATR3 pathogenesis. A separate RBP-targeted RNAi screen revealed that hnRNPM knockdown extends the lifespan of flies expressing Ser85Cys and Phe115Cys pathogenic mutants but not MATR3(WT). hnRNPM and MATR3 share many RNA substrates, and their respective binding sites are located in close proximity. It is therefore possible MATR3 acts in concert with hnRNPM to mediate RNA dysfunction and toxicity in *Drosophila*.

1.5.2 Mouse models

Multiple groups have attempted to model MATR3-related disease in mice. Homozygous knockout of murine *Matr3* is perinatally lethal, indicating that MATR3 is necessary for viability[99]. In a separate model, overexpression of human MATR3(WT) or MATR3(Phe115Cys) in skeletal muscle results in age-dependent muscle fiber degeneration with extensive vacuoles, internalized nuclei, and gross atrophy. Despite equivalent amounts of transgene mRNA, expression of MATR3(Phe115Cys) was greater than MATR3(WT), and only MATR3(Phe115Cys) animals demonstrated gross motor impairment, implying mutation-specific effects on translational control, turnover, or both[100]. For unknown reasons, neither MATR3(Phe115Cys) nor MATR3(WT) was detectable within the spinal cord of these animals, despite use of the MoPrP promoter, which typically drives high CNS expression[101].

Similar myopathic changes were observed by intramuscular AAV delivery of human MATR3(Ser85Cys) or MATR3(WT) in mice, including myofiber atrophy,

internalized nuclei, and upregulation of muscle repair genes[102]. Sarcoplasmic inclusions rich in MATR3 and p62/SQSTM1 were observed in transduced muscle sections, mirroring the pathology of inclusion body myopathy in humans[103]. Despite similar expression of exogenous protein, this phenotype was more severe with MATR3(Ser85Cys) than MATR3(WT), supporting enhanced pathogenicity of mutant MATR3. Notably, analogous sarcoplasmic aggregates rich in MATR3 and p62/SQSTM1 are observed in muscle tissue from patients with VCPDM who carry the Ser85Cys mutation, lending clinical relevance to these findings[73,78,104]. To investigate CNS-specific effects of MATR3 upregulation, Zhang and colleagues also generated transgenic mice expressing MATR3(Ser85Cys) under control of the CMV promoter. These animals develop age-dependent motor impairment with muscle degeneration, similar to that seen in AAV-injected animals, but also demonstrate progressive spinal cord pathology with motor neuron loss, astrogliosis, microgliosis, and mislocalization of MATR3 and TDP-43. While the striking CNS pathology is consistent with ALS, these observations are complicated by the unchanged levels of full-length MATR3 in transgenic mice compared to non-transgenic controls, and the lack of MATR3(WT) transgenic animals for comparison.

A Ser85Cys mutation knock-in model has also provided important pathogenic insights in the context of physiological MATR3 dosage[99]. Homozygous knock-in mice display age-dependent motor impairment, muscle denervation and pathology, and neuroinflammation. Strikingly, these animals also show marked cerebellar degeneration and loss of MATR3 within Purkinje neurons at end stage. While significant motor neuron loss was not noted, approximately half of spinal α-motor neurons in homozygous knock-

in mice also exhibit diminished MATR3 immunoreactivity, with many others staining positive for intranuclear MATR3 inclusions. This model raises fascinating questions for future studies regarding the effects of the Ser85Cys mutation on MATR3 regulation in Purkinje and motor neurons and the relevance of cerebellar pathology for human MATR3-linked neurodegeneration.

1.6 Similarity with other RBPs

MATR3 shares many similarities with other RBPs implicated in neuromuscular disease. MATR3 belongs to a subset of RBPs that are linked not only to the neurodegenerative disorders ALS and FTD but also to muscular disease. Although mutations in the genes encoding RBPs such as TDP-43 or FUS lead primarily to ALS, *MATR3* mutations can result in additional disorders such as FTD or VCPDM. Similar pleiotropy is also observed with *VCP*, *TIA1*, *hnRNPA1*, and *hnRNPA2B1* mutations, which can affect the CNS, skeletal muscle, and/or bone[105-107]. Individual differences among genes and clinical phenotypes may be important for disease mechanisms in each case. For instance, *VCP*, *hnRNPA1,* and *hnRNPA2B1* mutations cause multisystem proteinopathy (MSP) with Paget's disease of bone, inclusion body myopathy, ALS, and FTD, while *TIA1* and *MATR3* mutations result in distal myopathy in addition to ALS and FTD.

How mutations in these widely expressed proteins drive tissue-specific disease—and why their disease spectra differ—are currently not well understood. One promising explanation may lie in the dysregulation of pathways unique to certain cells. VCP degrades the NFκB inhibitor IκB, thereby suppressing osteoclast activity and bone

resorption[108,109]. Pathogenic *VCP* mutations promote IκB clearance, and VCP-mediated disease models show enhanced NFκB signaling and osteoclast activation phenotypes, suggesting mutant VCP instigates bone pathology by disinhibiting NFkB[110,111]. It is possible that similar cell type-specific functions for MATR3 and other RBPs dictate the range of phenotypes affecting muscle as well as neurons within the ventral spinal cord, motor cortex, and frontotemporal lobe.

All of these genes except *VCP* encode for IDR-containing RBPs that undergo phase separation as part of their normal functions in RNA splicing, degradation, sequestration, and transport. Notably, the physiological LLPS of RBPs is dynamic and reversible, with factors such as substrate binding and PTMs tuning self-assembly[56,112-118]. Disease-associated mutations may interrupt physiological LLPS regulation, promoting aberrant liquid-to-solid phase transitions that eventually lead to irreversible RBP aggregates characteristic of ALS, FTD, and inclusion body myopathy[106,107,119-123].

Upon RRM2 deletion, MATR3 rapidly undergoes LLPS, consistent with a model in which RNA binding pulls RBPs apart from each other. The extent to which MATR3 phase separation is necessary for its functions in nucleic acid processing remains unknown, as are the physiological factors regulating this process. Moreover, data from multiple groups suggest that the Ser85Cys mutant dramatically affects the biophysical properties of MATR3 liquid droplets, analogous to what has been reported for pathogenic mutations in other disease-linked RBPs[71,102].It is currently unclear whether other MATR3 mutations have similar effects on pathological phase transitions or if they drive disease through alternative mechanisms.

1.7 Summary and dissertation goals

Mutations in the gene encoding MATR3 are responsible for neuromuscular disease, implying this protein is critical for maintaining health in neurons as well as muscle. Potentially because of the similarity between MATR3 and other neurodegenerative disease-associated RBPs, the majority of investigations to date have focused on MATR3's influence on pre-mRNA splicing and RNA regulation. In contrast, much less in known about the consequences of MATR3 DNA binding and whether the dysregulation of MATR3 chromatin targets is involved in disease. Indeed, it is currently unclear if MATR3 binds chromatin directly *in vivo* or if it instead requires cell-specific factors for DNA association.

Despite the identification of MATR3 as a nuclear matrix component nearly three decades ago, important questions remain about its diverse functions in nucleic acid processing as well as its involvement in sporadic and inherited neuromuscular disorders. The goal of this dissertation work is to investigate the basic biology of MATR3 in neurons and how pathogenic mutations may impair physiological function and regulation. Chapter 2 discusses the effect of MATR3 abundance on neuron survival and presents data on MATR3 domain deletion and disease-associated mutants as they relate to neurotoxicity and biophysical properties of this protein. The focus of chapter 3 is the physiological regulation of MATR3 in neurons and how neuronal activity inhibits MATR3 RNA binding and results in its degradation, both of which occur through Ca^{2+}-dependent pathways. Chapter 4 concludes with a discussion of promising open questions in the field of MATR3 biology, with a focus on the potential relevance of findings from MATR3 to other RBPs in the context of neuronal physiology. Lastly,

appendix A details experiments aimed at elucidating the DNA targets of MATR3 in neurons that—while negative—nevertheless may shed light on MATR3's functions in nucleic acid regulation.

References

1. van Es, M. A. *et al.* Amyotrophic lateral sclerosis. *Lancet* **390,** 2084–2098 (2017).
2. Taylor, J. P., Brown, R. H. & Cleveland, D. W. Decoding ALS: from genes to mechanism. *Nature* **539,** 197–206 (2016).
3. Neumann, M. *et al.* Ubiquitinated TDP-43 in frontotemporal lobar degeneration and amyotrophic lateral sclerosis. *Science* **314,** 130–133 (2006).
4. Arai, T. *et al.* TDP-43 is a component of ubiquitin-positive tau-negative inclusions in frontotemporal lobar degeneration and amyotrophic lateral sclerosis. *Biochemical and Biophysical Research Communications* **351,** 602–611 (2006).
5. Nakayasu, H. & Berezney, R. Nuclear matrins: identification of the major nuclear matrix proteins. *Proc Natl Acad Sci USA* **88,** 10312–10316 (1991).
6. Belgrader, P., Dey, R. & Berezney, R. Molecular cloning of Matrin 3. A 125-kilodalton protein of the nuclear matrix contains an extensive acidic domain. *The Journal of Biological Chemistry* **266,** 9893–9899 (1991).
7. Hibino, Y., Ohzeki, H., Hirose, N. & Sugano, N. Involvement of phosphorylation in binding of nuclear scaffold proteins from rat liver to a highly repetitive DNA component. *Biochimica et Biophysica Acta (BBA) - Gene Structure and Expression* **1396,** 88–96 (1998).
8. Hibino, Y., Nakamura, K., Tsukada, S. & Sugano, N. Purification and characterization of nuclear scaffold proteins which bind to a highly repetitive bent DNA from rat liver. *Biochim. Biophys. Acta* **1174,** 162–170 (1993).
9. Hibino, Y., Tsukada, S. & Sugano, N. Properties of a DNA-binding protein from rat nuclear scaffold fraction. *Biochemical and Biophysical Research Communications* **197,** 336–342 (1993).
10. Brayer, K. J., Kulshreshtha, S. & Segal, D. J. The protein-binding potential of C2H2 zinc finger domains. *Cell Biochem. Biophys.* **51,** 9–19 (2008).
11. Burdach, J., O'Connell, M. R., Mackay, J. P. & Crossley, M. Two-timing zinc finger transcription factors liaising with RNA. *Trends Biochem. Sci.* **37,** 199–205 (2012).
12. Hibino, Y. *et al.* Molecular properties and intracellular localization of rat liver nuclear scaffold protein P130. *Biochimica et Biophysica Acta (BBA) - Gene Structure and Expression* **1759,** 195–207 (2006).
13. Craig, J. M., Boyle, S., Perry, P. & Bickmore, W. A. Scaffold attachments within the human genome. *J. Cell. Sci.* **110 (Pt 21),** 2673–2682 (1997).
14. Poljak, L. & Käs, E. Resolving the role of topoisomerase II in chromatin structure and function. *Trends Cell Biol.* **5,** 348–354 (1995).
15. Gerdes, M. G., Carter, K. C., Moen, P. T. & Lawrence, J. B. Dynamic changes in the higher-level chromatin organization of specific sequences revealed by in situ hybridization to nuclear halos. *J. Cell Biol.* **126,** 289–304 (1994).
16. Singh, G. B., Kramer, J. A. & Krawetz, S. A. Mathematical model to predict regions of chromatin attachment to the nuclear matrix. *Nucleic Acids Research* **25,** 1419–1425 (1997).
17. Nakayasu, H. & Berezney, R. Mapping replicational sites in the eucaryotic cell nucleus. *J. Cell Biol.* **108,** 1–11 (1989).

18. Nayler, O. *et al.* SAF-B protein couples transcription and pre-mRNA splicing to SAR/MAR elements. *Nucleic Acids Research* **26,** 3542–3549 (1998).
19. Bidwell, J. P. *et al.* Osteocalcin gene promoter-binding factors are tissue-specific nuclear matrix components. *Proc Natl Acad Sci USA* **90,** 3162–3166 (1993).
20. Zeitz, M. J., Malyavantham, K. S., Seifert, B. & Berezney, R. Matrin 3: Chromosomal distribution and protein interactions. *J. Cell. Biochem.* **108,** 125–133 (2009).
21. Malyavantham, K. S. *et al.* Identifying functional neighborhoods within the cell nucleus: proximity analysis of early S-phase replicating chromatin domains to sites of transcription, RNA polymerase II, HP1gamma, matrin 3 and SAF-A. *J. Cell. Biochem.* **105,** 391–403 (2008).
22. Hibino, Y., Ohzeki, H., Sugano, N. & Hiraga, K. Transcription Modulation by a Rat Nuclear Scaffold Protein, P130, and a Rat Highly Repetitive DNA Component or Various Types of Animal and Plant Matrix or Scaffold Attachment Regions. *Biochemical and Biophysical Research Communications* **279,** 282–287 (2000).
23. Skowronska-Krawczyk, D. *et al.* Required enhancer–matrin-3 network interactions for a homeodomain transcription program. *Nature* 1–13 (2014). doi:10.1038/nature13573
24. Fujita, T. & Fujii, H. Direct identification of insulator components by insertional chromatin immunoprecipitation. *PLoS ONE* **6,** e26109 (2011).
25. Desideri, F. *et al.* Intronic Determinants Coordinate Charme lncRNA Nuclear Activity through the Interaction with MATR3 and PTBP1. *Cell Rep* **33,** 108548 (2020).
26. Salton, M., Lerenthal, Y., Wang, S.-Y., Chen, D. J. & Shiloh, Y. Involvement of Matrin 3 and SFPQ/NONO in the DNA damage response. *Cell Cycle* **9,** 1568–1576 (2014).
27. Shi, L. *et al.* Matrin3 promotes homologous recombinational repair by regulation of RAD51. *J. Biochem.* **166,** 343–351 (2019).
28. Chaudhary, R. *et al.* Prosurvival long noncoding RNA PINCR regulates a subset of p53 targets in human colorectal cancer cells by binding to Matrin 3. *Elife* **6,** 861 (2017).
29. Rajgor, D., Hanley, J. G. & Shanahan, C. M. Identification of novel nesprin-1 binding partners and cytoplasmic matrin-3 in processing bodies. **27,** 3894–3902 (2016).
30. Höck, J. *et al.* Proteomic and functional analysis of Argonaute-containing mRNA-protein complexes in human cells. *EMBO Rep.* **8,** 1052–1060 (2007).
31. Salton, M. *et al.* Matrin 3 Binds and Stabilizes mRNA. *PLoS ONE* **6,** e23882–7 (2011).
32. Luo, E.-C. *et al.* Large-scale tethered function assays identify factors that regulate mRNA stability and translation. *Nat. Struct. Mol. Biol.* **24,** 416–12 (2020).
33. Ayala, Y. M. *et al.* Human, Drosophila, and C.elegans TDP43: nucleic acid binding properties and splicing regulatory function. *J. Mol. Biol.* **348,** 575–588 (2005).

34. Kuo, P.-H., Doudeva, L. G., Wang, Y.-T., Shen, C.-K. J. & Yuan, H. S. Structural insights into TDP-43 in nucleic-acid binding and domain interactions. *Nucleic Acids Research* **37,** 1799–1808 (2009).
35. Buratti, E. & Baralle, F. E. Characterization and functional implications of the RNA binding properties of nuclear factor TDP-43, a novel splicing regulator of CFTR exon 9. *The Journal of Biological Chemistry* **276,** 36337–36343 (2001).
36. Coelho, M. B. *et al.* Nuclear matrix protein Matrin3 regulates alternative splicing and forms overlapping regulatory networks with PTB. *The EMBO Journal* **34,** 653–668 (2015).
37. Weiss, K., Treiber, T., Meister, G. & Schratt, G. The nuclear matrix protein Matr3 regulates processing of the synaptic microRNA-138-5p. *Neurobiol Learn Mem* **159,** 36–45 (2019).
38. Ray, D. *et al.* A compendium of RNA-binding motifs for decoding gene regulation. *Nature* **499,** 172–177 (2013).
39. Uemura, Y. *et al.* Matrin3 binds directly to intronic pyrimidine-rich sequences and controls alternative splicing. *Genes Cells* **22,** 785–798 (2017).
40. Sun, J., Bai, J., Jiang, T., Gao, Y. & Hua, Y. Modulation of PDCD1 exon 3 splicing. *RNA Biol* **16,** 1794–1805 (2019).
41. Joshi, A. *et al.* Crystallographic analysis of polypyrimidine tract-binding protein-Raver1 interactions involved in regulation of alternative splicing. *Structure* **19,** 1816–1825 (2011).
42. Attig, J. *et al.* Heteromeric RNP Assembly at LINEs Controls Lineage-Specific RNA Processing. *Cell* **174,** 1067–1081.e17 (2018).
43. Morchikh, M. *et al.* HEXIM1 and NEAT1 Long Non-coding RNA Form a Multi-subunit Complex that Regulates DNA-Mediated Innate Immune Response. *Mol. Cell* **67,** 387–399.e5 (2017).
44. Yamaguchi, A. & Takanashi, K. FUS interacts with nuclear matrix-associated protein SAFB1 as well as Matrin3 to regulate splicing and ligand-mediated transcription. *Scientific Reports* **6,** 35195–14 (2016).
45. Damianov, A. *et al.* Rbfox Proteins Regulate Splicing as Part of a Large Multiprotein Complex LASR. *Cell* **165,** 606–619 (2016).
46. Li, Y. *et al.* Immunoprecipitation and mass spectrometry defines an extensive RBM45 protein-protein interaction network. *Brain Research* **1647,** 79–93 (2016).
47. Tenzer, S. *et al.* Proteome-wide characterization of the RNA-binding protein RALY-interactome using the in vivo-biotinylation-pulldown-quant (iBioPQ) approach. *J. Proteome Res.* **12,** 2869–2884 (2013).
48. Erazo, A. & Goff, S. P. Nuclear matrix protein Matrin 3 is a regulator of ZAP-mediated retroviral restriction. *Retrovirology* 1–12 (2015). doi:10.1186/s12977-015-0182-4
49. Ling, S.-C. *et al.* ALS-associated mutations in TDP-43 increase its stability and promote TDP-43 complexes with FUS/TLS. *Proc. Natl. Acad. Sci. U.S.A.* **107,** 13318–13323 (2010).
50. Leonard, D., Ajuh, P., Lamond, A. I. & Legerski, R. J. hLodestar/HuF2 interacts with CDC5L and is involved in pre-mRNA splicing. *Biochemical and Biophysical Research Communications* **308,** 793–801 (2003).

51. Boehringer, A. *et al.* ALS Associated Mutations in Matrin 3 Alter Protein-Protein Interactions and Impede mRNA Nuclear Export. *Scientific Reports* 1–14 (2017). doi:10.1038/s41598-017-14924-6
52. Iradi, M. C. G. *et al.* Characterization of gene regulation and protein interaction networks for Matrin 3 encoding mutations linked to amyotrophic lateral sclerosis and myopathy. *Scientific Reports* **8,** 4049 (2018).
53. Gallego-Iradi, M. C. *et al.* N-terminal sequences in matrin 3 mediate phase separation into droplet-like structures that recruit TDP43 variants lacking RNA binding elements. *Lab. Invest.* **99,** 1030–1040 (2019).
54. Flores, B. N. *et al.* An Intramolecular Salt Bridge Linking TDP43 RNA Binding, Protein Stability, and TDP43-Dependent Neurodegeneration. *Cell Rep* **27,** 1133–1150.e8 (2019).
55. Maharana, S. *et al.* RNA buffers the phase separation behavior of prion-like RNA binding proteins. *Science* eaar7366 (2018). doi:10.1126/science.aar7366
56. Mann, J. R. *et al.* RNA Binding Antagonizes Neurotoxic Phase Transitions of TDP-43. *Neuron* **102,** 321–338.e8 (2019).
57. Banerjee, A., Vest, K. E., Pavlath, G. K. & Corbett, A. H. Nuclear poly(A) binding protein 1 (PABPN1) and Matrin3 interact in muscle cells and regulate RNA processing. *Nucleic Acids Research* **45,** 10706–10725 (2017).
58. Depreux, F. F. *et al.* Disruption of the lamin A and matrin-3 interaction by myopathic LMNAmutations. *Human Molecular Genetics* **24,** 4284–4295 (2015).
59. Quintero-Rivera, F. *et al.* MATR3 disruption in human and mouse associated with bicuspid aortic valve, aortic coarctation and patent ductus arteriosus. *Human Molecular Genetics* **24,** 2375–2389 (2015).
60. Chen, H. *et al.* Long-Read RNA Sequencing Identifies Alternative Splice Variants in Hepatocellular Carcinoma and Tumor-Specific Isoforms. *Hepatology* **70,** 1011–1025 (2019).
61. Rayaprolu, S. *et al.* Heterogeneity of Matrin 3 in the developing and aging murine central nervous system. *Journal of Comparative Neurology* **524,** 2740–2752 (2016).
62. Giordano, G. *et al.* Activation of NMDA receptors induces protein kinase A-mediated phosphorylation and degradation of matrin 3. Blocking these effects prevents NMDA-induced neuronal death. *Journal of Neurochemistry* **94,** 808–818 (2005).
63. Alexander Valencia, C., Ju, W. & Liu, R. Matrin 3 is a Ca2+/calmodulin-binding protein cleaved by caspases. *Biochemical and Biophysical Research Communications* **361,** 281–286 (2007).
64. Cheng, C., Fass, D. M. & Reynolds, I. J. Emergence of excitotoxicity in cultured forebrain neurons coincides with larger glutamate-stimulated [Ca(2+)](i) increases and NMDA receptor mRNA levels. *Brain Research* **849,** 97–108 (1999).
65. Hisada-Ishii, S., Ebihara, M., Kobayashi, N. & KITAGAWA, Y. Bipartite nuclear localization signal of matrin 3 is essential for vertebrate cells. *Biochemical and Biophysical Research Communications* **354,** 72–76 (2007).

66. Goldstein, L. & Trescott, O. H. Characterization of RNAs that do and do not migrate between cytoplasm and nucleus. *Proc Natl Acad Sci USA* **67,** 1367–1374 (1970).
67. Erazo, A., Yee, M. B., Banfield, B. W. & Kinchington, P. R. The Alphaherpesvirus US3/ORF66 Protein Kinases Direct Phosphorylation of the Nuclear Matrix Protein Matrin 3. *Journal of Virology* **85,** 568–581 (2010).
68. Niimori-Kita, K., Tamamaki, N., Koizumi, D. & Niimori, D. Matrin-3 is essential for fibroblast growth factor 2-dependent maintenance of neural stem cells. *Scientific Reports* **8,** 13412 (2018).
69. Yamazaki, F. *et al.* pY RNA1-s2: a highly retina-enriched small RNA that selectively binds to Matrin 3 (Matr3). *PLoS ONE* **9,** e88217 (2014).
70. Feit, H. *et al.* Vocal Cord and Pharyngeal Weakness with Autosomal Dominant Distal Myopathy: Clinical Description and Gene Localization to 5q31. *The American Journal of Human Genetics* **63,** 1732–1742 (1998).
71. Senderek, J. *et al.* Autosomal-Dominant Distal Myopathy Associated with a Recurrent Missense Mutation in the Gene Encoding the Nuclear Matrix Protein, Matrin 3. *The American Journal of Human Genetics* **84,** 511–518 (2009).
72. Kraya, T., Schmidt, B., MüLLER, T. & Hanisch, F. Impairment of respiratory function in late-onset distal myopathy due to MATR3 Mutation. *Muscle & Nerve* **51,** 916–918 (2015).
73. Palmio, J. *et al.* Re-evaluation of the phenotype caused by the common MATR3 p.Ser85Cys mutation in a new family. *J. Neurol. Neurosurg. Psychiatry* **87,** 448–450 (2016).
74. Müller, T. J. *et al.* Phenotype of matrin-3-related distal myopathy in 16 German patients. *Ann. Neurol.* **76,** 669–680 (2014).
75. Mensch, A. *et al.* Whole-body muscle MRI of patients with MATR3-associated distal myopathy reveals a distinct pattern of muscular involvement and highlights the value of whole-body examination. *J. Neurol.* **14,** 434 (2020).
76. Mensch, A. *et al.* The p.S85C-mutation in MATR3 impairs stress granule formation in Matrin-3 myopathy. *Exp. Neurol.* **306,** 222–231 (2018).
77. Johnson, J. O. *et al.* Mutations in the Matrin 3 gene cause familial amyotrophic lateral sclerosis. *Nat Neurosci* **17,** 664–666 (2014).
78. Yamashita, S. *et al.* Clinicopathological features of the first Asian family having vocal cord and pharyngeal weakness with distal myopathy due to a MATR3 mutation. *Neuropathol. Appl. Neurobiol.* **41,** 391–398 (2015).
79. Hanisch, F., Kraya, T., Müller, T. & Kornhuber, M. Needle electromyography findings in patients with MATR3 mutation â€“ A prospective study. *Clinical Neurophysiology* **127,** 2085–2086 (2016).
80. Hanisch, F., Kronenberger, C., Zierz, S. & Kornhuber, M. The significance of pathological spontaneous activity in various myopathies. *Clin Neurophysiol* **125,** 1485–1490 (2014).
81. Lin, K.-P. *et al.* Mutational analysis of MATR3 in Taiwanese patients with amyotrophic lateral sclerosis. *Neurobiology of Aging* **36,** 2005.e1–2005.e4 (2015).

82. Origone, P. *et al.* A novel Arg147Trp MATR3 missense mutation in a slowly progressive ALS Italian patient. *Amyotrophic Lateral Sclerosis and Frontotemporal Degeneration* **16,** 530–531 (2015).
83. Leblond, C. S. *et al.* Replication study of MATR3 in familial and sporadic amyotrophic lateral sclerosis. *Neurobiology of Aging* **37,** 209.e17–209.e21 (2016).
84. Marangi, G. *et al.* Matrin 3 variants are frequent in Italian ALS patients. *Neurobiology of Aging* **49,** 218.e1–218.e7 (2017).
85. Narain, P. *et al.* Identification and characterization of novel and rare susceptible variants in Indian amyotrophic lateral sclerosis patients. *Neurogenetics* **20,** 197–208 (2019).
86. Lamp, M. *et al.* Twenty years of molecular analyses in amyotrophic lateral sclerosis: genetic landscape of Italian patients. *Neurobiology of Aging* **66,** 179.e5–179.e16 (2018).
87. Barp, A. *et al.* The first French case of MATR3-related distal myopathy: Clinical, radiological and histopathological characterization. *Rev. Neurol. (Paris)* **174,** 752–755 (2018).
88. Dreser, A. *et al.* The ALS-linked E102Q mutation in Sigma receptor-1 leads to ER stress-mediated defects in protein homeostasis and dysregulation of RNA-binding proteins. 1–17 (2017). doi:10.1038/cdd.2017.88
89. Jones, A. R. *et al.* Stratified gene expression analysis identifies major amyotrophic lateral sclerosis genes. *Neurobiology of Aging* **36,** 2006.e1–9 (2015).
90. Tada, M. *et al.* Matrin 3 is a component of neuronal cytoplasmic inclusions of motor neurons in sporadic amyotrophic lateral sclerosis. *The American Journal of Pathology* 1–36 (2017). doi:10.1016/j.ajpath.2017.10.007
91. Yamoah, A. *et al.* Aggregates of RNA Binding Proteins and ER Chaperones Linked to Exosomes in Granulovacuolar Degeneration of the Alzheimer's Disease Brain. *J. Alzheimers Dis.* **75,** 139–156 (2020).
92. Zatsepina, O. G. *et al.* Amyloid-β with isomerized Asp7 cytotoxicity is coupled to protein phosphorylation. *Scientific Reports* **8,** 3518–10 (2018).
93. Gallego-Iradi, M. C. *et al.* Subcellular Localization of Matrin 3 Containing Mutations Associated with ALS and Distal Myopathy. *PLoS ONE* **10,** e0142144–15 (2015).
94. Hayes, L. R., Duan, L., Bowen, K., Kalab, P. & Rothstein, J. D. C9orf72 arginine-rich dipeptide repeat proteins disrupt karyopherin-mediated nuclear import. *Elife* **9,** 807 (2020).
95. Xu, G. *et al.* Identification of proteins sensitive to thermal stress in human neuroblastoma and glioma cell lines. *PLoS ONE* **7,** e49021 (2012).
96. Bajc Česnik, A., Motaln, H. & Rogelj, B. The Impact of ALS-Associated Genes hnRNPA1, MATR3, VCP and UBQLN2 on the Severity of TDP-43 Aggregation. *Cells* **9,** 1791 (2020).
97. Zhao, M. *et al.* Knockdown of genes involved in axonal transport enhances the toxicity of human neuromuscular disease-linked MATR3 mutations in Drosophila. *FEBS Lett.* **27,** 4103 (2020).

98. Ramesh, N., Kour, S., Anderson, E. N., Rajasundaram, D. & Pandey, U. B. RNA-recognition motif in Matrin-3 mediates neurodegeneration through interaction with hnRNPM. *Acta Neuropathologica Communications* **8,** 138 (2020).
99. Kao, C. S. *et al.* Selective neuronal degeneration in MATR3 S85C knock-in mouse model of early-stage ALS. *Nature Communications* **11,** 5304–17 (2020).
100. Moloney, C. *et al.* Analysis of spinal and muscle pathology in transgenic mice overexpressing wild-type and ALS-linked mutant MATR3. *Acta Neuropathologica Communications* **6,** 137–13 (2018).
101. Borchelt, D. R. *et al.* A vector for expressing foreign genes in the brains and hearts of transgenic mice. *Genet. Anal.* **13,** 159–163 (1996).
102. Zhang, X. *et al.* A mutant MATR3 mouse model to explain multisystem proteinopathy. *J. Pathol.* **249,** 182–192 (2019).
103. Askanas, V., Engel, W. K. & Nogalska, A. Sporadic inclusion-body myositis: A degenerative muscle disease associated with aging, impaired muscle protein homeostasis and abnormal mitophagy. *Biochim. Biophys. Acta* **1852,** 633–643 (2015).
104. Johnson, J. O. *et al.* Mutations in the Matrin 3 gene cause familial amyotrophic lateral sclerosis supplemental. *Nat Neurosci* **17,** 664–666 (2014).
105. Johnson, J. O. *et al.* Exome sequencing reveals VCP mutations as a cause of familial ALS. *Neuron* **68,** 857–864 (2010).
106. Kim, H. J. *et al.* Mutations in prion-like domains in hnRNPA2B1 and hnRNPA1 cause multisystem proteinopathy and ALS. *Nature* **495,** 467–473 (2013).
107. Mackenzie, I. R. *et al.* TIA1 Mutations in Amyotrophic Lateral Sclerosis and Frontotemporal Dementia Promote Phase Separation and Alter Stress Granule Dynamics. *Neuron* **95,** 808–816.e9 (2017).
108. Dai, R. M., Chen, E., Longo, D. L., Gorbea, C. M. & Li, C. C. Involvement of valosin-containing protein, an ATPase Co-purified with IkappaBalpha and 26 S proteasome, in ubiquitin-proteasome-mediated degradation of IkappaBalpha. *The Journal of Biological Chemistry* **273,** 3562–3573 (1998).
109. Dai, R. M. & Li, C. C. Valosin-containing protein is a multi-ubiquitin chain-targeting factor required in ubiquitin-proteasome degradation. *Nature Cell Biology* **3,** 740–744 (2001).
110. Custer, S. K., Neumann, M., Lu, H., Wright, A. C. & Taylor, J. P. Transgenic mice expressing mutant forms VCP/p97 recapitulate the full spectrum of IBMPFD including degeneration in muscle, brain and bone. *Human Molecular Genetics* **19,** 1741–1755 (2010).
111. Badadani, M. *et al.* VCP associated inclusion body myopathy and paget disease of bone knock-in mouse model exhibits tissue pathology typical of human disease. *PLoS ONE* **5,** e13183 (2010).
112. Burke, K. A., Janke, A. M., Rhine, C. L. & Fawzi, N. L. Residue-by-Residue View of In Vitro FUS Granules that Bind the C-Terminal Domain of RNA Polymerase II. *Mol. Cell* **60,** 231–241 (2015).
113. Monahan, Z. *et al.* Phosphorylation of the FUS low-complexity domain disrupts phase separation, aggregation, and toxicity. *The EMBO Journal* **36,** 2951–2967 (2017).

114. Murray, D. T. *et al.* Structure of FUS Protein Fibrils and Its Relevance to Self-Assembly and Phase Separation of Low- Complexity Domains. *Cell* **171,** 615–620.e16 (2017).
115. Qamar, S. *et al.* FUS Phase Separation Is Modulated by a Molecular Chaperone and Methylation of Arginine Cation-π Interactions. *Cell* **173,** 720–734.e15 (2018).
116. Hofweber, M. *et al.* Phase Separation of FUS Is Suppressed by Its Nuclear Import Receptor and Arginine Methylation. *Cell* **173,** 706–719.e13 (2018).
117. Vijayakumar, J. *et al.* The prion-like domain of Drosophila Imp promotes axonal transport of RNP granules in vivo. *Nature Communications* **10,** 2593–14 (2019).
118. Yang, P. *et al.* G3BP1 Is a Tunable Switch that Triggers Phase Separation to Assemble Stress Granules. *Cell* **181,** 325–345.e28 (2020).
119. Murakami, T. *et al.* ALS/FTD Mutation-Induced Phase Transition of FUS Liquid Droplets and Reversible Hydrogels into Irreversible Hydrogels Impairs RNP Granule Function. *Neuron* **88,** 678–690 (2015).
120. Patel, A. *et al.* A Liquid-to-Solid Phase Transition of the ALS Protein FUS Accelerated by Disease Mutation. *Cell* **162,** 1066–1077 (2015).
121. Conicella, A. E., Zerze, G. H., Mittal, J. & Fawzi, N. L. ALS Mutations Disrupt Phase Separation Mediated by α-Helical Structure in the TDP-43 Low-Complexity C-Terminal Domain. *Structure* **24,** 1537–1549 (2016).
122. Gopal, P. P., Nirschl, J. J., Klinman, E. & Holzbaur, E. L. F. Amyotrophic lateral sclerosis-linked mutations increase the viscosity of liquid-like TDP-43 RNP granules in neurons. *Proc Natl Acad Sci USA* **114,** E2466–E2475 (2017).
123. Mateju, D. *et al.* An aberrant phase transition of stress granules triggered by misfolded protein and prevented by chaperone function. *The EMBO Journal* **36,** 1669–1687 (2017).
124. Peng K, Radivojac P, Vucetic S, Dunker AK, Obradovic Z. Length-dependent prediction of protein intrinsic disorder. *BMC Bioinformatics* 2006;7(1):208.

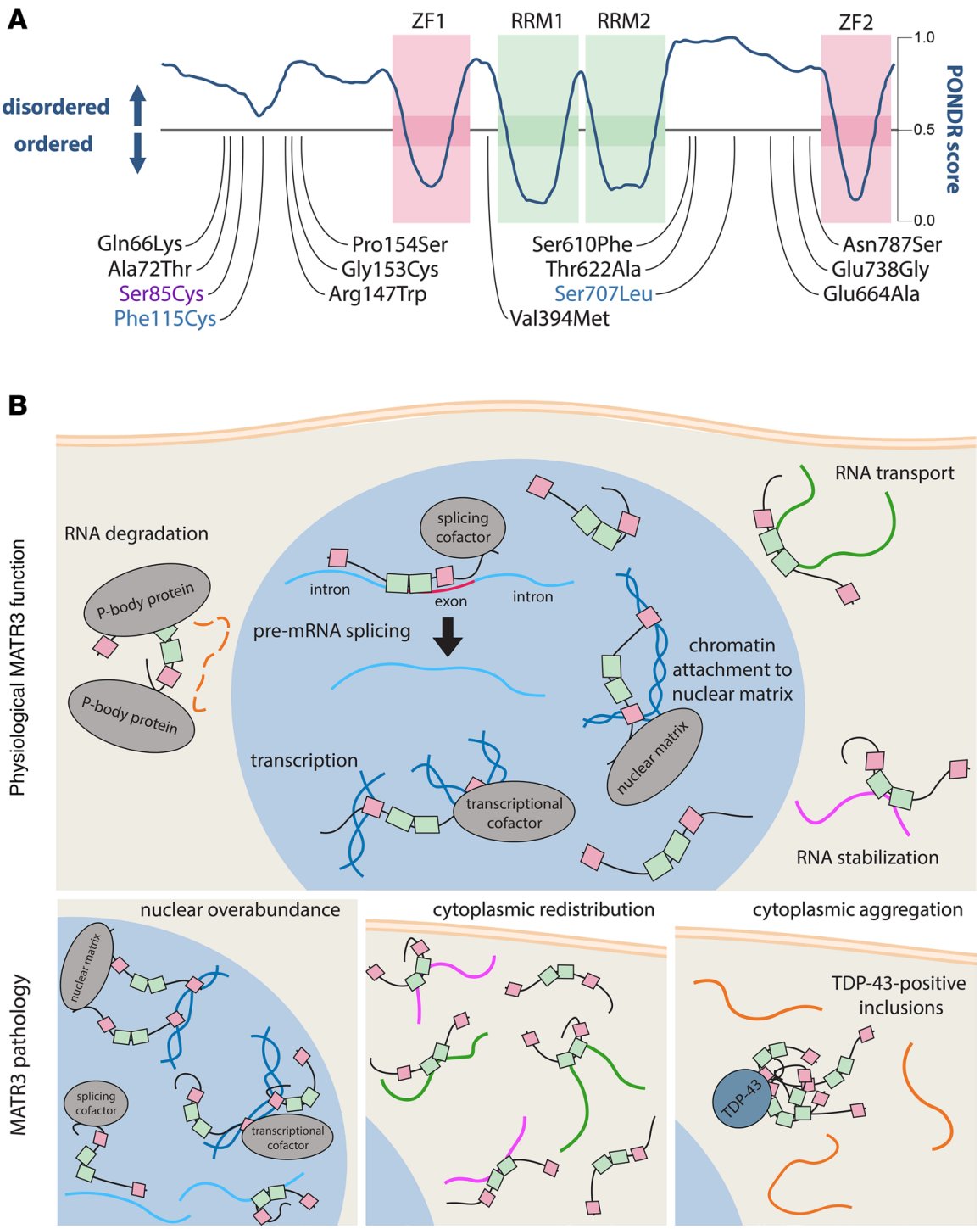

Figure 1.1. MATR3 domain structure and functions in normal and pathological contexts. (**A**) MATR3 has two zinc finger (ZF) and two RNA-recognition motif (RRM) domains, with the remainder of the protein consisting of an intrinsically disordered sequence as measured by a high Predictor of Natural Disordered Regions (PONDR) score[124]. Pathogenic mutations are located across the disordered stretches of MATR3;

although the majority of mutations reported to date are linked to ALS, a subset is implicated in ALS/distal myopathy (violet) or ALS/dementia (blue). (**B**) Although predominantly localized in the nucleus, MATR3 is tied to several nucleic acid–related processes in both nuclear and cytoplasmic compartments. Three distinct but not mutually exclusive patterns of MATR3 pathology are observed in neuromuscular disease: nuclear enrichment, cytoplasmic redistribution, and cytoplasmic aggregation. Nuclear overabundance is predicted to drive chromatin, transcriptional, and splicing aberrations. In addition, MATR3 redistribution and aggregation in the cytoplasm — representing cytosolic gain and loss of function, respectively — may disrupt RNA stability and transport.

Chapter 2: MATR3-Dependent Neurotoxicity is Modified by Nucleic Acid Binding and Nucleocytoplasmic Localization[2]

2.1 Abstract

Abnormalities in nucleic acid processing are associated with the development of amyotrophic lateral sclerosis (ALS) and frontotemporal dementia (FTD). Mutations in *Matrin 3* (*MATR3*), a poorly understood DNA- and RNA-binding protein, cause familial ALS/FTD, and MATR3 pathology is a feature of sporadic disease, suggesting that MATR3 dysfunction is integrally linked to ALS pathogenesis. Using a rat primary neuron model to assess MATR3-mediated toxicity, we noted that neurons were bidirectionally vulnerable to MATR3 levels, with pathogenic MATR3 mutants displaying enhanced toxicity. MATR3's zinc finger domains partially modulated toxicity, but elimination of its RNA recognition motifs had no effect on survival, instead facilitating its self-assembly into liquid-like droplets. In contrast to other RNA-binding proteins associated with ALS, cytoplasmic MATR3 redistribution mitigated neurodegeneration, suggesting that nuclear MATR3 mediates toxicity. Our findings offer a foundation for understanding MATR3-related neurodegeneration and how nucleic acid binding functions, localization, and pathogenic mutations drive sporadic and familial disease.

[2] This chapter is adapted from the following publication: Malik A.M., Miguez R.A., Li X., Ho Y.S., Feldman E.L., and Barmada S.J. Matrin 3-dependent neurotoxicity is modified by nucleic acid binding and nucleocytoplasmic localization. 2018. *Elife* 7:e35977. doi: 10.7554/eLife.35977

2.2 Introduction

Amyotrophic lateral sclerosis (ALS) is a progressive neurodegenerative disorder resulting in the death of upper and lower motor neurons. Mounting evidence indicates that RNA-binding proteins (RBPs) are integrally involved in the pathogenesis of ALS[1]. The majority (>95%) of ALS patients display cytoplasmic mislocalization and deposition of the RBP TDP-43 (TAR DNA/RNA-binding protein of 43 kDa) in affected tissue[2]. Moreover, over 40 different ALS-associated mutations have been identified in the gene encoding TDP-43, and mutations in several different RBPs have been similarly linked to familial ALS[3-8]. These mutations often cluster in intrinsically disordered domains that facilitate reversible liquid-liquid phase separation (LLPS), thereby creating ribonucleoprotein granules important for RNA processing, shuttling of mRNAs to sites of local translation, or sequestration of transcripts during stress. Pathogenic mutations in the genes encoding TDP-43 and related RBPs, including FUS and TIA1, shift the equilibrium towards irreversible phase separation and the formation of cytoplasmic aggregates analogous to those observed in post-mortem tissues from patients with ALS[9-12]. The downstream implications of abnormal LLPS on RNA misprocessing, RBP pathology, and neurodegeneration in ALS are unknown, however.

Matrin 3 (MATR3) is a DNA- and RNA-binding protein with wide-ranging functions in nucleic acid metabolism including gene transcription, the DNA damage response, splicing, RNA degradation, and the sequestration of hyperedited RNAs[13-19]. The S85C mutation in *MATR3* leads to autosomal dominant distal myopathy with vocal cord and pharyngeal weakness[20,21]. A more recent report reclassified a subset of

patients with this diagnosis as having ALS and noted several additional *MATR3* mutations in individuals with ALS and frontotemporal dementia (FTD), placing *MATR3* in a family of genes implicated in familial ALS, FTD, and myopathy. This family also includes *TIA1*, *VCP*, *p62/SQSTM1*, *hnRNPA1*, and *hnRNPA2/B1*, mutations in which lead to multisystem proteinopathy characterized by variable involvement of muscle and bone in addition to the central nervous system[8,12,22-27]. More than a dozen pathogenic *MATR3* mutations have now been identified, most of which result in amino acid substitutions within disordered stretches of the MATR3 protein (Fig. 2.1A). Additionally, post-mortem analyses demonstrated MATR3 pathology—consisting of cytoplasmic MATR3 accumulation as well as strong nuclear immunostaining—in patients with sporadic ALS and familial disease due to *C9orf72* hexanucleotide expansions and *FUS* mutations[28,29]. Together, these observations suggest that MATR3 may be a common mediator of disease even in those without *MATR3* mutations.

Even so, little is known about MATR3's functions in health or in disease, and the mechanisms underlying MATR3-dependent neurotoxicity remain unclear. Here, we establish an *in vitro* model of MATR3-mediated neurodegeneration and take advantage of this model to investigate the intrinsic properties and domains of MATR3 required for toxicity. Furthermore, we examine how disease-associated MATR3 mutations affect these properties to enhance neurodegeneration.

2.3 Results

2.3.1 MATR3 levels modulate neuronal survival in an *in vitro* model of neurodegeneration.

We first asked how MATR3 expression is related to neurodegeneration using longitudinal fluorescence microscopy (LFM), a sensitive high-content imaging system that we assembled for assessing neuronal function and survival at the single-cell level. As *MATR3* mutations cause a spectrum of disease that includes ALS and FTD, we modeled neurotoxicity in primary mixed cortical cultures, a system that recapitulates key features of ALS/FTD pathogenesis[30-32]. Primary neurons were transfected with diffusely localized mApple to enable visualization of neuronal cell bodies and processes by fluorescence microscopy. In addition, cells were co-transfected with constructs encoding enhanced green fluorescent protein (EGFP) or MATR3 fused with EGFP. Cultures were imaged by fluorescence microscopy at 24 h intervals for 10 days, and custom scripts used to generate uniquely labeled regions of interest (ROIs) corresponding to each cell (Fig. 2.1B). Rounding of the soma, retraction of neurites or loss of fluorescence indicated cell death; these criteria proved to be sensitive markers of neurodegeneration in previous studies[33]. We used the time of death for individual cells to calculate an overall risk of death, expressed as a hazard ratio (HR), corresponding to the likelihood of cell death in each population relative to a control or reference group[34]. In doing so, we observed that MATR3-EGFP overexpression significantly increases the risk of death compared to EGFP alone, with a HR of 1.48 (Fig. 2.1C).

Next, we investigated the dose-dependency of this MATR3 toxicity. Transient transfection delivers a different amount of vector to each cell, resulting in substantial variability in protein expression for individual cells. Such variability can be difficult to appreciate using population-based approaches such as Western blotting but are readily visualized by single-cell techniques including immunofluorescence[32,35,36]. Therefore, to

estimate the degree of MATR3 overexpression in individual neurons, we measured MATR3 antibody reactivity by quantitative immunofluorescence in neurons transfected with EGFP or MATR3-EGFP (Fig. 2.1D). There was no significant difference in MATR3 antibody reactivity between EGFP transfected and untransfected cells (Fig. 2.1E). In comparison, MATR3-EGFP transfected cells showed a 2.8-fold increase in MATR3 antibody reactivity compared to untransfected cells. Further, and in agreement with previous work relating single-cell fluorescence intensity to immunoreactivity[35], we detected a linear relationship between EGFP fluorescence intensity and anti-MATR3 antibody reactivity in individual neurons expressing MATR-EGFP (Fig. 2.1F). These data confirm that GFP intensity provides a reliable, single-cell estimate of EGFP or MATR3-EGFP expression.

We took advantage of this relationship to analyze the association between EGFP or MATR3-EGFP expression (measured 24 h after transfection) and neuronal survival using penalized splines[32,36]. These models enable us to predict the impact of single-cell protein expression on the risk of death within separate populations of cells expressing either EGFP (Fig. 2.1G) or MATR3-EGFP (Fig. 2.1H). Consistent with the results of prior studies, we detected a reduced risk of death in association with higher EGFP expression levels[36], implying that unhealthy or dying neurons are unable to express high amounts of EGFP. Conversely, we noted a significant increase in the risk of death for cells expressing high levels of MATR3-EGFP (Fig. 2.1H); this relationship is similar to that observed for other proteins associated with neurodegenerative disorders, including TDP-43 (ALS/FTD)[32] and mutant huntingtin (Huntington's disease)[36]. Taken together, these data support a dose-dependent toxicity of MATR3-EGFP in primary neurons.

Several *MATR3* mutations are responsible for familial ALS, FTD, and hereditary distal myopathy[21,27,37-43]. To determine if disease-associated *MATR3* mutations accentuate neurodegeneration, we created MATR3-EGFP fusion proteins harboring one of four mutations originally implicated in familial disease: S85C, F115C, P154S, and T622A (Fig. 1A). Primary rodent cortical neurons expressing these mutant MATR3-EGFP constructs exhibited the same granular nuclear distribution as MATR3(WT)-EGFP, without obvious aggregation or cytoplasmic mislocalization, in accordance with prior reports (Fig. 2.2A)[44,45]. Even so, all four displayed a modest but significant increase in toxicity over MATR3(WT)-EGFP when overexpressed in primary neurons (Fig. 2.2B), consistent with either gain-of-function or dominant negative loss-of-function mechanisms contributing to mutant MATR3-associated neurodegeneration.

To determine if loss of endogenous MATR3 function is sufficient for neurodegeneration, we transfected primary neurons with mApple and siRNA targeting the amino (N)-terminal coding region of rodent *Matr3* or a scrambled siRNA control. Three days after transfection, Matr3 immunoreactivity was used to quantify efficacy of knockdown in transfected cells (Fig. 2.2C). Compared to scrambled siRNA-transfected cells, we noted consistent depletion of the endogenous rat Matr3 by approximately 65% in those transfected with siRNA targeting *Matr3* (Fig. 2.2D). Having confirmed knockdown, we imaged a separate set of transfected cells for 10 days to assess the effect of *Matr3* knockdown on neuronal survival. In doing so, we observed a 20% increase in the risk of death upon *Matr3* depletion in comparison to scrambled siRNA (Fig. 2.2E). These data suggest that neurons are vulnerable to both increases and decreases in MATR3 levels and function; further, pathogenic *MATR3* mutations may

elicit neurodegeneration via gain- or loss-of-function mechanisms, or through elements of both.

2.3.2 MATR3's zinc finger domains modulate overexpression toxicity, but its RNA recognition motifs mediate self-association.

To identify the functional domains involved in MATR3-mediated neurodegeneration, we systematically deleted each of the annotated MATR3 domains and evaluated subsequent toxicity upon overexpression in primary neurons (Fig. 2.3A). MATR3 has two zinc-finger (ZF) domains of the C2H2 variety, which bind DNA but may also recognize RNA and/or mediate protein-protein interactions[46,47]. Deletions of ZF1, ZF2, or both had no observable effect on MATR3-EGFP localization (Fig. 2.3B), and ZF1 deletion by itself did not significantly alter toxicity compared to full-length MATR3-EGFP. In contrast, ZF2 deletion, either in isolation or combined with ZF1 deletion, partially rescued MATR3-EGFP overexpression toxicity (Fig. 2.3C).

We next created deletion variants of MATR3's RNA recognition motifs (RRMs) to test their contribution to MATR3-mediated neurodegeneration. As with the MATR3 ZF domains, RRMs are capable of recognizing both RNA and DNA[48]. While deletion of RRM1 failed to affect MATR3-EGFP localization, we noted a striking redistribution of MATR3(ΔRRM2)-EGFP into intranuclear granules in a subset of transfected neurons (Fig. 2.3D). Deletion of RRM1 in combination with RRM2 produced the same phenotype, suggesting that RRM2 normally prevents such redistribution. These nuclear granules formed by MATR3(ΔRRM2)-EGFP and MATR3(ΔRRM1/2)-EGFP were uniformly spherical in shape, and their presence was accompanied by a reduction in the

intensity of diffusely distributed MATR3 within the nucleus, suggesting that they represent hyperconcentrated MATR3 puncta. Evidence from previous studies indicates that RNA recognition by MATR3 may be largely—but not solely—driven by RRM2. Consistent with this, our finding that RRM2 deletion induces the formation of nuclear condensates suggests that RNA binding normally keeps MATR3 diffuse by preventing an intrinsic tendency for self-association. We detected no colocalization of MATR3(ΔRRM2)-EGFP or MATR3(ΔRRM1/2)-EGFP with markers of nucleoli, nuclear speckles, or PML bodies (Supplemental Fig. 2.1), indicating that MATR3 lacking its RRM2 does not join these organelles. Despite the dramatic shift in MATR3-EGFP distribution with RRM2 deletion, there was no associated change in the toxicity of MATR3-EGFP lacking RRM1, RRM2, or both in comparison to MATR3(WT)-EGFP (Fig. 2.3E). This finding stands in contrast to what has been observed for other ALS/FTD-associated RBPs, for which the ability to bind RNAs is a key mediator of overexpression toxicity[49-51].

2.3.3 The toxicity of RNA binding deficient MATR3 variants is highly dependent on their subcellular distribution

One of the hallmarks of neurodegenerative diseases, including ALS and FTD, is the formation of protein-rich aggregates[2,52]. Prior investigations suggest that these aggregates may be toxic, innocuous, or representative of a coping response that ultimately prolongs neuronal survival[30,35]. To determine if the formation of nuclear puncta by MATR3(ΔRRM2)-EGFP and MATR3(ΔRRM1/2)-EGFP affected neuronal lifespan, we turned to LFM. We employed a modified version of the automated analysis

script to draw ROIs around the nuclear perimeter within each transfected cell (Fig. 2.4A) and then calculated a coefficient of variation (CV) for the MATR3(ΔRRM1/2)-EGFP signal within each nuclear ROI. The CV, or the ratio of the standard deviation of GFP intensity to the mean GFP intensity for the ROI, is directly proportional to the spatial variability of fluorescence intensity within each ROI. Therefore, we reasoned that this measure might be useful for rapidly and reliably identifying puncta in an unbiased and high-throughput manner. We first validated the use of CV for detecting puncta by creating a receiver-operator characteristic (ROC) curve; in doing so, we observed that a CV threshold of 0.92 was 87.2% sensitive and 93.9% specific in discriminating cells with nuclear granules from those with diffuse protein (Fig. 2.4B). We therefore utilized this CV threshold to assess the frequency of nuclear granule formation in primary rodent cortical neurons, noting that 24 h after transfection, 76.1% (2081/2734) of neurons transfected with MATR3(ΔRRM2)-EGFP displayed nuclear granules compared to 91.2% (1590/1743) of MATR3(ΔRRM1/2)-EGFP cells (Fig. 2.4C). We also observed the time-dependent formation of nuclear granules as neurons expressed increasing amounts of MATR3-EGFP (Fig. 2.4D), suggesting that granule formation may be proportional to expression level. To investigate this relationship further, we identified neurons exhibiting a diffuse distribution of MATR3(ΔRRM2)-EGFP at day 1 and followed these cells for an additional 3 days by automated microscopy. We then measured the GFP intensity for each cell at day 1 and related this value to the risk of granule formation over the ensuing 72 h period using penalized splines models. Notably, we failed to observe a significant relationship between GFP intensity on day 1 and granule formation by day 3 (Fig. 2.3E). We also assessed the relative change in expression level on a per-cell

basis, as quantified by the ratio of GFP intensity at day 2 to the GFP intensity at day 1, to determine if the net rate of MATR3(ΔRRM2)-EGFP production better predicted granule formation. The probability of granule formation was directly proportional to the time-dependent change in MATR3(ΔRRM2)-EGFP levels (Fig. 2.4F), suggesting that granule formation is favored by the rapid accumulation of MATR3(ΔRRM2)-EGFP.

Our previous studies demonstrated that deletion of RRM1, RRM2, or both had no effect upon the toxicity of MATR3-EGFP when expressed in primary neurons (Fig. 2.3E). These analyses included all neurons within a given condition, consisting of cells with diffuse nuclear MATR3 as well as those with MATR3 redistributed into granules. To determine if the presence of nuclear MATR3-EGFP granules impacted the survival of neurons, we utilized the nuclear CV threshold (Fig. 2.4B) to divide neurons expressing MATR3(ΔRRM2)-EGFP and MATR3(ΔRRM1/2)-EGFP into three categories: cells with diffuse protein at day 1, those with granules at day 1, or all cells. We then tracked neurons in each category for the following 9 days by LFM and compared their survival by Cox proportional hazards analysis. By these measures, neurons displaying nuclear MATR3(ΔRRM2)-EGFP granules fared significantly better than the population as a whole, while those exhibiting a diffuse distribution demonstrated an increased risk of death (Fig. 2.4G). Similar results were obtained for neurons expressing MATR3(ΔRRM1/2)-EGFP; here, the relative protection associated with nuclear MATR3(ΔRRM1/2)-EGFP granules was modest, but the toxicity of diffusely distributed MATR3(ΔRRM1/2)-EGFP was more pronounced (Fig. 2.4H). The marked toxicity of diffuse MATR3(ΔRRM1/2)-EGFP may explain why so few cells with diffuse protein are seen at day 1 (Fig. 2.4D). Taken together, these results suggest that diffuse MATR3 is

highly neurotoxic when it cannot bind RNA. Furthermore, the sequestration of RNA binding-deficit MATR3 variants into nuclear granules is associated with a survival advantage.

2.3.4 MATR3 granules formed by deletion of the RNA-binding domains display liquid-like properties that are affected by a pathogenic mutation

As part of their normal function, many RBPs reversibly undergo LLPS, involving the formation of droplets with liquid-like properties from diffuse or soluble proteins[53,54]. Disease-associated mutations in the genes encoding these proteins may promote LLPS or impair the reversibility of phase separation[8,10,53,55]. We wondered whether the intranuclear granules formed by MATR3(ΔRRM2)-EGFP and MATR3(ΔRRM1/2)-EGFP represent liquid droplets and also whether pathogenic MATR3 mutations affect the intrinsic properties of these puncta. Indeed, nuclear granules exhibited dynamic properties, not only growing in size over time but also moving freely within the nucleus and fusing if they encountered other granules (Fig. 2.5A), indicative of liquid-like behavior.

We then asked if these structures displayed internal rearrangement characteristic of liquid droplets and whether pathogenic *MATR3* mutations affect their dynamics[56,57]. To answer this, we introduced disease-associated mutations into MATR3(ΔRRM1/2)-EGFP and transfected rodent primary cortical neurons with each construct (Fig. 2.5B). Nuclear puncta were photobleached 2-4 days after transfection, and the recovery of fluorescence intensity tracked within the bleached and unbleached ROIs by laser scanning confocal microscopy. Granules formed by WT MATR3(ΔRRM1/2)-EGFP

displayed internal rearrangement over the course of minutes consistent with liquid-like properties, as did all tested disease mutants on the ΔRRM1/2 background (Fig. 2.5C-D). The S85C mutation, however, severely slowed fluorescence recovery, suggesting reduced exchange of molecules within each droplet. Using the Stokes-Einstein equation, we calculated viscosity estimates for each MATR3(ΔRRM1/2)-EGFP variant based on return time and bleached area size (Fig. 2.5E). Consistent with the observed effect of this mutation on fluorescence recovery, the S85C mutation led to a pronounced increase in viscosity over that of WT and other disease-associated mutants.

We wondered whether this phenotype was specific to nuclear droplets formed by MATR3(ΔRRM1/2)-EGFP, or if full-length MATR3 carrying pathogenic mutations would also display reduced mobility. For this, we transfected primary neurons with full-length versions of MATR3(WT)-EGFP or disease-associated MATR3-EGFP variants and then bleached a circular area in the center of the nucleus (Fig. 2.5F). In each case, we noted rapid return of fluorescence, and the recovery rate was unaffected by pathogenic *MATR3* point mutations (Fig. 2.5G). To account for the rapidity of return as well as the area of the bleached region, we calculated a diffusion coefficient (DC) for each construct. Comparison of the DCs for WT and mutant MATR3-EGFP variants showed no significant differences (Fig. 2.5H). Our data therefore suggest that the S85C point mutation selectively affects the droplet properties of MATR3. To test whether this feature is shared among disease-associated mutations affecting the MATR3 N-terminus, we generated two additional pathogenic mutants, Q66K and A72T, on the ΔRRM1/2 background (Supplemental Fig. 2.2). Unlike the S85C variant, these mutations had no effect on granule viscosity, indicating that the S85C mutant is unique

among N-terminal low-complexity domain mutations in its ability to affect the mobility of phase-separated MATR3.

2.3.5 Mapping the sequence determinants of MATR3 localization in neurons

Cytoplasmic inclusions composed of the RBP TDP-43 are characteristic of ALS and the majority of FTD[2,52]. Moreover, pathogenic mutations in the gene encoding TDP-43 enhance cytoplasmic mislocalization concordant with enhanced neurotoxicity, and reductions in cytoplasmic TDP-43 prolong neuronal survival[30,31]. To determine if MATR3 localization is likewise an important determinant of neurodegeneration, we sought to disrupt the MATR3 nuclear localization signal (NLS). However, since multiple sequences have been associated with nuclear MATR3 localization[58,59], we systematically identified regions enriched in positively-charged amino acids (arginine, lysine) that may mediate nuclear import via importin-α. We then deleted each of the 7 regions defined in this manner, including two that had been identified as controlling nuclear localization in previous studies, and assessed their localization by transfection in rodent primary cortical neurons followed by fluorescence microscopy (Fig. 2.6A).

Deletions of putative NLS (pNLS) 1, 2, 3, 5, 6, and 7 had little to no effect on neuronal MATR3 distribution (Fig. 2.6B). While the ΔpNLS3 mutation did not change nuclear MATR3 localization *per se*, it did induce the formation of many small, nuclear granules. This effect is consistent with the position of pNLS3 within RRM2 and the observed formation of nuclear puncta upon RRM2 deletion (Fig. 2.3). In contrast, and in accord with previous studies[59], deletion of the bipartite pNLS4 elicited a marked reduction in nuclear MATR3-EGFP accompanied by enhanced cytoplasmic localization

and the formation of small MATR3-EGFP granules within the cytoplasm. In DT40 and HeLa cells, both arms of this NLS were critical for MATR3 nuclear localization. To determine if this is the case in neurons, we sequentially deleted the N- and C-terminal arms (ΔpNLS4N and ΔpNLS4C, respectively) and tested their localization by transfection into primary cortical neurons. These studies demonstrated that only the N-terminal arm is necessary for nuclear localization, as MATR3(ΔpNLS4N)-EGFP exhibits nuclear clearing and punctate distribution in the cytoplasm and neuronal processes, while MATR3(ΔpNLS4C)-EGFP has the same distribution as MATR3(WT)-EGFP (Fig. 2.6C-D). To test whether pNLS4N was sufficient for nuclear localization, we generated a construct in which the eight amino acids corresponding to pNLS4N were appended to EGFP and compared the subcellular distribution of this construct in primary neurons to EGFP alone or EGFP fused to the canonical NLS from the SV40 large T antigen (Supplemental Fig. 2.3)[60]. These studies demonstrated comparable nuclear localization of pNLS4N-EGFP and SV40-NLS-EGFP, indicating that the MATR3 pNLS4N sequence is both necessary and sufficient for nuclear protein localization in primary neurons.

Having identified the N-terminal arm of the bipartite pNLS4 as the key sequence regulating MATR3 localization in neurons, we asked whether driving MATR3 into the cytoplasm by deletion of this sequence could modify toxicity. Rodent primary cortical neurons were transfected with mApple and either EGFP, MATR3(WT)-EGFP, or MATR3(ΔpNLS4N)-EGFP and imaged at regular intervals by LFM. Automated survival analysis of neuronal populations expressing these constructs demonstrated that the ΔpNLS4N mutation and resulting cytoplasmic localization significantly reduced MATR3-dependent toxicity compared to the MATR3(WT)-EGFP (Fig. 2.6E). Therefore, unlike

TDP-43 and FUS, two RBPs whose cytoplasmic mislocalization is tightly tied to neurodegeneration in ALS/FTD models, cytoplasmic MATR3 retention mitigates toxicity, suggesting that nuclear MATR3 functions are required for neurodegeneration[30,61].

Given the observed relationship between MATR3 localization and toxicity, we wondered if subtle changes in nucleocytoplasmic MATR3 distribution could be responsible for the increased toxicity of MATR3 bearing disease-associated mutations. Rodent primary cortical neurons transfected with each of the pathogenic MATR3-EGFP variants showed no obvious difference in subcellular localization in comparison with MATR3(WT)-EGFP (Fig. 2.2A). To investigate MATR3-EGFP localization in a quantitative manner, we developed a customized image-based analysis script to draw ROIs around the nucleus and soma of each neuron, measure MATR3-EGFP content separately within each compartment, and calculate a nucleocytoplasmic ratio for MATR3-EGFP in individual cells (Fig. 2.6F). This analysis confirmed our initial observations, showing no significant differences in the localization of mutant MATR3-EGFP variants compared to MATR3(WT)-EGFP.

In a complementary series of experiments, we utilized biochemical fractionation to assess the distribution of MATR3-EGFP in a human cell line. MATR3(WT)-EGFP or versions of MATR3-EGFP bearing the S85C, F115C, P154S, and T622A disease-associated mutations were transfected into HEK293T cells, and the nuclear and cytoplasmic fractions subjected to SDS-PAGE and Western blotting. In agreement with single-cell data from transfected primary neurons, we noted no difference in the nucleocytoplasmic distribution of any of the MATR3-EGFP variants tested here (Fig. 2.6G). Nevertheless, we consistently observed far less of the S85C variant in both

nuclear and cytoplasmic fractions, compared to MATR3(WT)-EGFP and other disease-associated mutants. These data suggest that the S85C mutation may destabilize MATR3-EGFP; alternatively, this mutation may prevent adequate solubilization and detection of MATR3-EGFP via SDS-PAGE and Western blotting.

2.3.6 A subset of pathogenic MATR3 mutations affect protein solubility and stability

To discriminate among these possibilities, we first investigated the turnover of WT and mutant MATR3 variants using optical pulse labeling (OPL), a technique enabling non-invasive determinations of protein clearance in living cells[31]. For these experiments, MATR3 was fused to Dendra2—a photoconvertable protein that irreversibly switches from a green to red fluorescent state upon illumination with low-wavelength light[62]—and expressed in primary cortical neurons. One day after transfection, neurons were illuminated with blue light to photoconvert Dendra2, and the time-dependent loss of red fluorescence signal used to calculate protein half-life (Fig. 2.7A) [31]. Previous studies validated the accuracy and utility of OPL for determinations of protein half-life; importantly, and in contrast to biochemical techniques for calculating half-life that depend on radioactive labeling or translational inhibitors, OPL allows us to measure protein clearance on a single-cell level for thousands of neurons simultaneously (Fig. 2.7B). Most disease-associated mutations had no effect upon the turnover of MATR3-Dendra2 in primary cortical neurons. However, we noted subtle destabilization of MATR3(S85C)-Dendra2 in comparison to other pathogenic mutant variants and MATR3(WT)-Dendra2 (Fig. 2.7C-D). Even so, the magnitude of the effect

was relatively small, making it unlikely that differences in protein turnover fully explain the reduced abundance of MATR3(S85C)-EGFP noted in cell lysates (Fig. 2.6G).

We next asked if the S85C mutation altered MATR3 solubility. HEK293T cells transfected with WT and mutant MATR3-EGFP variants were lysed using a harsher protocol that involved sonication in RIPA buffer; additionally, we used urea buffer to extract all RIPA-insoluble proteins. In stark contrast to mild conditions (Fig. 2.6G), harsher lysis resulted in equivalent levels of all MATR3 variants on Western blot, suggesting that the S85C mutation reduced MATR3 solubility (Fig. 2.7E). In accordance with this interpretation, the urea-soluble fraction was markedly enriched for MATR3(S85C)-EGFP and modestly enriched for MATR3(T622A)-EGFP. These data show that the S85C and T622A mutations reduce the solubility of MATR3, without drastically affecting its stability. As shown in Fig. 2.1A, both mutations lie within areas of predicted disorder, consistent with their effects on MATR3 aggregation and solubility.

2.4 Discussion

In this study, we modeled MATR3-mediated neurodegeneration by overexpressing WT or disease-associated MATR3 variants in primary neurons. In doing so, we found that neurons were highly susceptible to increases or decreases in MATR3 levels, and disease-associated MATR3 variants exhibited enhanced toxicity in comparison to MATR3(WT). Structure-function studies demonstrated that the ZF2 domain modulates overexpression-related toxicity, while RRM2 prevents MATR3 phase separation into mobile nuclear puncta. Biophysical analysis of these puncta confirmed their liquid-like nature and further indicated that the pathogenic S85C mutation

substantially increased the viscosity of these structures. We also determined that the N-terminal arm of a bipartite NLS drives MATR3 nuclear localization in neurons; forcing MATR3 into the cytoplasm by deleting this sequence blocked toxicity from MATR3 overexpression. While we did not observe any differences in the distribution of pathogenic MATR3 variants, we noted that the S85C mutation significantly reduced MATR3 solubility and, to a lesser extent, stability. The T622A mutant displayed similar but more muted effects on MATR3 solubility, suggesting that disease-associated mutations located in distinct MATR3 domains may operate through convergent pathogenic mechanisms.

Both MATR3 overexpression and knockdown elicited significant and comparable toxicity in neurons. These data suggest that neurons are bidirectionally vulnerable to changes in MATR3 levels. Post-mortem studies of MATR3 distribution in sporadic and familial ALS patients demonstrated stronger MATR3 nuclear staining as well as the presence of cytoplasmic MATR3 aggregates in motor neurons[28,29]. While the impact of these findings is unknown, MATR3 mislocalization or sequestration into aggregates may reflect a reduction in normal function, a new and abnormal function, or both. In mice, homozygous *Matr3* knockout is perinatally lethal, supporting our findings that MATR3 reduction is toxic[63]. Overexpression of MATR3(WT), MATR3(Ser85Cys), or MATR3(Phe115Cys) in mice results in severe muscle disease consisting of fore- and hindlimb muscle atrophy accompanied by vacuolization[64,65]. While overexpression of WT protein is toxic in these mouse models, pathogenic mutants show stronger phenotypes, in close accordance with our findings in cortical neurons (Fig. 2.2A).

MATR3 is unique among ALS/FTD-associated RBPs in possessing not just two tandem RRMs but also two ZF domains that can bind repetitive DNA elements found in the nuclear scaffold[66]. MATR3 binds thousands of RNAs via a pyrimidine-rich consensus sequence (AUCUU)[17,19,67]; these binding events are concentrated within introns and most often associated with exon repression. We found that genetic ablation of either or both of MATR3's RRMs had no overall effect on overexpression-mediated toxicity. Conversely, ZF2 deletion mitigated MATR3 overexpression-mediated toxicity, suggesting that aberrant DNA binding by overexpressed MATR3 may be partially responsible for neurodegeneration in these systems. MATR3's genomic targets remain uncharacterized, however, and further studies are required to identify relevant MATR3 DNA substrates that participate in MATR3 overexpression-related toxicity.

Our data support a model in which RNA binding prevents MATR3 self-association into droplets. Consistent with this interpretation, deletion of RRM2—either alone or in combination with RRM1—resulted in the formation of phase-separated intranuclear droplets. We also observed small, mobile MATR3 granules in the cytoplasm and neuronal processes when the bipartite NLS was disrupted (Fig. 2.6D). Cytoplasmic RNA concentrations are more than an order of magnitude lower than those in the nucleus, a gradient that may favor the coalescence of MATR3(ΔpNLS4N)-EGFP into puncta within the neuronal soma and processes[68]. Similarly, phase transitions of two other RBPs implicated in ALS and FTD—TDP-43 and FUS—are blocked by high RNA concentrations in the nucleus and facilitated by low RNA concentrations in the cytoplasm, indicating that this phenomenon is not exclusive to MATR3[69].

In C2C12 myoblast cells, MATR3 formed intranuclear spherical structures with liquid-like properties upon deletion of RRM2, though these granules were smaller and more numerous than those we detected in primary neurons, a difference that may be due to expression level and cell type[70]. RRM2 deletion in C2C12 cells led to a large increase in protein binding partners, many with low-complexity domains. In the absence of effective RNA binding, therefore, MATR3 may be free to interact with other proteins and itself through its low-complexity domains, driving LLPS.

The functional importance of the individual RRM domains for MATR3's RNA binding activity is unclear; while some studies suggest that both RRM1 and RRM2 bind RNA, other investigations indicated that RRM2 is primarily responsible for RNA binding[58,71]. Our data show that deletion of RRM2 is sufficient to elicit MATR3 phase separation, suggesting that RNA recognition by MATR3 is mediated largely by RRM2. We also noted no significant difference in the survival of neuronal populations overexpressing ΔRRM1, ΔRRM2, and ΔRRM1/2 variants of MATR3-EGFP, implying that RNA binding *per se* is unrelated to MATR3-mediated neurodegeneration. This interpretation is strengthened by detailed analyses of neurons expressing MATR3(ΔRRM2) and MATR3(ΔRRM1/2). When neurons with and without droplets were assessed separately, we noted that neurons exhibiting diffuse MATR3(ΔRRM2) or MATR3(ΔRRM1/2) displayed a significantly higher risk of death than those with droplets. These results imply that diffuse MATR3, when not bound to RNA, can be highly toxic. Conversely, sequestration of RNA-binding deficient MATR3 into puncta is associated with extended neuronal survival. Our data further indicate that diffuse MATR3(ΔRRM1/2) is more toxic than diffuse MATR3(ΔRRM2) (compare the diffuse

population in Fig. 2.4G to the diffuse population in Fig. 2.4H). Since RRM1 may be capable of recognizing some RNA even without RRM2, these observations suggest that neurodegeneration is inversely proportional to the ability of MATR3 to bind RNA when diffusely localized within the nucleus. In disease models involving related RBPs, including TDP-43 and FUS, toxicity requires the presence of RNA binding motifs as well as low-complexity domains that enable LLPS[50,72,73]. As with MATR3, abrogation of RNA binding may disinhibit self-association, resulting in the sequestration of otherwise toxic diffuse protein within droplets.

Investigating the liquid-like properties of MATR3(ΔRRM1/2)-EGFP droplets, we noted a selective effect of the S85C mutation on droplet viscosity. Low-complexity, intrinsically disordered domains are required for phase separation and self-assembly of RBPs. Apart from its nucleic acid binding domains, MATR3 displays a high degree of predicted disorder based on its primary amino acid sequence (Fig. 2.1A). Among the pathogenic mutations studied here, only the S85C mutation significantly affected MATR3(ΔRRM2)-EGFP droplet viscosity; notably, S85C is also the only disease-associated mutation associated with a primary myopathy as well as neurodegeneration[20,21]. In myoblasts, MATR3(ΔRRM2) carrying the S85C mutation did not form spherical droplets but rather coalesced into irregular nuclear clusters, pointing to cell type-specific differences in MATR3 behavior that may be relevant for myopathic or neurodegenerative phenotypes[70]. Whether full-length MATR3 is capable of phase-separation under physiological circumstances, and what relevance this process has for disease, is currently unclear.

Conflicting evidence[58,59] suggests that MATR3 nuclear import is driven by distinct sequences in different cell types. For example, while amino acids 701-718 are essential for nuclear localization of rat MATR3 in Ac2F cells, deletion of the homologous sequence (amino acids 701-720) in human MATR3 has no effect on neuronal distribution (Fig. 2.6B). To identify the sequences responsible for MATR3 nuclear import within neurons, we undertook a systematic analysis of arginine/lysine-rich sequences in MATR3 resembling NLSs. In accord with an earlier report[59], we found that MATR3's bipartite pNLS controlled its nuclear enrichment in neurons, but only the N-terminal arm of this pNLS was necessary and sufficient for MATR3 nuclear localization in neurons. Pathogenic *TARDBP* and *FUS* mutations promote cytoplasmic mislocalization of TDP-43 and FUS, respectively, and cytoplasmic enrichment of these proteins is tightly linked to toxicity[30,74]. In stark contrast, however, we observed that cytoplasmic MATR3 redistribution extended neuronal survival, suggesting—along with the partial rescue we observed for MATR3(ΔZF2)-EGFP and MATR3(ΔZF1/2)-EGFP—that MATR3 overexpression elicits neurodegeneration through nuclear DNA binding activity, mediated at least in part by ZF2.

Given previously established relationships between the distribution and aggregation of RBPs and neurodegeneration in ALS models[8,9,30,61,74,75], we wondered whether the enhanced toxicity of pathogenic MATR3 variants arises from mutation-associated changes in MATR3 localization or solubility. We noted no significant differences in the subcellular distribution of mutant MATR3 variants in comparison to MATR3(WT) but instead consistently observed reduced levels of MATR3(S85C) in transfected cell lysates. A similar pattern was noted in previous investigations and

attributed to reduced MATR3(S85C) stability[27]. Using OPL, a sensitive method for measuring protein turnover *in situ*[31,76], we detected only a very modest shortening of MATR3(S85C) half-life compared to MATR3(WT). Nevertheless, we observed a marked change in the solubility of MATR3(S85C) and, less so, MATR3(T622A). This is in partial agreement with initial studies of MATR3(S85C) in patient tissues that noted equivalent amounts of MATR3(WT) and MATR3(S85C) in insoluble fractions but reduced MATR3(S85C) in nuclear fractions[21] and in close accord with the insolubility of MATR3(Ser85Cys) observed since the publication of our data in fly and mouse models[65,77,78]. Both the S85C and T622A mutations lie within domains predicted to be disordered (Fig. 2.1A). Furthermore, both mutations disrupt potential phosphorylation sites, and phosphorylation within the intrinsically disordered domain of FUS inhibits self-association of the protein through negative-negative charge repulsion between phosphate groups[79]. Of the 13 pathogenic mutations identified to date in MATR3, four (S85C, S610F, T622A, S707L) eliminate phosphorylatable residues, suggesting that inadequate phosphorylation and subsequent disinhibited self-association of MATR3 may be a conserved feature of MATR3 mutants.

MATR3's possesses broad functions in DNA/RNA processing[13-15,17-19,71]. Its presence within cytoplasmic aggregates in approximately half of patients with sporadic ALS[29] implies that MATR3 pathology causes or is caused by cellular alterations in RNA and protein homeostasis, many of which may contribute to neurodegeneration in ALS and related disorders. Our work confirms that MATR3 is essential for maintaining neuronal survival and furthermore shows that MATR3 accumulation results in neurodegeneration in a manner that depends on its subcellular localization and ZF

domains. Additional studies are needed to further delineate the impact of disease-associated MATR3 mutations on the function, behavior, and liquid-like properties of MATR3.

2.5 Materials and methods

Plasmids

Full-length human *MATR3* cDNA was obtained from Addgene (#32880) and cloned into the pCMV-Tag2B vector (Agilent Technologies, #211172) using BamHI and XhoI endonucleases, tagging the amino-terminus with a FLAG epitope. To generate MATR3-EGFP, the *EGFP* open reading frame with a 14 amino acid N-terminal linker was amplified from pGW1-EGFP by PCR using forward primer 5'-AGC TAC TAG TAC TAG AGC TGT TTG GGA C-3' and reverse primer 5'-TAT TGG GCC CCT ATT ACT TGT ACA GCT CGT CCA T-3'. The resulting amplicon was digested with SpeI and ApaI and cloned into the corresponding sites in pKS to generate pKS-EGFP. To create pKS-MATR3-EGFP, the *FLAG-MATR3* open reading frame from pCMV-Tag2B was amplified by PCR with forward primer 5'-GAT CTC TAG AGC GGC CGC CAC CAT GGA T-3' and reverse primer 5'-AGC TAC TAG TCA TAG TTT CCT TCT TCT GTC T-3', digested with XbaI and SpeI, and inserted into the corresponding sites in pKS-EGFP. pGW1-MATR3-EGFP was generated by digesting pKS-MATR3-EGFP with XbaI and ApaI, purifying the ensuing fragment containing MATR3-EGFP, and inserting into the corresponding sites of pGW1. To create Dendra2-tagged MATR3 variants, the *EGFP* coding region of each construct was removed by PCR amplification of the pGW1-MATR3-EGFP vector using primers that flank the *EGFP* open reading frame. The *Dendra2* open reading frame was

then removed from pGW1-Dendra2[31] by digestion with ApaI and MfeI and inserted into pGW1-MATR3. All constructs were confirmed by sequencing prior to transfection in neurons and HEK293T cells.

Domain deletion mutants were created using Q5 Hot Start High-Fidelity DNA Polymerase (New England Biolabs) and primers flanking the regions to be deleted for nucleic acid-binding domain (Table 1) and putative nuclear localization signal (Table 2) deletions. All disease-associated point mutations were created with site-directed mutagenesis (Table 3).

To generate NLS-EGFP fusion protein variants, the pNLS4N sequence (5'-AAA AAA GAT AAA TCC CGA AAA AGA-3') and SV40 large T antigen NLS sequence (5'-CCA AAA AAG AAG AGA AAG GTA-3') were synthesized as oligonucleotides flanked with ends complementary to ApaI/AgeI sites and BsrGI/EcoRI sites, respectively. These were heated to 95 °C for 5 min, annealed overnight at room temperature (RT), and phosphorylated with T4 Polynucleotide Kinase (New England Biolabs). pGW1-EGFP and FUGW-EGFP vectors were digested with ApaI/AgeI and BsrGI/EcoRI, respectively, after which the corresponding annealed NLS-containing oligonucleotides were ligated.

Primary neuron cell culture and transfection

Cortices from embryonic day (E)19-20 Long-Evans rat embryos were dissected and disassociated, and primary neurons plated at a density of 6 x 10^5 cells/mL in 96-well plates, as described previously[80]. At *in vitro* day (DIV) 4-5, neurons were transfected with 100 ng of pGW1-mApple[31] to mark cells bodies and 100 ng of an experimental construct (i.e. pGW1-MATR3-EGFP) using Lipofectamine 2000, as

before[30]. Following transfection, cells were placed into either Neurobasal with B27 supplement (Gibco; for all survival experiments) or NEUMO photostable medium (Cell Guidance Systems; for optical pulse labeling experiments). For siRNA knockdown experiments, neurons were transfected with 100 ng of pGW1-mApple per well and siRNA at a final concentration of 90 nM. Cells were treated with either scrambled siRNA (Dharmacon) or siRNA targeting the N-terminal coding region of rat Matr3 (5'-GUC AUU CCA GCA GUC AUC UUU-3').

Longitudinal fluorescence microscopy and automated image analysis

Neurons were imaged as described previously[32] using a Nikon Eclipse Ti inverted microscope with PerfectFocus3 and a 20X objective lens. Detection was accomplished with an Andor iXon3 897 EMCCD camera or Andor Zyla4.2 (+) sCMOS camera. A Lambda XL Xenon lamp (Sutter) with 5 mm liquid light guide (Sutter Instrument Company) was used to illuminate samples, and custom scripts written in Beanshell for use in μManager controlled all stage movements, shutters, and filters. Custom ImageJ/Fiji macros and Python scripts (https://github.com/barmadaslab/survival-analysis and https://github.com/barmadaslab/measurements; copies archived at https://github.com/elifesciences-publications/ survival-analysis and https://github.com/elifesciences-publications/measurements) were used to identify neurons and draw regions of interest (ROIs) based upon size, morphology, and fluorescence intensity. Criteria for marking cell death involved rounding of the soma, loss of fluorescence and degeneration of neuritic processes. Custom scripts

(https://github.com/barmadaslab/nuclear-fractionation; copy archived at https://github.com/elifesciences-publications/nuclear-fractionation) were also used to identify and draw bounding ROIs around nuclei of transfected cells based upon MATR3-EGFP or Hoechst 33258 (ThermoFisher) fluorescence. Coefficient of variation (CV) was calculated as the standard deviation of fluorescence intensity divided by the mean fluorescence intensity within an ROI.

Immunocytochemistry

Neurons were fixed with 4% paraformaldehyde, rinsed with phosphate buffered saline (PBS), and permeabilized with 0.1% Triton X-100 in PBS. After brief treatment with 10 mM glycine in PBS, cells were placed in blocking solution (0.1% Triton X-100, 2% fetal calf serum, and 3% bovine serum albumin (BSA), all in PBS) at RT for 1 h before incubation overnight at 4 °C in primary antibody at the following dilutions in blocking solution: rabbit anti-MATR3 (Abcam EPR10635(B); RRID: AB_2491618 for Fig. 2.1 and EPR10634(B) for Fig. 2.2) diluted 1:1000, mouse anti-fibrillarin (Abcam 38F3; RRID: AB_304523) diluted 1:1000, mouse anti-SC35 (Novus Biologicals NB100-1774SS; RRID: AB_526734) diluted 1:2000, mouse anti-PML (Santa Cruz Biotechnology sc-377390) diluted 1:50. Cells were then washed 3x in PBS, and incubated at RT with secondary antibody, goat anti-rabbit 647 (Jackson ImmunoResearch 111-605-003; RRID: AB_2338072) or goat anti-mouse 647 (Jackson ImmunoResearch 115-605-003; RRID: AB_2338902) diluted 1:1000 in blocking solution, for 1 h at RT. Following 3x rinses in PBS containing 1:5000 Hoechst 33258

dye (ThermoFisher), neurons were imaged by fluorescence microscopy, as described above.

Fluorescence recovery after photobleaching

Primary neurons were dissected as above and plated in LAB-TEK 8-well borosilicate chambers (ThermoFisher). On DIV 3, they were transfected as before but using 200 µg of pGW1-mApple and 200 µg of pGW1-MATR3-EGFP variants per well. Cell were imaged 2-4 days after transfection using a Nikon A1 confocal microscope operated by Nikon Elements, a 60X objective lens, and a heating chamber with CO_2 pre-warmed to 37 °C. For MATR3(ΔRRM1/2)-EGFP variants, an ROI corresponding to half of the granule was outlined with Elements and photobleached using a 488 nm laser set at 30% power, 1 pulse per sec x 7 sec. Fluorescence recovery was monitored up to 10 min after photobleaching. For full-length MATR3 variants, ROIs for photobleaching were drawn in the center of the nucleus for each cell, and recovery was monitored for 6 min.

Image analysis was conducted in FIJI. Rigid body stack registration was used to fix the granules in place relative to the frame. The GFP integrated density for the whole granule was calculated from pre-bleach measurements, as was the fraction of granule integrated density corresponding to the ROI to be photobleached. The decline in this fraction immediately after photobleaching was then calculated and used as the floor, and the return was plotted as the percent recovery within the ROI as a fraction of the original pre-bleach granule integrated density.

Recovery data were fit to the equation $y(t) = A(1-e^{-\tau t})$, where A is the return curve plateau, τ is the time constant, and t is the time post-bleach. The fitted τ from each curve was then used to calculate the time to half-return ($t_{1/2}$) using the equation $t_{1/2} = \ln(0.5)/-\tau$. To estimate the diffusion coefficient (D) of these molecules, we used the equation $D = (0.88w^2)/(4t_{1/2})$, where w is the ROI radius[11]. This equation assumes spot bleach with a circular stimulation ROI and diffusion limited to the x-y plane. Since we could not be confident that these assumptions were met, we estimated D and downstream parameters by dividing ROI areas by π to approximate w^2 and solving for D. This estimated value was used in the Einstein-Stokes equation, $D = k_BT/(6\pi\eta r)$, where k_B is the Boltzmann constant, T is temperature in K, η is viscosity, and r is the Stokes radius of the particle. As there is no applicable structural data on MATR3, we estimated a Stokes radius of 3.13 nm by applying the MATR3(ΔRRM1/2)-EGFP fusion protein's combined molecular weight of 106.4 kDa to the equation $R_{min} = 0.66M^{1/3}$, where R_{min} is the minimal radius in nm of a sphere that could bound a globular protein with a molecular weight of M[81]. Using these constants and the estimated D for each granule, the Einstein-Stokes equation was rearranged to solve for η.

Photobleaching data from full-length MATR3-EGFP was analyzed in a similar fashion. After calculating the nuclear integrated density, the fraction attributable to photobleaching within the ROI was used for normalization. Intensity data were fit to the $y(t) = A(1-e^{-\tau t})$ equation, $t_{1/2}$ values were calculated as before, and D determined by the equation $D = (0.88w^2)/(4t_{1/2})$.

Nuclear/cytoplasmic fractionation and differential solubility

HEK293T cells (STR profiling-validated and mycoplasma-negative; ATCC CRL-3216; RRID: CVCL_0063) were transfected in a 6-well plate with 3 µg of DNA per well using Lipofectamine 2000 according to the manufacturer's instructions. For nuclear/cytoplasmic fractionation, cells were washed with cold PBS 24 h after transfection, collected with resuspension buffer (10 mM Tris, 10 mM NaCl, 3 mM $MgCl_2$, pH 7.4), and transferred to a pre-chilled 1.5 mL conical tube to sit on ice for 5 min. An equal volume of resuspension buffer with 0.6% Igepal (Sigma) was then added to rupture cell membranes and release cytoplasmic contents, with occasional inversion for 5 min on ice. Nuclei were pelleted at 100 x g at 4 °C for 10 min using a tabletop centrifuge. The supernatant (cytosolic fraction) was collected, and the nuclei were rinsed twice in resuspension buffer without Igepal. To collect nuclear fractions, pelleted nuclei were lysed in RIPA buffer (Pierce) with cOmplete protease inhibitors (Roche) on ice for 30 min with occasional inversion. Samples were centrifuged at 9,400 x g at 4 °C for 10 min, and the supernatant was saved as the nuclear fraction.

For differential solubility experiments, transfected HEK293T were collected in cold PBS 24 h after transfection and transferred to a pre-chilled conical tube on ice. Cells were then centrifuged at 100 x g for 5 min at 4 °C to pellet cells, the PBS was aspirated, and cells were resuspended in RIPA buffer with protease inhibitors. Following lysis on ice for 15 min with occasional inversion, cells were sonicated at 80% amplitude with 5 sec on/5 sec off for 2 min using a Fisherbrand Model 505 Sonic Dismembrenator (ThermoFisher). Samples were centrifuged at 41,415 x g for 15 min at 4 °C to pellet RIPA-insoluble material, with the supernatant removed and saved as the RIPA-soluble fraction. The RIPA-insoluble pellet was washed in RIPA once, and contents

resuspended vigorously in urea buffer (7 M urea, 2 M thiourea, 4% CHAPS, 30 mM Tris, pH 8.5). Samples were again centrifuged at 41,415 x g for 15 min at 4 °C, and the supernatant was saved as the RIPA-insoluble, urea-soluble fraction.

For SDS-PAGE, stock sample buffer (10% SDS, 20% glycerol, 0.0025% bromophenol blue, 100 mM EDTA, 1 M DTT, 20 mM Tris, pH 8) was diluted 1:10 in lysates and all samples except urea fractions were boiled for 10 min before 5-15 µg of protein were loaded onto 4-15% gradient gels (Bio-Rad). For urea fractions, total protein concentration was too low to quantify and so equal volumes of sample across conditions were mixed 1:1 with water and loaded. After electrophoresis, samples were transferred at 30 V overnight at 4 °C onto an activated 2 µm nitrocellulose membrane (Bio-Rad), blocked with 3% BSA in 0.2% Tween-20 in Tris-buffered saline (TBST), and blotted overnight at 4 °C with the following primary antibodies: rabbit anti-MATR3 (Abcam EPR10634(B)), mouse anti-GAPDH (Millipore Sigma MAB374; RRID: AB_2107445), and rabbit anti-H2B (Novus Biologicals NB100-56347; RRID: AB_838347), all diluted 1:1000 in 3% BSA, 0.2% TBST. The following day, blots were washed in 0.2% TBST, incubated at RT for 1 h with AlexaFluor goat anti-mouse 594 (ThermoFisher A-11005; RRID: AB_141372) and goat anti-rabbit 488 (ThermoFisher A-11008; RRID: AB_143165), both diluted 1:10,000 in 3% BSA in 0.2% TBST. Following treatment with secondary antibody, blots were washed in 0.2% TBST, placed in Tris-buffered saline, and imaged using an Odyssey CLx Imaging System (LI-COR Biosciences).

Statistical analysis

Statistical analyses were performed in R or Prism 7 (GraphPad). For primary neuron survival analysis, the publicly available R survival package was used to determine hazard ratios describing the relative survival among populations through Cox proportional hazards analysis. For half-life calculations, a custom R script (https://github.com/barmadaslab/measurements; copy archived at https://github.com/elifesciences-publications/measurements), was applied to fit log-transformed TRITC intensity data to a linear equation. Photobleaching recovery data were fit to the $y(t) = A(1-e^{-\tau t})$ equation using non-linear regression in R. siRNA knockdown data were plotted using Prism 7, and significance determined via the two-tailed t-test. One-way ANOVA with Tukey's post-test was used to assess for significant differences among nuclear/cytoplasmic ratios, viscosities, D values, and half-lives. Data are shown as mean ± SEM unless otherwise stated.

2.6 Acknowledgements

We thank Dr. Stephen Lentz for his assistance with confocal microscopy, Drs. Claudia Figueroa-Romero and Hilary Archbold for their experimental advice, and Brittany Flores for technical assistance in assembling the manuscript.

The present work was supported in part by funding from the National Institutes of Health (NIH) National Institute for Neurological Disorders and Stroke (NINDS) R01 NS097542 (S.J.B.), National Institute for Aging (NIA) P30 AG053760 (S.J.B.), and National Institute of General Medical Sciences (NIGMS) T32 GM007863 (A.M.M.); the Protein Folding Diseases Initiative at the University of Michigan (S.J.B.); the Program for Neurology Research and Discovery (E.L.F.); and the A. Alfred Taubman Medical

Research Institute (S.J.B., E.L.F.). Confocal microscopy was performed at the Microscopy & Image Analysis Core of the Michigan Diabetes Research Center funded by NIH grant P60DK020572 from the National Institute of Diabetes and Digestive and Kidney Diseases (NIDDK).

References

1. Taylor, J. P., Brown, R. H. & Cleveland, D. W. Decoding ALS: from genes to mechanism. *Nature* **539,** 197–206 (2016).
2. Neumann, M. *et al.* Ubiquitinated TDP-43 in frontotemporal lobar degeneration and amyotrophic lateral sclerosis. *Science* **314,** 130–133 (2006).
3. Kabashi, E. *et al.* TARDBP mutations in individuals with sporadic and familial amyotrophic lateral sclerosis. *Nat. Genet.* **40,** 572–574 (2008).
4. Kwiatkowski, T. J. *et al.* Mutations in the FUS/TLS gene on chromosome 16 cause familial amyotrophic lateral sclerosis. *Science* **323,** 1205–1208 (2009).
5. Vance, C. *et al.* Mutations in FUS, an RNA processing protein, cause familial amyotrophic lateral sclerosis type 6. *Science* **323,** 1208–1211 (2009).
6. Barmada, S. J. & Finkbeiner, S. Pathogenic TARDBP mutations in amyotrophic lateral sclerosis and frontotemporal dementia: disease-associated pathways. *Rev Neurosci* **21,** 251–272 (2010).
7. Ticozzi, N. *et al.* Mutational analysis reveals the FUS homolog TAF15 as a candidate gene for familial amyotrophic lateral sclerosis. *Am. J. Med. Genet. B Neuropsychiatr. Genet.* **156B,** 285–290 (2011).
8. Kim, H. J. *et al.* Mutations in prion-like domains in hnRNPA2B1 and hnRNPA1 cause multisystem proteinopathy and ALS. *Nature* **495,** 467–473 (2013).
9. Johnson, B. S. *et al.* TDP-43 is intrinsically aggregation-prone, and amyotrophic lateral sclerosis-linked mutations accelerate aggregation and increase toxicity. *The Journal of Biological Chemistry* **284,** 20329–20339 (2009).
10. Patel, A. *et al.* A Liquid-to-Solid Phase Transition of the ALS Protein FUS Accelerated by Disease Mutation. *Cell* **162,** 1066–1077 (2015).
11. Gopal, P. P., Nirschl, J. J., Klinman, E. & Holzbaur, E. L. F. Amyotrophic lateral sclerosis-linked mutations increase the viscosity of liquid-like TDP-43 RNP granules in neurons. *Proc Natl Acad Sci USA* **114,** E2466–E2475 (2017).
12. Mackenzie, I. R. *et al.* TIA1 Mutations in Amyotrophic Lateral Sclerosis and Frontotemporal Dementia Promote Phase Separation and Alter Stress Granule Dynamics. *Neuron* **95,** 808–816.e9 (2017).
13. Belgrader, P., Dey, R. & Berezney, R. Molecular cloning of Matrin 3. A 125-kilodalton protein of the nuclear matrix contains an extensive acidic domain. *The Journal of Biological Chemistry* **266,** 9893–9899 (1991).
14. Hibino, Y., Ohzeki, H., Sugano, N. & Hiraga, K. Transcription Modulation by a Rat Nuclear Scaffold Protein, P130, and a Rat Highly Repetitive DNA Component or Various Types of Animal and Plant Matrix or Scaffold Attachment Regions. *Biochemical and Biophysical Research Communications* **279,** 282–287 (2000).
15. Zhang, Z. & Carmichael, G. G. The Fate of dsRNA in the Nucleus: A p54nrb-Containing Complex Mediates the Nuclear Retention of Promiscuously A-to-I Edited RNAs. *Cell* **106,** 465–476 (2001).
16. Salton, M., Lerenthal, Y., Wang, S.-Y., Chen, D. J. & Shiloh, Y. Involvement of Matrin 3 and SFPQ/NONO in the DNA damage response. *Cell Cycle* **9,** 1568–1576 (2014).

17. Coelho, M. B. *et al.* Nuclear matrix protein Matrin3 regulates alternative splicing and forms overlapping regulatory networks with PTB. *The EMBO Journal* **34,** 653–668 (2015).
18. Rajgor, D., Hanley, J. G. & Shanahan, C. M. Identification of novel nesprin-1 binding partners and cytoplasmic matrin-3 in processing bodies. **27,** 3894–3902 (2016).
19. Uemura, Y. *et al.* Matrin3 binds directly to intronic pyrimidine-rich sequences and controls alternative splicing. *Genes Cells* **22,** 785–798 (2017).
20. Feit, H. *et al.* Vocal Cord and Pharyngeal Weakness with Autosomal Dominant Distal Myopathy: Clinical Description and Gene Localization to 5q31. *The American Journal of Human Genetics* **63,** 1732–1742 (1998).
21. Senderek, J. *et al.* Autosomal-Dominant Distal Myopathy Associated with a Recurrent Missense Mutation in the Gene Encoding the Nuclear Matrix Protein, Matrin 3. *The American Journal of Human Genetics* **84,** 511–518 (2009).
22. Hocking, L. J. *et al.* Domain-specific mutations in sequestosome 1 (SQSTM1) cause familial and sporadic Paget's disease. *Human Molecular Genetics* **11,** 2735–2739 (2002).
23. Fecto, F. *et al.* SQSTM1 mutations in familial and sporadic amyotrophic lateral sclerosis. *Arch. Neurol.* **68,** 1440–1446 (2011).
24. Kimonis, V. E. *et al.* Clinical studies in familial VCP myopathy associated with Paget disease of bone and frontotemporal dementia. *Am. J. Med. Genet. A* **146A,** 745–757 (2008).
25. Johnson, J. O. *et al.* Exome sequencing reveals VCP mutations as a cause of familial ALS. *Neuron* **68,** 857–864 (2010).
26. Klar, J. *et al.* Welander distal myopathy caused by an ancient founder mutation in TIA1 associated with perturbed splicing. *Hum. Mutat.* **34,** 572–577 (2013).
27. Johnson, J. O. *et al.* Mutations in the Matrin 3 gene cause familial amyotrophic lateral sclerosis. *Nat Neurosci* **17,** 664–666 (2014).
28. Dreser, A. *et al.* The ALS-linked E102Q mutation in Sigma receptor-1 leads to ER stress-mediated defects in protein homeostasis and dysregulation of RNA-binding proteins. 1–17 (2017). doi:10.1038/cdd.2017.88
29. Tada, M. *et al.* Matrin 3 is a component of neuronal cytoplasmic inclusions of motor neurons in sporadic amyotrophic lateral sclerosis. *The American Journal of Pathology* 1–36 (2017). doi:10.1016/j.ajpath.2017.10.007
30. Barmada, S. J. *et al.* Cytoplasmic mislocalization of TDP-43 is toxic to neurons and enhanced by a mutation associated with familial amyotrophic lateral sclerosis. *J. Neurosci.* **30,** 639–649 (2010).
31. Barmada, S. J. *et al.* Autophagy induction enhances TDP43 turnover and survival in neuronal ALS models. *Nature Chemical Biology* **10,** 677–685 (2014).
32. Barmada, S. J. *et al.* Amelioration of toxicity in neuronal models of amyotrophic lateral sclerosis by hUPF1. *Proc. Natl. Acad. Sci. U.S.A.* **112,** 7821–7826 (2015).
33. Arrasate, M. & Finkbeiner, S. Automated microscope system for determining factors that predict neuronal fate. *Proc Natl Acad Sci USA* **102,** 3840–3845 (2005).
34. Christensen, E. Multivariate survival analysis using Cox's regression model. *Hepatology* **7,** 1346–1358 (1987).

35. Arrasate, M., Mitra, S., Schweitzer, E. S., Segal, M. R. & Finkbeiner, S. Inclusion body formation reduces levels of mutant huntingtin and the risk of neuronal death. *Nature* **431,** 805–810 (2004).
36. Miller, J. *et al.* Quantitative relationships between huntingtin levels, polyglutamine length, inclusion body formation, and neuronal death provide novel insight into huntington's disease molecular pathogenesis. *J. Neurosci.* **30,** 10541–10550 (2010).
37. Millecamps, S. *et al.* Genetic analysis of matrin 3 gene in French amyotrophic lateral sclerosis patients and frontotemporal lobar degeneration with amyotrophic lateral sclerosis patients. *Neurobiology of Aging* **35,** 2882.e13–2882.e15 (2014).
38. Lin, K.-P. *et al.* Mutational analysis of MATR3 in Taiwanese patients with amyotrophic lateral sclerosis. *Neurobiology of Aging* **36,** 2005.e1–2005.e4 (2015).
39. Origone, P. *et al.* A novel Arg147Trp MATR3 missense mutation in a slowly progressive ALS Italian patient. *Amyotrophic Lateral Sclerosis and Frontotemporal Degeneration* **16,** 530–531 (2015).
40. Leblond, C. S. *et al.* Replication study of MATR3 in familial and sporadic amyotrophic lateral sclerosis. *Neurobiology of Aging* **37,** 209.e17–209.e21 (2016).
41. Xu, L., Li, J., Tang, L., Zhang, N. & Fan, D. MATR3 mutation analysis in a Chinese cohort with sporadic amyotrophic lateral sclerosis. *Neurobiology of Aging* **38,** 218.e3–218.e4 (2016).
42. Marangi, G. *et al.* Matrin 3 variants are frequent in Italian ALS patients. *Neurobiology of Aging* **49,** 218.e1–218.e7 (2017).
43. Narain, P. *et al.* Identification and characterization of novel and rare susceptible variants in Indian amyotrophic lateral sclerosis patients. *Neurogenetics* **20,** 197–208 (2019).
44. Gallego-Iradi, M. C. *et al.* Subcellular Localization of Matrin 3 Containing Mutations Associated with ALS and Distal Myopathy. *PLoS ONE* **10,** e0142144–15 (2015).
45. Boehringer, A. *et al.* ALS Associated Mutations in Matrin 3 Alter Protein-Protein Interactions and Impede mRNA Nuclear Export. *Scientific Reports* 1–14 (2017). doi:10.1038/s41598-017-14924-6
46. Brayer, K. J., Kulshreshtha, S. & Segal, D. J. The protein-binding potential of C2H2 zinc finger domains. *Cell Biochem. Biophys.* **51,** 9–19 (2008).
47. Burdach, J., O'Connell, M. R., Mackay, J. P. & Crossley, M. Two-timing zinc finger transcription factors liaising with RNA. *Trends Biochem. Sci.* **37,** 199–205 (2012).
48. Inagaki, H. *et al.* A large DNA-binding nuclear protein with RNA recognition motif and serine/arginine-rich domain. *The Journal of Biological Chemistry* **271,** 12525–12531 (1996).
49. Elden, A. C. *et al.* Ataxin-2 intermediate-length polyglutamine expansions are associated with increased risk for ALS. *Nature* **466,** 1069–1075 (2010).
50. Daigle, J. G. *et al.* RNA-binding ability of FUS regulates neurodegeneration, cytoplasmic mislocalization and incorporation into stress granules associated with FUS carrying ALS-linked mutations. *Human Molecular Genetics* **22,** 1193–1205 (2013).

51. Flores, B. N. *et al.* An Intramolecular Salt Bridge Linking TDP43 RNA Binding, Protein Stability, and TDP43-Dependent Neurodegeneration. *Cell Rep* **27,** 1133–1150.e8 (2019).
52. Arai, T. *et al.* TDP-43 is a component of ubiquitin-positive tau-negative inclusions in frontotemporal lobar degeneration and amyotrophic lateral sclerosis. *Biochemical and Biophysical Research Communications* **351,** 602–611 (2006).
53. Molliex, A. *et al.* Phase separation by low complexity domains promotes stress granule assembly and drives pathological fibrillization. *Cell* **163,** 123–133 (2015).
54. Murray, D. T. *et al.* Structure of FUS Protein Fibrils and Its Relevance to Self-Assembly and Phase Separation of Low- Complexity Domains. *Cell* **171,** 615–620.e16 (2017).
55. Conicella, A. E., Zerze, G. H., Mittal, J. & Fawzi, N. L. ALS Mutations Disrupt Phase Separation Mediated by α-Helical Structure in the TDP-43 Low-Complexity C-Terminal Domain. *Structure* **24,** 1537–1549 (2016).
56. Lin, Y., Protter, D. S. W., Rosen, M. K. & Parker, R. Formation and Maturation of Phase-Separated Liquid Droplets by RNA-Binding Proteins. *Mol. Cell* **60,** 208–219 (2015).
57. Shin, Y. & Brangwynne, C. P. Liquid phase condensation in cell physiology and disease. *Science* **357,** eaaf4382–13 (2017).
58. Hibino, Y. *et al.* Molecular properties and intracellular localization of rat liver nuclear scaffold protein P130. *Biochimica et Biophysica Acta (BBA) - Gene Structure and Expression* **1759,** 195–207 (2006).
59. Hisada-Ishii, S., Ebihara, M., Kobayashi, N. & KITAGAWA, Y. Bipartite nuclear localization signal of matrin 3 is essential for vertebrate cells. *Biochemical and Biophysical Research Communications* **354,** 72–76 (2007).
60. Kalderon, D., Roberts, B. L., Richardson, W. D. & Smith, A. E. A short amino acid sequence able to specify nuclear location. *Cell* **39,** 499–509 (1984).
61. Qiu, H. *et al.* ALS-associated mutation FUS-R521C causes DNA damage and RNA splicing defects. *J. Clin. Invest.* **124,** 981–999 (2014).
62. Chudakov, D. M., Lukyanov, S. & Lukyanov, K. A. Tracking intracellular protein movements using photoswitchable fluorescent proteins PS-CFP2 and Dendra2. *Nat Protoc* **2,** 2024–2032 (2007).
63. Kao, C. S. *et al.* Selective neuronal degeneration in MATR3 S85C knock-in mouse model of early-stage ALS. *Nature Communications* **11,** 5304–17 (2020).
64. Moloney, C. *et al.* Analysis of spinal and muscle pathology in transgenic mice overexpressing wild-type and ALS-linked mutant MATR3. *Acta Neuropathologica Communications* **6,** 137–13 (2018).
65. Zhang, X. *et al.* A mutant MATR3 mouse model to explain multisystem proteinopathy. *J. Pathol.* **249,** 182–192 (2019).
66. Hibino, Y., Ohzeki, H., Hirose, N. & Sugano, N. Involvement of phosphorylation in binding of nuclear scaffold proteins from rat liver to a highly repetitive DNA component. *Biochimica et Biophysica Acta (BBA) - Gene Structure and Expression* **1396,** 88–96 (1998).
67. Ray, D. *et al.* A compendium of RNA-binding motifs for decoding gene regulation. *Nature* **499,** 172–177 (2013).

68. Goldstein, L. & Trescott, O. H. Characterization of RNAs that do and do not migrate between cytoplasm and nucleus. *Proc Natl Acad Sci USA* **67,** 1367–1374 (1970).
69. Maharana, S. *et al.* RNA buffers the phase separation behavior of prion-like RNA binding proteins. *Science* eaar7366 (2018). doi:10.1126/science.aar7366
70. Iradi, M. C. G. *et al.* Characterization of gene regulation and protein interaction networks for Matrin 3 encoding mutations linked to amyotrophic lateral sclerosis and myopathy. *Scientific Reports* **8,** 4049 (2018).
71. Salton, M. *et al.* Matrin 3 Binds and Stabilizes mRNA. *PLoS ONE* **6,** e23882–7 (2011).
72. Johnson, B. S., McCaffery, J. M., Lindquist, S. & Gitler, A. D. A yeast TDP-43 proteinopathy model: Exploring the molecular determinants of TDP-43 aggregation and cellular toxicity. *Proc. Natl. Acad. Sci. U.S.A.* **105,** 6439–6444 (2008).
73. Ihara, R. *et al.* RNA binding mediates neurotoxicity in the transgenic Drosophila model of TDP-43 proteinopathy. *Human Molecular Genetics* **22,** 4474–4484 (2013).
74. Dormann, D. *et al.* ALS-associated fused in sarcoma (FUS) mutations disrupt Transportin-mediated nuclear import. *The EMBO Journal* **29,** 2841–2857 (2010).
75. Igaz, L. M. *et al.* Dysregulation of the ALS-associated gene TDP-43 leads to neuronal death and degeneration in mice. *J. Clin. Invest.* **121,** 726–738 (2011).
76. Gupta, R. *et al.* The Proline/Arginine Dipeptide from Hexanucleotide Repeat Expanded C9ORF72 Inhibits the Proteasome. *eNeuro* **4,** ENEURO.0249–16.2017 (2017).
77. Ramesh, N., Kour, S., Anderson, E. N., Rajasundaram, D. & Pandey, U. B. RNA-recognition motif in Matrin-3 mediates neurodegeneration through interaction with hnRNPM. *Acta Neuropathologica Communications* **8,** 138 (2020).
78. Zhao, M. *et al.* Knockdown of genes involved in axonal transport enhances the toxicity of human neuromuscular disease-linked MATR3 mutations in Drosophila. *FEBS Lett.* **27,** 4103 (2020).
79. Monahan, Z. *et al.* Phosphorylation of the FUS low-complexity domain disrupts phase separation, aggregation, and toxicity. *The EMBO Journal* **36,** 2951–2967 (2017).
80. Saudou, F., Finkbeiner, S., Devys, D. & Greenberg, M. E. Huntingtin acts in the nucleus to induce apoptosis but death does not correlate with the formation of intranuclear inclusions. *Cell* **95,** 55–66 (1998).
81. Erickson, H. P. Size and shape of protein molecules at the nanometer level determined by sedimentation, gel filtration, and electron microscopy. *Biol Proced Online* **11,** 32–51 (2009).
82. Peng K, Radivojac P, Vucetic S, Dunker AK, Obradovic Z. Length-dependent prediction of protein intrinsic disorder. *BMC Bioinformatics* 2006;7(1):208.

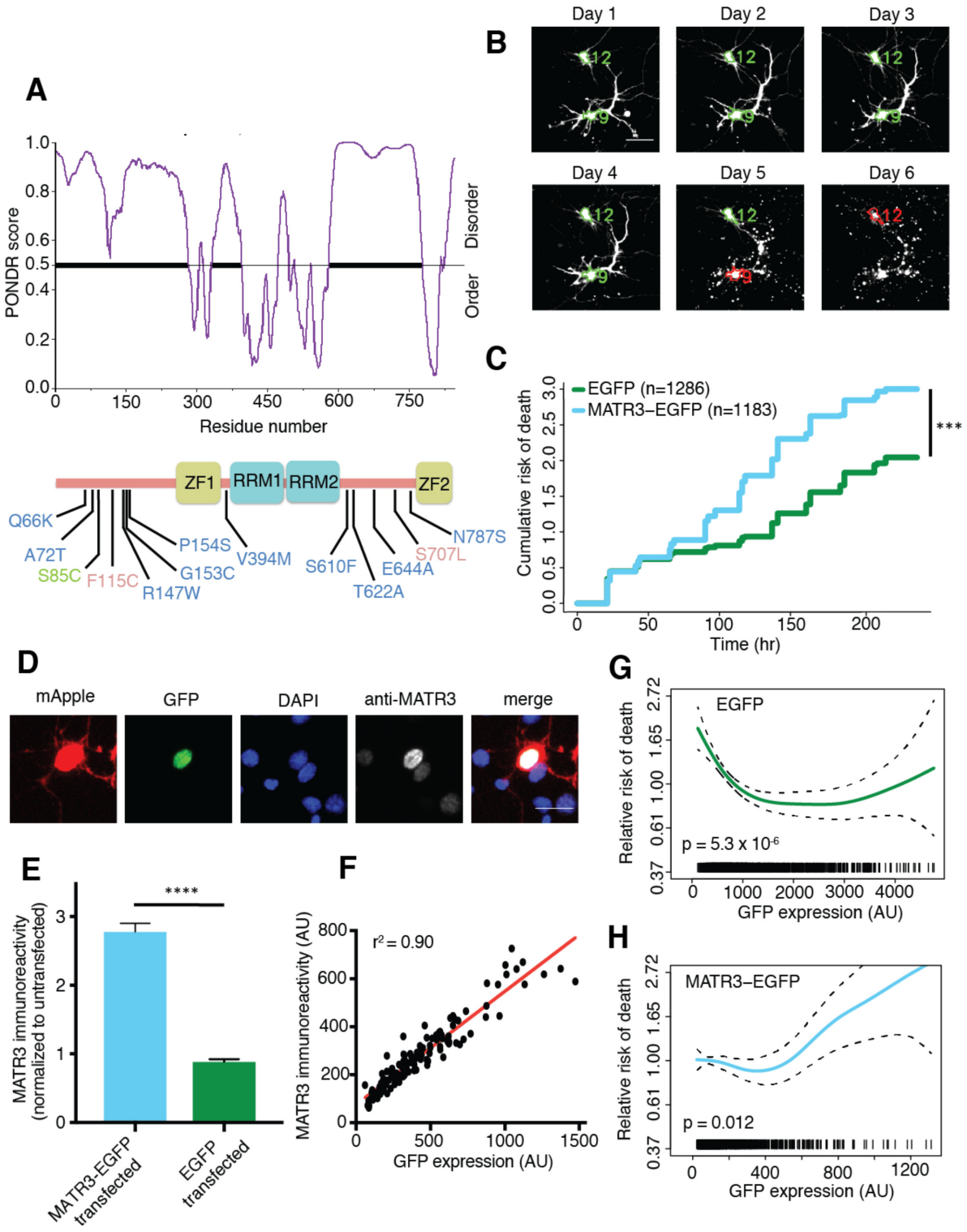

Figure 2.1. MATR3 overexpression results in dose-dependent neurodegeneration. **A.** Diagram of MATR3 showing nucleic acid-binding domains as well as the distribution of pathogenic mutations implicated in ALS (blue), ALS/FTD (red), and ALS/distal myopathy (green) within domains predicted to be disordered by PONDR VSL2[82]. **B.**

Longitudinal fluorescence microscopy (LFM) allows unique identification and tracking of thousands of primary neurons (green outlines) transfected with fluorescent proteins, as well as monitoring of cell death (red outlines), indicated by loss of fluorescence signal and changes in morphology. **C.** MATR3-EGFP expressing neurons exhibited a higher risk of death compared to neurons expressing only EGFP, as quantified by the hazard ratio (HR) (HR = 1.48; EGFP n = 1286, MATR3-EGFP n = 1183; *** $p < 2 \times 10^{-16}$, Cox proportional hazards). **D-E.** Transfection of neurons with MATR3-EGFP resulted in a 2.8-fold increase in anti-MATR3 immunoreactivity over untransfected cells (MATR3-EGFP n = 133, untransfected n = 136, EGFP n = 113, **** $p < 0.0001$, one-way ANOVA with Tukey's post-hoc test). **F.** On a single-cell basis, GFP fluorescence is directly proportional to anti-MATR3 reactivity ($p < 0.0001$, $r^2 = 0.90$; linear regression). **G.** Penalized spline modeling confirmed a protective effect associated with higher EGFP expression that plateaus at ~1500 arbitrary units (AU); ($p = 5.3 \times 10^{-6}$, penalized spline regression). **H**. However, penalized spline analysis showed no relationship between expression and survival at low and medium expression but a significant increase in risk of death with high MATR3-EGFP levels ($p = 0.012$; penalized spline regression). Scale bars in **(B)** and **(D)**, 20 μm.

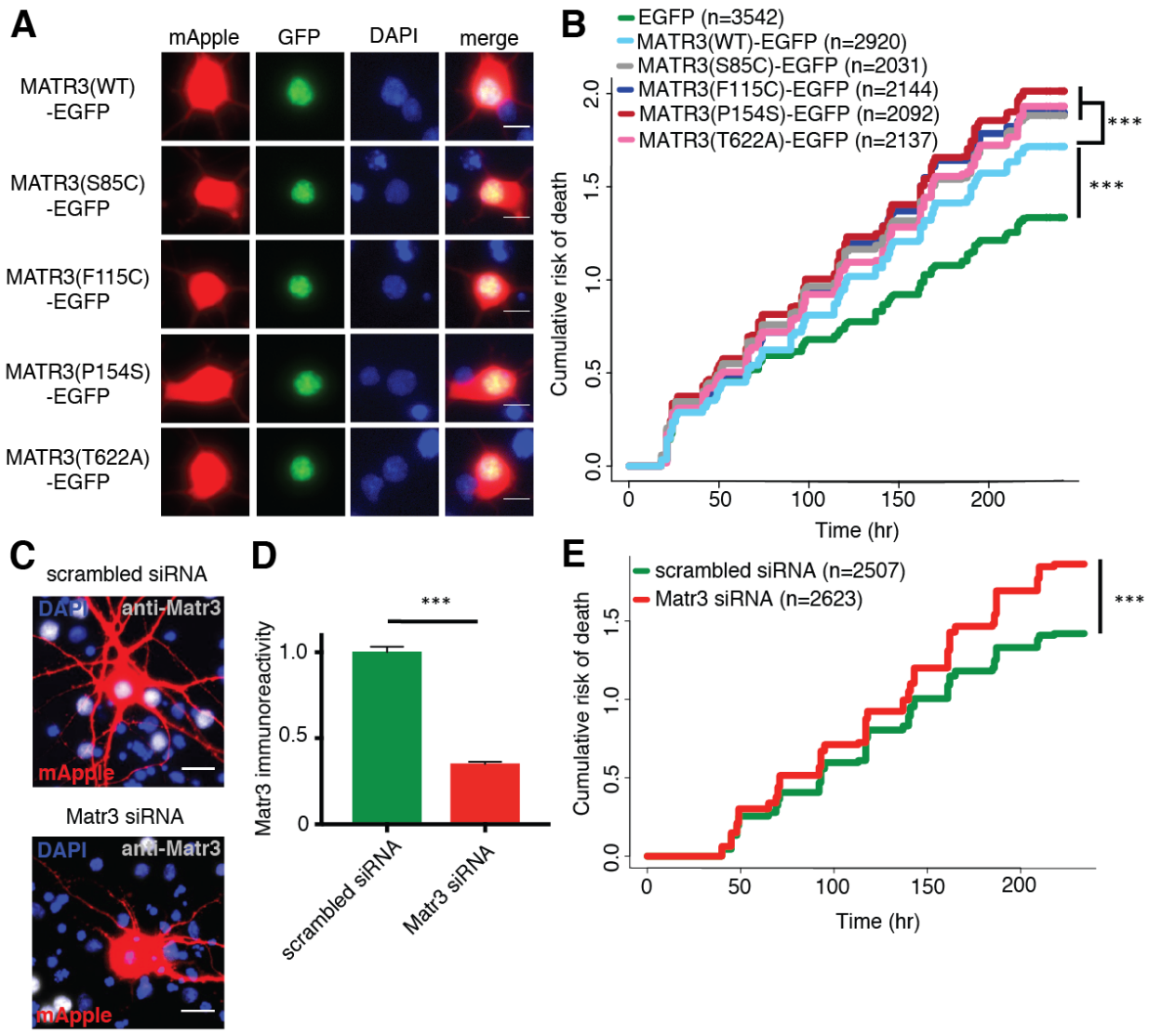

Figure 2.2. Neurons are susceptible to both gain-of-function and loss-of-function MATR3 toxicity. A. In primary rodent cortical neurons, the S85C, F115C, P154S, and T622A disease-associated MATR3 mutants have the same granular nuclear distribution as MATR3(WT)-EGFP. **B.** All four disease mutations display a subtle but significant increase in toxicity compared to MATR3(WT)-EGFP (comparing to MATR3(WT)-EGFP, n = 2920: MATR3(S85C)-EGFP, HR = 1.16, n = 2031, *** $p = 3.79 \times 10^{-6}$; MATR3(F115C)-EGFP, HR = 1.14, n = 2144, *** $p = 5.57 \times 10^{-5}$; MATR3(P154S)-EGFP, HR = 1.24, n = 2092, *** $p = 1.77 \times 10^{-11}$; MATR3(T622A)-EGFP, HR = 1.14, n = 2137, *** $p = 6.02 \times 10^{-5}$; Cox proportional hazards). **C-D.** siRNA targeting the endogenous rat *Matr3* reduced MATR3 antibody reactivity by approximately 65% (scrambled siRNA, n = 576; anti-Matr3 siRNA, n = 508; $p < 0.0001$, two-tailed t-test). **E.** Neurons transfected with anti-Matr3 siRNA displayed a higher risk of death compared to those transfected with scrambled siRNA (HR = 1.20; scrambled siRNA, n = 2507; anti-Matr3, n = 2623; *** $p = 2.05 \times 10^{-8}$, Cox proportional hazards). Scale bars in **(A)**, 10 μm; scale bars in **(C)**, 20 μm.

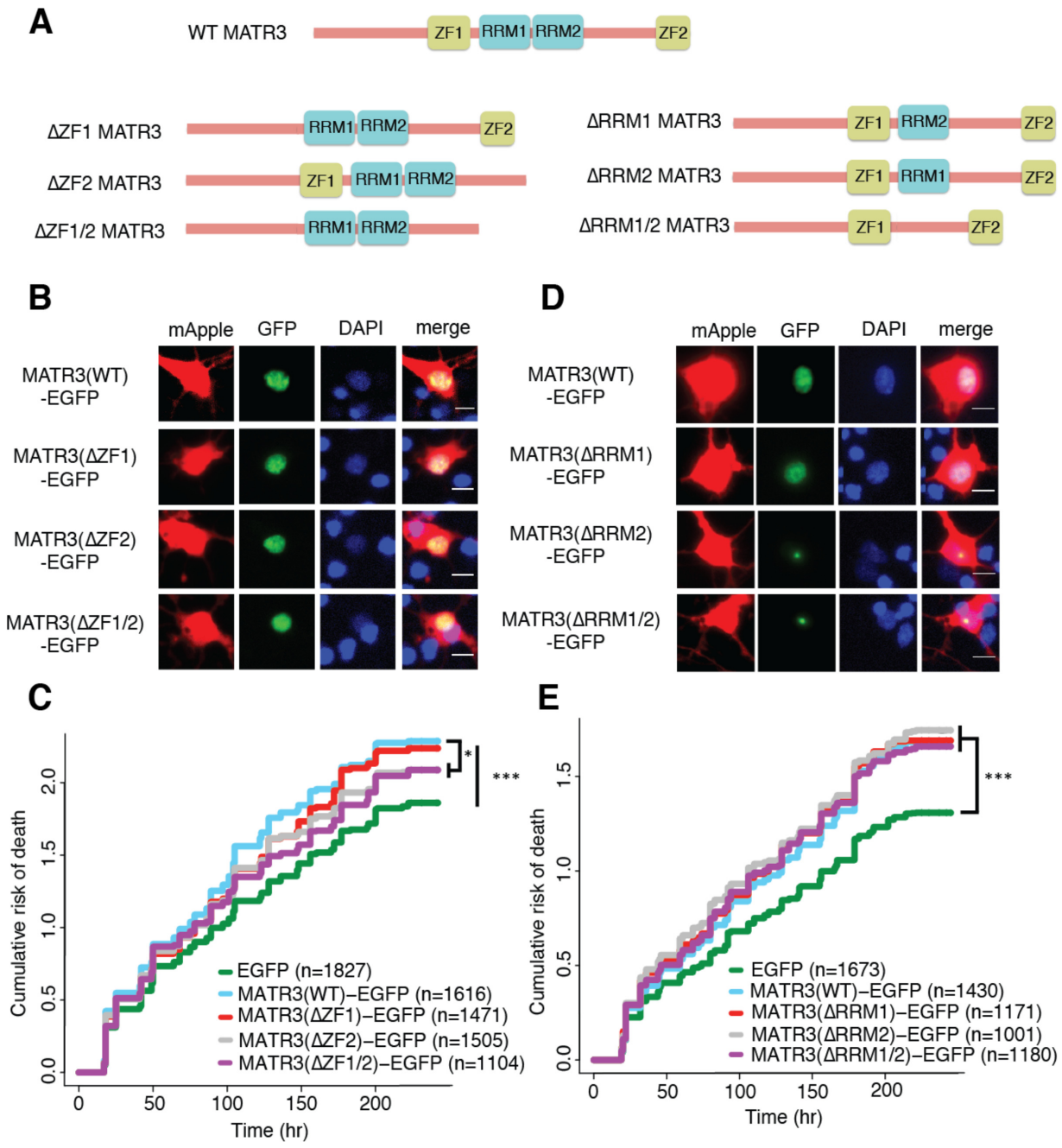

Figure 2.3. MATR3's ZFs mediate overexpression toxicity, and its RRMs regulate subcellular distribution. A. Schematic of MATR3 domain deletion mutants. **B.** Zinc finger (ZF) domain deletions do not change the localization of MATR3-EGFP compared to the full-length protein. **C.** ZF2 deletion, either in isolation or combination with ZF1, results in modest rescue of overexpression toxicity (comparing to MATR3(WT)-EGFP, n = 1616: MATR3(ΔZF1)-EGFP, HR = 0.94, n = 1471, p = 0.10; MATR3(ΔZF2)-EGFP, HR =0.93, n = 1505, * p = 0.040; MATR3(ΔZF1/2)-EGFP, HR = 0.90, n = 1104, ** p = 0.0093; Cox proportional hazards). **D.** While MATR3(ΔRRM1)-EGFP exhibits the same localization as MATR3(WT)-EGFP, deletion of RRM2 results in redistribution into

intranuclear granules. **E.** RRM deletion had little effect on MATR3-mediated toxicity (comparing to MATR3(WT)-EGFP n = 1430: MATR3(ΔRRM1)-EGFP, HR = 1.05, n = 1171, p = 0.25; MATR3(ΔRRM2)-EGFP, HR = 1.09, n = 1001, p = 0.066; MATR3(ΔRRM1/2)-EGFP, HR = 1.04, n = 1180, p = 0.42). Scale bars in **(B)** and **(D)**, 10 μm.

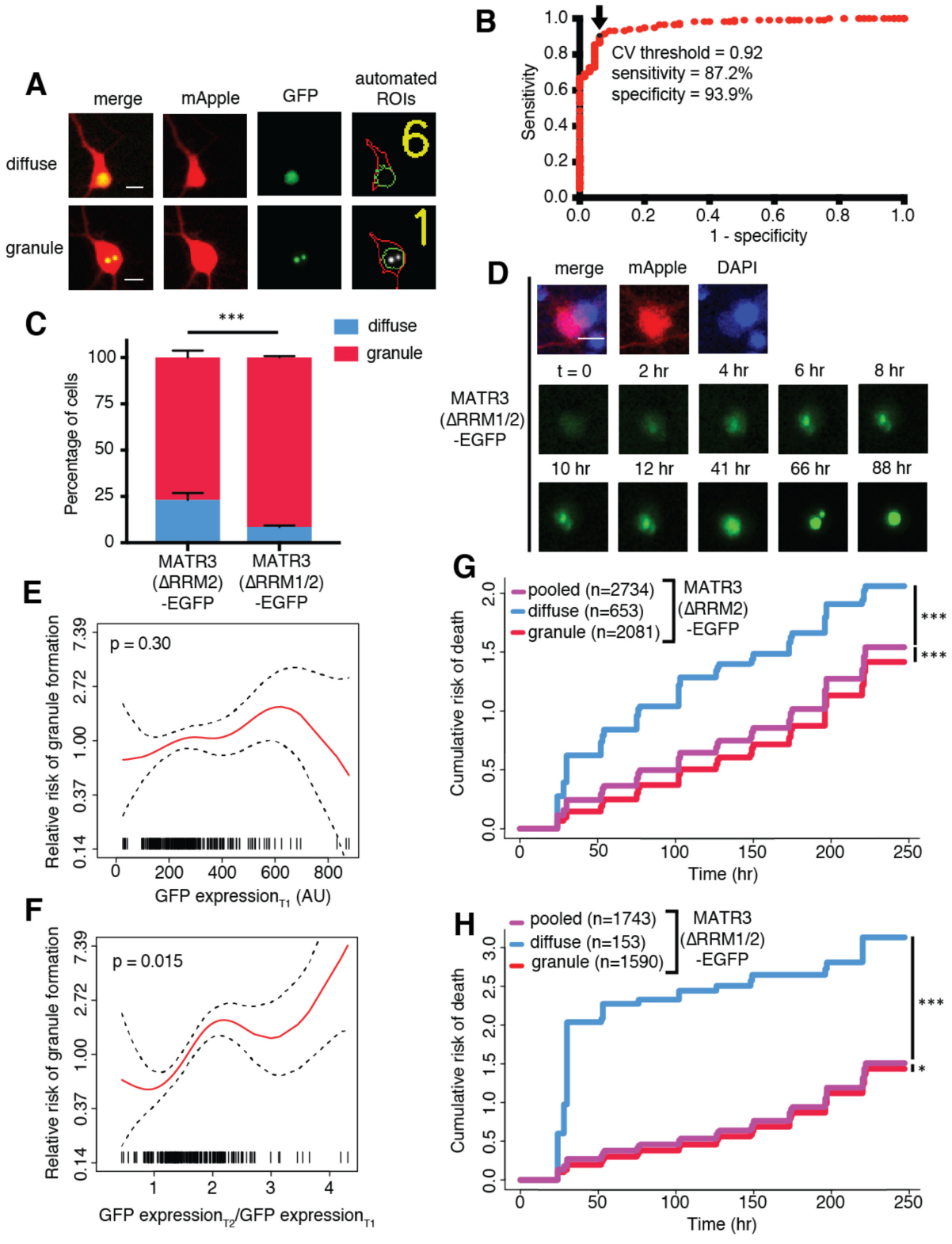

Figure 2.4. MATR3(ΔRRM2)-EGFP and MATR3(ΔRRM1/2)-EGFP are highly neurotoxic in their diffuse form. A. Automated analysis of MATR3-EGFP distribution

in transfected primary cortical neurons. Regions of interest (ROIs) were drawn around the cell body (marked by mApple fluorescence, red) and diffuse MATR3-EGFP (indicated by GFP fluorescence, green), and used to calculate a coefficient of variation (CV) representing MATR3-EGFP distribution within each ROI. **B**. Receiver operating characteristic (ROC) curve for MATR3-EGFP CV values. A CV threshold of 0.92 (arrow/black point) identified cells with intranuclear MATR3-EGFP granules with 87.2% sensitivity and 93.9% specificity. **C.** Using this cutoff, we determined that 1 day after transfection, 76.1% (2081/2734) of MATR3(ΔRRM2)-EGFP neurons displayed intranuclear granules compared to 91.2% (1590/1743) of MATR3(ΔRRM1/2)-EGFP cells (*** $p < 0.00001$, Fisher's exact test). **D.** Intranuclear granules form in a time-dependent manner in neurons expressing MATR3(ΔRRM2)-EGFP and MATR3(ΔRRM1/2)-EGFP. **E-F.** Penalized spline models depicting the relationship between MATR3(ΔRRM2)-EGFP expression on day 1 (**E**) or change in GFP expression between day 1 and day 2 (**F**), and risk of developing an intranuclear granule by day 3. Expression level at day 1 was not significantly associated with risk of granule formation (**E**; $p = 0.30$, penalized spline regression), but the relative increase in expression from day 1 to day 2 is (**F**; $p = 0.015$, penalized spline regression). **G.** For MATR3(ΔRRM2)-EGFP, neurons exhibiting granules by day 1 displayed improved survival compared to the pooled combination of all cells. Conversely, neurons with diffusely distributed MATR3(ΔRRM2)-EGFP fared far worse (comparing to the pooled condition: cells with granules n = 2081, HR = 0.86, *** $p = 1.02 \times 10^{-5}$; cells with diffuse protein n = 653, HR = 1.75, *** $p < 2 \times 10^{-16}$; Cox proportional hazards). **H.** Neurons with MATR3(ΔRRM1/2)-EGFP granules by day 1 similarly displayed a reduced risk of death in comparison to the pooled group, while diffuse MATR3(ΔRRM1/2)-EGFP was highly toxic (comparing to the pooled condition: cells with granules, n = 1590, HR = 0.92, * $p = 0.03$; cells with diffuse protein, n = 153, HR = 3.78, *** $p = 2 \times 10^{-16}$; Cox proportional hazards). Scale bars in **(A)** and **(B)**, 10 μm.

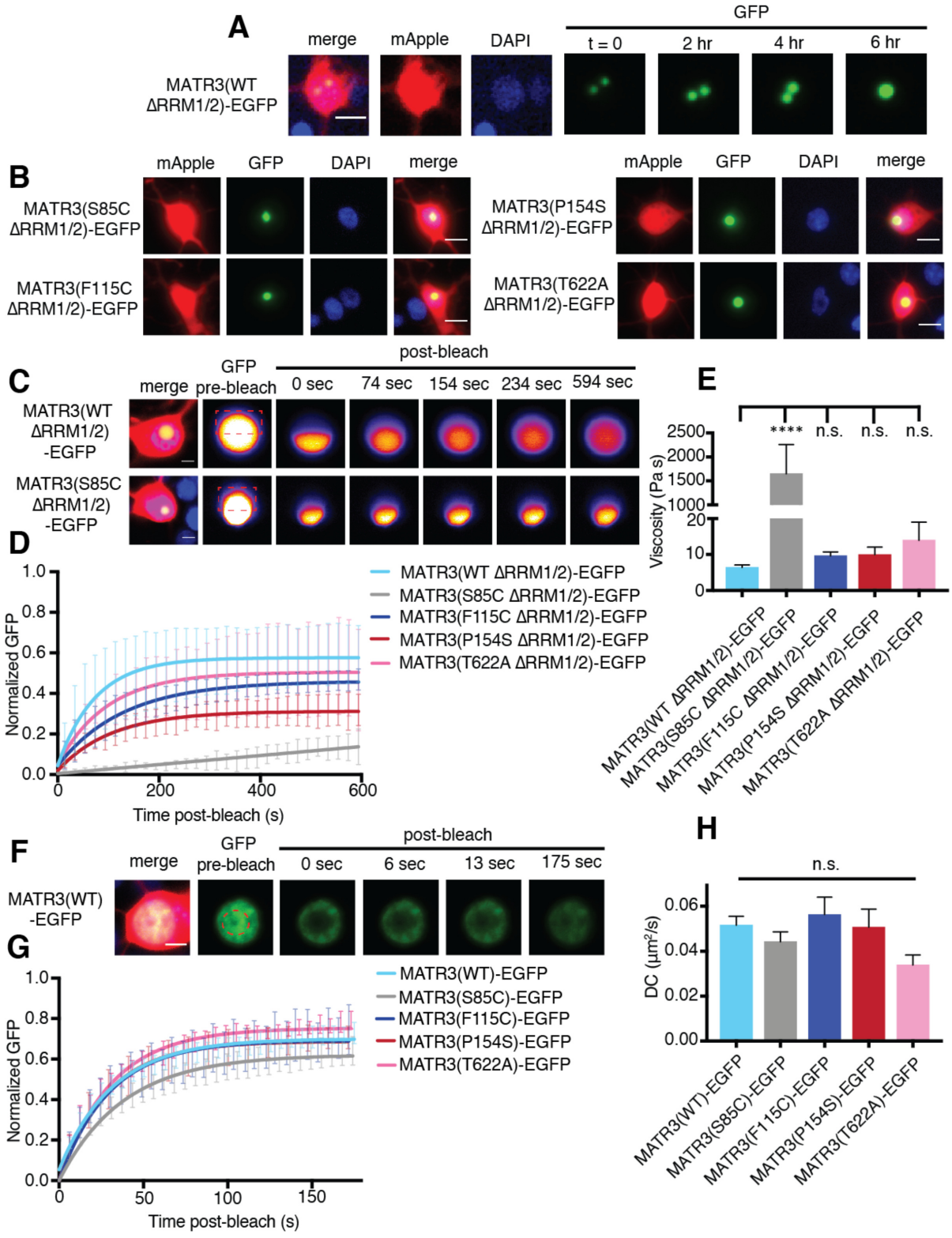

Figure 2.5. MATR3(ΔRRM1/2)-EGFP droplets display liquid-like properties that are affected by the S85C mutation. A. MATR3(ΔRRM2)-EGFP and MATR3(ΔRRM1/2)-EGFP droplets show liquid-like properties such as mobility and fusion. **B.** Pathogenic

MATR3 mutations on the ΔRRM1/2 background result in similar phase-separated droplets. **C-D.** Fluorescence recovery after photobleaching (FRAP) of MATR3(ΔRRM1/2)-EGFP droplets shows internal rearrangement consistent with liquid-like behavior, but the recovery of MATR3(S85C ΔRRM1/2)-EGFP droplets was significantly delayed. **E.** MATR3(S85C ΔRRM1/2)-EGFP droplets displayed significantly higher viscosity in comparison to MATR3(WT ΔRRM1/2)-EGFP (comparing to MATR3(WT ΔRRM1/2)-EGFP, n = 5: MATR3(S85C ΔRRM1/2)-EGFP, n = 5, **** $p < 0.0001$; MATR3(F115C ΔRRM1/2)-EGFP, n = 5, $p > 0.9999$; MATR3(P154S ΔRRM1/2)-EGFP, n = 5, $p > 0.9999$; MATR3(T622A ΔRRM1/2)-EGFP, n = 4, $p > 0.9999$; one-way ANOVA with Tukey's post-hoc test). **F-G.** FRAP experiments involving full-length MATR3-EGFP variants showed no differences in rates of return. **H.** Similarly, there were no differences in diffusion coefficients (DC) among full-length MATR3 variants (MATR3(WT)-EGFP, n = 5; MATR3(S85C)-EGFP, n = 5; MATR3(F115C)-EGFP; n = 5, MATR3(P154S)-EGFP, n = 5; MATR3(T622A)-EGFP, n = 4; $p = 0.17$, one-way ANOVA). Scale bars in **(A)** and **(B)**, 10 μm; scale bars in **(C)** and **(F)**, 5 μm. Curves in **(D)** and **(G)** show fitted curves ± SD.

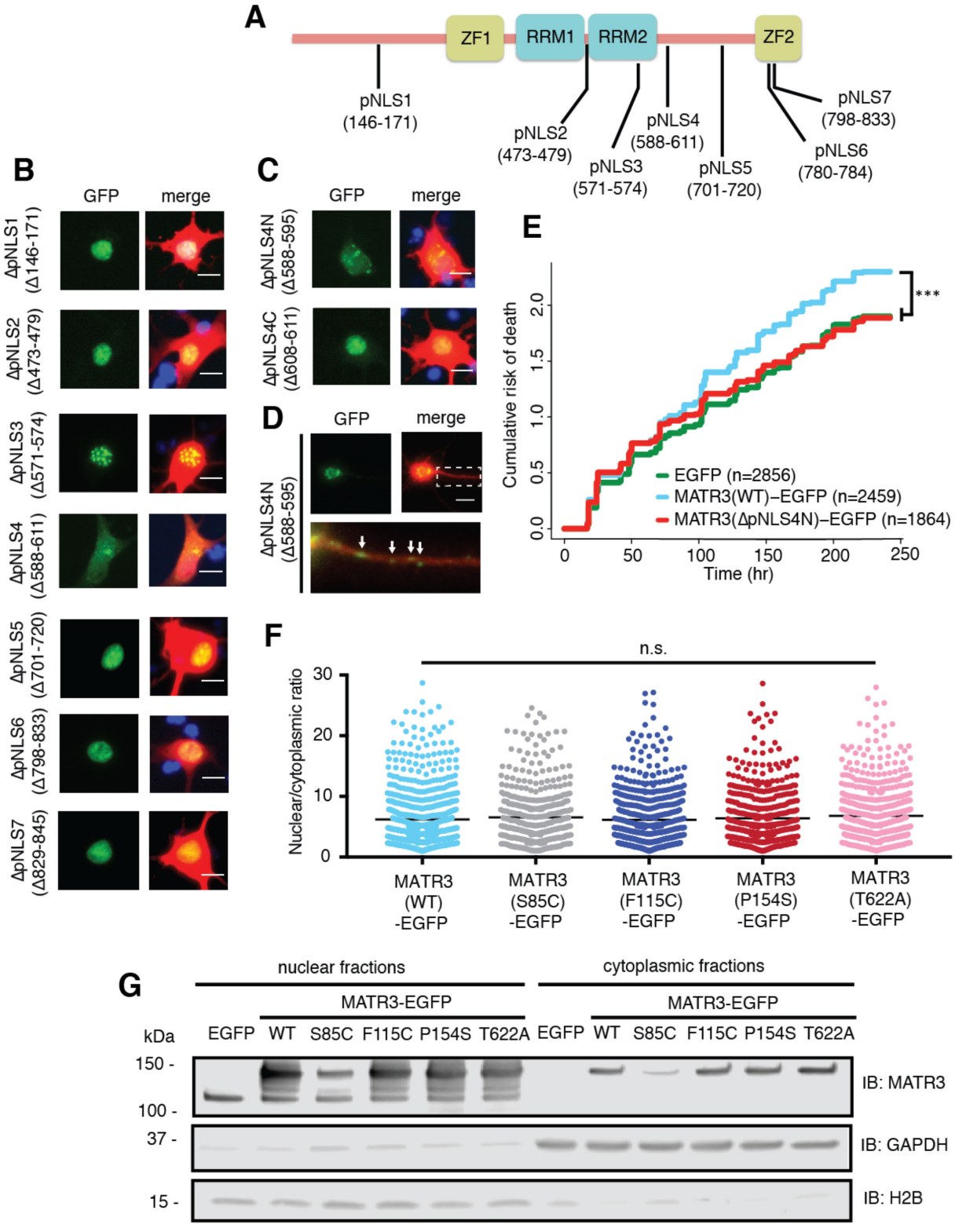

Figure 2.6. Reducing MATR3 nuclear localization mitigates overexpression toxicity. A. Schematic showing putative MATR3 nuclear localization signals (pNLS). **B-**

C. Deletion of the N-terminal arm of NLS4 (ΔpNLS4N) led to nuclear MATR3 clearance in neurons. **D.** MATR3(ΔpNLS4N)-EGFP forms granular structures in the cytoplasm and neuronal processes (white arrows). **E.** Disrupting nuclear localization of MATR3 prevents neurotoxicity from overexpression (compared to MATR3(WT)-EGFP, n = 2459: MATR3(ΔpNLS4N)-EGFP, n = 1864, HR = 0.89, *** p = 0.00041, Cox proportional hazards). **F-G.** Pathogenic MATR3 mutants display no difference in subcellular protein localization as assessed by automated image nuclear/cytoplasmic analysis (**F**; MATR3(WT)-EGFP, n = 824; MATR3(S85C)-EGFP, n = 499; MATR3(F115C)-EGFP, n = 634; MATR3(P154S)-EGFP, n = 554; MATR3(T622A)-EGFP, n = 677; p = 0.067, one-way ANOVA) or biochemical fractionation in transfected HEK293T cells (**G**). Western blot demonstrated reduced abundance of the S85C mutant in transfected HEK293T cells. Scale bars in **(B)** and **(C)**, 10 μm; scale bar in (D), 50 μm.

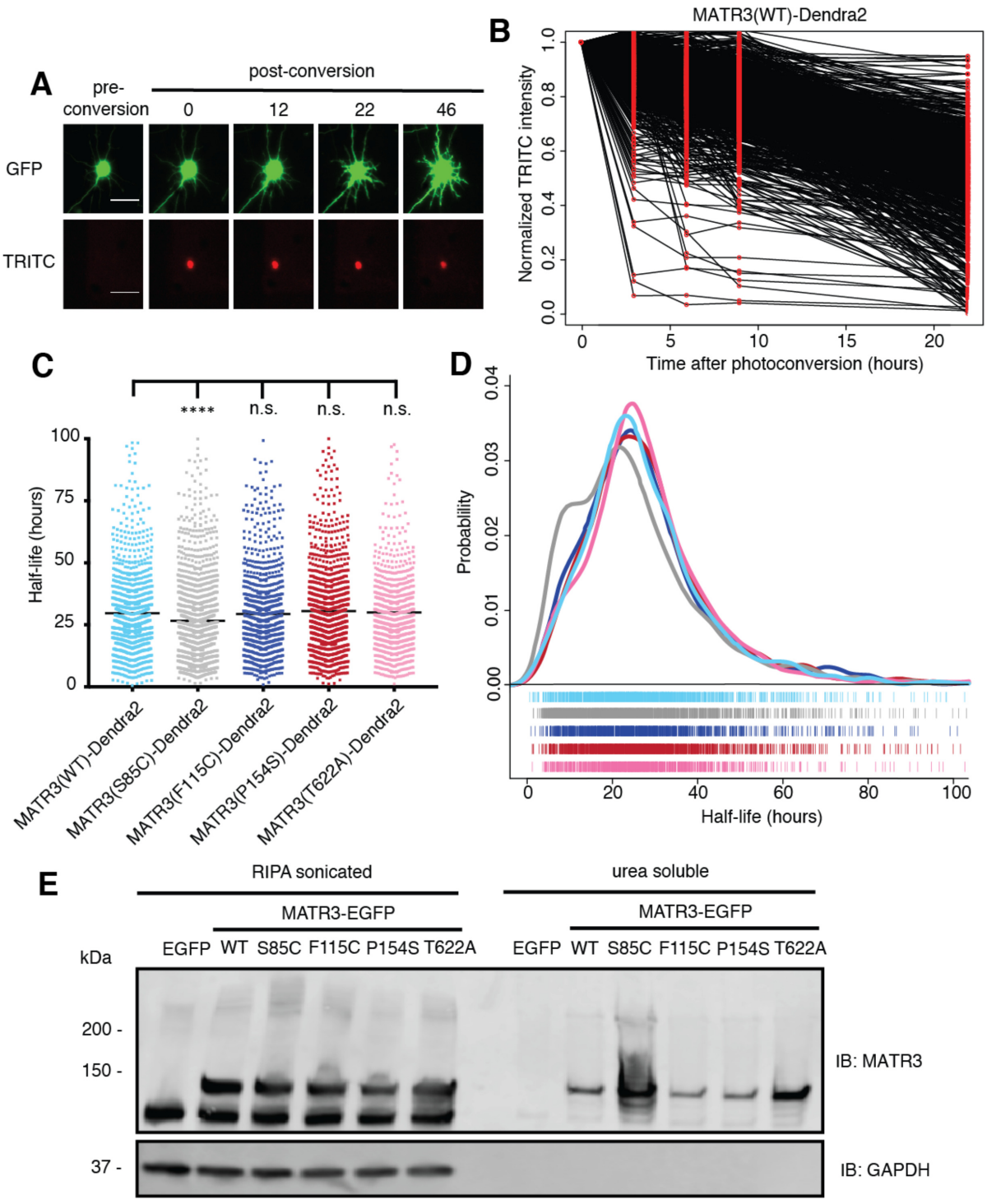

Figure 2.7. Pathogenic MATR3 mutations have little effect on MATR3 turnover, but a subset reduce solubility. A. Optical pulse labeling of Dendra2-tagged MATR3 variants. Each neuron is transfected with EGFP alone to outline the cell body, as well as MATR3-Dendra2, which fluoresces in the red channel (TRITC) upon photoconversion. Scale bar, 50 μm. **B.** Normalized red fluorescence (TRITC) signal for individual neurons.

The time-dependent decay of red fluorescence over time is used to calculate MATR3-Dendra2 half-life for each neuron. **C-D.** MATR3(S85C)-Dendra2 displayed a subtle but significant reduction in half-life compared to MATR3(WT)-Dendra2 (comparing to MATR3(WT)-Dendra2, n = 1269: MATR3(S85C)-Dendra2, n = 1670, **** $p < 0.0001$; MATR3(F115C)-Dendra2, n = 1122, $p > 0.9999$; MATR3(P154S)-Dendra2, n = 1509, $p = 0.9309$; MATR3(T622A)-Dendra2, n = 923, $p = 0.9989$; one-way ANOVA with Tukey's post-hoc test). **E.** Sonication in RIPA resulted in equivalent amounts of all MATR3 variants by Western blotting. The S85C variant was markedly enriched in the RIPA-insoluble, urea-soluble fraction, while the T622A variant showed more modest enrichment.

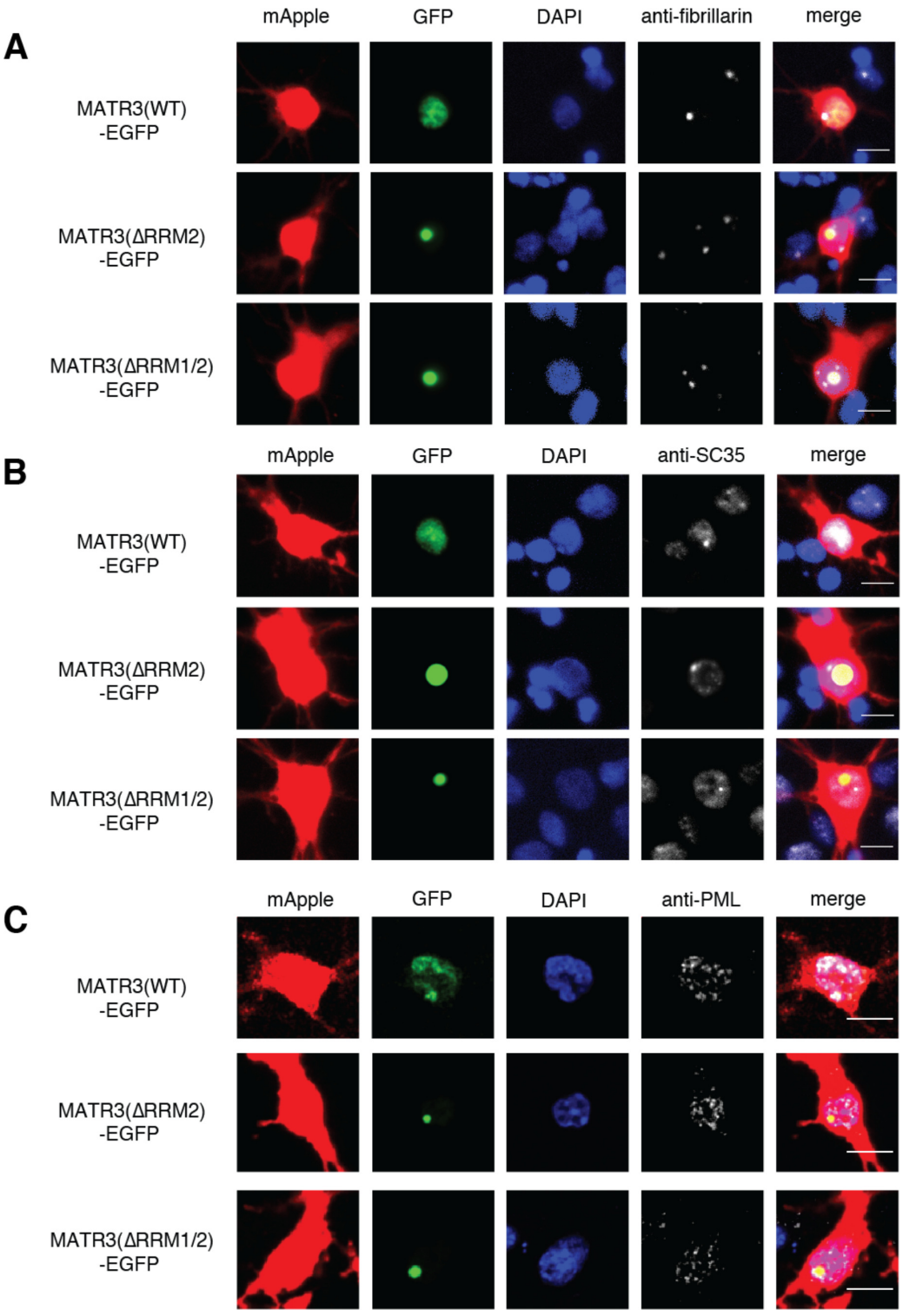

Supplemental Figure 2.1. MATR3(ΔRRM2)-EGFP and MATR3(ΔRRM1/2)-EGFP do not join preexisting subnuclear organelles. A-C. Immunostaining for nucleoli, speckles, and PML bodies using antibodies against fibrillarin, SC35, and PML, respectively, show no colocalization between MATR3(ΔRRM2)-EGFP and

MATR3(ΔRRM1/2)-EGFP granules and these nuclear structures. Scale bars in **(A)**, **(B)**, and **(C)**, 10 μm.

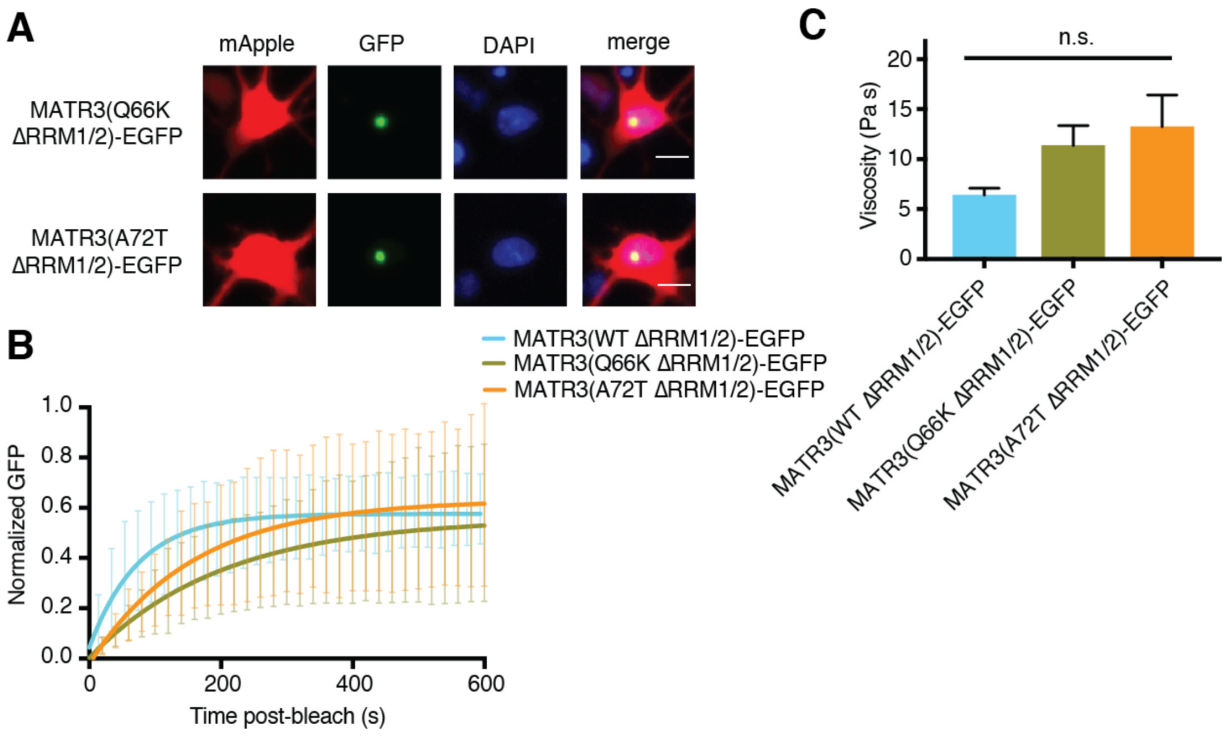

Supplemental Figure 2.2. Pathogenic N-terminal domain mutations other than S85C on the ΔRRM1/2 background do not affect granule viscosity. A. When expressed in rodent primary cortical neurons, the Q66K and A72T disease-associated mutations on MATR3(ΔRRM1/2)-EGFP form intranuclear granules. Scale bar, 10 μm. **B-C.** However, these mutants do not alter droplet viscosity (MATR3(WT ΔRRM1/2)-EGFP n = 5, MATR3(Q66K ΔRRM1/2)-EGFP n = 6, MATR3(A72T ΔRRM1/2)-EGFP n = 6; p = 0.11; one-way ANOVA). Curves in **(B)** show fitted curves ± SD.

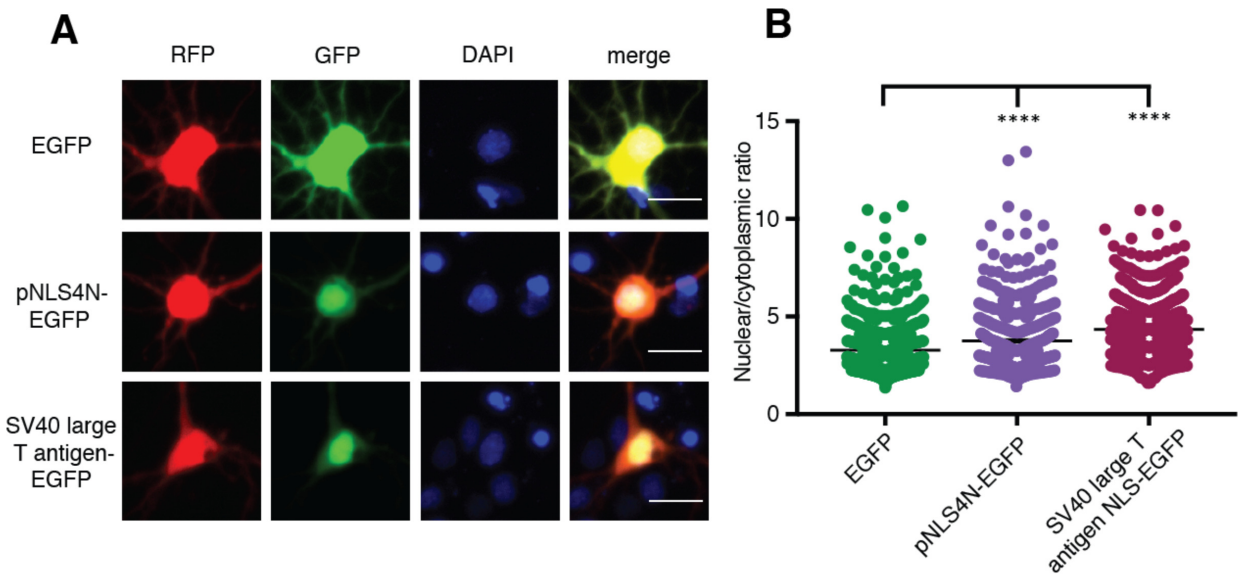

Supplemental Figure 2.3. The N-terminal arm of MATR3's bipartite NLS is capable of driving nuclear enrichment of a heterologous protein. A-B. Appending the eight amino acids of the pNLS4N sequence onto EGFP results in enhanced nuclear localization, comparable to the effect of the canonical SV40 large T cell antigen NLS (comparing to EGFP n = 877: pNLS4N-EGFP n = 601, $p < 0.0001$; SV40 large T cell antigen NLS-EGFP n = 1095, **** $p < 0.0001$; one-way ANOVA with Tukey's post-hoc test). Scale bar, 20 μm.

Table 2.1. Primer sequences for generating MATR3 domain deletions

Deletion mutation	Amino acids	Primers	Sequences
ΔZF1	288 –322	Forward	5'-CTT GAA ATC TAC CCA GAA TG-3'
		Reverse	5'-CTT CGG TAA GAG TCC ATG-3'
ΔZF2	798 – 833	Forward	5'-CTG AAT AAA TTG GCA GAA GAA C-
		Reverse	5'-AGG TAT CAC ATA GTC TAT ACC-3'
ΔRRM1	398 – 473	Forward	5'-TAT AAA AGA ATA AAG AAA CCT
		Reverse	5'-GCT AGT TTC CAC TCT GCC-3'
ΔRRM2	496 – 575	Forward	5'-GTT CTG AGG ATT CCA AAC AG-3'
		Reverse	5'-TCC AAG CTC TTG CTT TTG-3'

Table 2.2. Primer sequences for generating putative MATR3 NLS deletions

Deletion mutation	Amino acids	Primers	Sequences
ΔpNLS1	146 – 171	Forward	5'-AGA GTA CCT AGG GAT GAT TG-3'
		Reverse	5'-AAG CTG TAG AAG GAT TTG G-3'
ΔpNLS2	473 – 479	Forward	5'-CCT GAA GGA AAG CCA GAT C-3'
		Reverse	5'-CTG GGA TAA ATG AAC TCT CAC-3'
ΔpNLS3	571 – 574	Forward	5'-CTG GTT CTG AGG ATT CCA ACC-3'
		Reverse	5'-CTC AGA CAG GTC AAC CTT C-3'
ΔpNLS4	588 – 611	Forward	5'-ACT GAT GGT TCC CAG AAG-3'
		Reverse	5'-CAG TAA ATC AAT GCC TCT G-3'
ΔpNLS5	701– 720	Forward	5'-GAG GAA CTT GAT CAA GAA AAC-3'
		Reverse	5'-CAC AGC TTT ATC TGA TGG TTC-3'
ΔpNLS6	780 – 784	Forward	5'-CAG CCC AAT GTT CCT GTT G-3'
		Reverse	5'-ATA CTC ATC TGG GAT TGT ATA G-3'
ΔpNLS7	798 – 833	Forward	5'-GAA ACT ATG ACT AGT ACT AGA G-3'
		Reverse	5'-CTG ATA ATG AGG AAG GCT G-3'
ΔpNLS4N	588 – 595	Forward	5'-TCT TAC TCT CCA GAT GGC-3'
		Reverse	5'-CAG TAA ATC AAT GCC TCT G-3'
ΔpNLS4C	608 – 611	Forward	5'-ACT GAT GGT TCC CAG AAG-3'
		Reverse	5'-ATC ACT TGG AGA TTC TTT GC-3'

Table 2.3. Primer sequences for site-directed mutagenesis for pathogenic mutants

Mutation	Primers	Sequences
Q66K	Forward	5'-TTC TTC ATT GAA TAA ACA AGG AGC TC-
	Reverse	5'-GAG CTC CTT GTT TAT TCA ATG AAG AA-
A72T	Forward	5'-AAG GAG CTC ATA GTA CAC TGT CT-3'
	Reverse	5'-AGA CAG TGT ACT ATG AGC TCC TT-3'
S85C	Forward	5'-AAT TTG CAG TGT ATA TTT AAC ATT GG-3'
	Reverse	5'-ATG GGA AGA AGT ACT AGC AGA-3'
F115C	Forward	5'-ATT TTG GCC AGC TGT GGT CTG TCT
	Reverse	5'-GTT ACT GGC CTG GTC TGC ATC-3'
P154S	Forward	5'-GAA GAA GGC TCT ACC TTG AGT TAT GG-
	Reverse	5'-AGT TCT CCT CCT TTT AAG CTG-3'
T622A	Forward	5'-GAG AGT TCA GCC GAA GGT AAA GAA C-
	Reverse	5'-AGT CTT CTG GGA ACC ATC AGT-3'

Chapter 3: Neuronal Activity Regulates MATR3 Through Calpain-Mediated Degradation and Calmodulin-Dependent Inhibition of RNA Binding

3.1 Abstract

RNA-binding protein (RBP) dysfunction is a fundamental hallmark of amyotrophic lateral sclerosis (ALS) and related neuromuscular disorders. Alterations in neuronal activity are observed in patients and in disease models, though little is known about how activity-dependent processes regulate RBP levels and functions. Mutations in the gene encoding the DNA- and RNA-binding protein Matrin 3 (MATR3) cause familial disease, and MATR3 pathology has also been observed in sporadic ALS, suggesting a key role for MATR3 in pathogenesis. Here, we show that glutamatergic activity drives MATR3 degradation through a NMDAR-, Ca^{2+}-, and calpain-dependent mechanism and that the most common pathogenic mutation in MATR3 renders it resistant to calpain degradation. We also demonstrate that Ca^{2+} regulates MATR3 through a non-degradative process involving the binding of Ca^{2+}/calmodulin (CaM) to MATR3 and inhibition of its RNA-binding ability. These findings indicate that neuronal activity reduces MATR3 abundance and impairs its RNA-binding functions and provides a foundation for further study of Ca^{2+}-coupled regulation of RBPs implicated in ALS and related neurological diseases.

3.2 Introduction

Amyotrophic lateral sclerosis (ALS) is a neurodegenerative disease involving the death of both upper and lower motor neurons and resulting in muscle weakness, paralysis, and ultimately death. ALS shares clinical, genetic, and pathological overlap with frontotemporal dementia (FTD), a disorder characterized by the degeneration of neurons in frontal and temporal cortices that results in markedly altered behavior and speech[1]. Accumulating evidence points to dysfunction in RNA-binding proteins (RBPs) as underlying ALS/FTD spectrum disease, with the vast majority of patients with ALS and approximately half of those with FTD displaying aggregation and/or mislocalization of the RBP TDP-43 in affected tissues on autopsy[2,3]. Moreover, while most cases of ALS and FTD are sporadic, rare mutations including many in genes encoding RBPs can cause inherited, familial disease[4-7].

To date, a number of disease-linked RBPs have been identified, and for a subset of these the phenotypic spectrum extends beyond neurons to skeletal muscle, manifesting as myopathies[8,9]. One such RBP is Matrin 3 (MATR3), a nuclear protein with two zinc finger (ZF) domains and two RNA recognition motifs (RRMs) and the capacity to bind both DNA and RNA targets[10-12]. Over a dozen point mutations in MATR3 have been reported in ALS, combined ALS/FTD, or a form of distal myopathy to date[13-21], and MATR3 pathology—consisting of mislocalization, changes in abundance, and aggregation—has been found in motor neurons of sporadic ALS patients[22,23], suggesting a fundamental link between MATR3 dyshomeostasis and neuromuscular disease.

Alterations in neuronal activity have been linked to the pathogenesis of ALS and related disorders in patients[24-26] and in a variety of models, with both hypo- and hyperexcitability phenotypes reported depending on neuronal population studied, model system, and disease progression[27-31]. Although regulation of RBP abundance and function in response to activity is incompletely understood, there are numerous examples of RBPs controlled by receptor activation or depolarization[32-35]. This indicates that investigations of disease-linked RBPs in the context of neuronal activity may shed light onto both basic physiology and pathogenic mechanisms. In previous studies, MATR3 was found to be degraded in cerebellar granule neurons after treatment with N-methyl-D-aspartate (NMDA) in a protein kinase A (PKA)-dependent manner. Additionally, it was reported to bind *in vitro* to Ca^{2+}-bound calmodulin (CaM), a major protein in Ca^{2+} signal transduction that after binding Ca^{2+} changes conformation and rapidly shuttles to the nucleus to drive the expression of plasticity-related transcriptional programs[36-40]. These findings from the literature motivated us to investigate the mechanism and functional consequences of activity-dependent regulation of MATR3.

In this study, we present data showing that MATR3 in primary cortical neurons is degraded after glutamatergic stimulation through an NMDAR-, Ca^{2+}-, and calpain-dependent pathway and that similar clearance occurs *ex vivo* in cerebellar Purkinje neurons. On a shorter timescale than degradation, MATR3's interaction with Ca^{2+}/CaM inhibits its ability to bind RNAs, and we present data hinting that binding to Ca^{2+}/CaM may similarly tune the function of many other RBPs associated with ALS/FTD spectrum disorders.

3.3 Results

3.3.1 Glutamatergic stimulation reduces MATR3 through an NMDAR-dependent mechanism

We first sought to determine whether NMDAergic stimulation of rodent primary cortical neurons leads to MATR3 degradation in accordance with previous reports. We found that treatment of NMDAergically mature DIV14-16 cultures with NMDA resulted in a rapid, time-dependent decrease in MATR3 protein abundance (Fig. 3.1A-B). Notably, and in contrast to previous work, we observed only a small blunting of NMDA-dependent MATR3 clearance by the PKA inhibitor H89 (Supplemental Fig. 3.1A-B). Additionally, while we noted an increase in phosphorylated MATR3 as assessed via a PKA phospho-substrate antibody upon short NMDA treatment, this enhanced phosphorylation was not blocked by H89 (Supplemental Fig. 3.1C-D), suggesting that another kinase phosphorylates MATR3 at a residue recognized by this antibody. These points of departure from studies done in cerebellar granule neurons led us to conclude that phosphorylation of MATR3 by PKA did not drive MATR3 clearance and instead motivated us to closely examine the mechanism of MATR3 reduction in cortical neurons in response to NMDA stimulation.

To dissect the neuropharmacology of this process, we asked whether glutamate, the endogenous agonist for NMDARs as well as all other glutamatergic receptors, likewise results in MATR3 decrease. Treatment with equivalent doses of NMDA or glutamate for 3 hours resulted in comparable reduction of MATR3 immunoreactivity in MAP2-positive neurons without aggregation or changes in nucleocytoplasmic distribution, indicating that MATR3 clearance occurs in the nuclear compartment in

response to both agonists (Fig. 3.1C-D). Dose-response experiments with NMDA and glutamate likewise confirmed that both compounds were able to effectively drive reduction of MATR3 protein (Fig. 3.1E-G).

Neurons express a variety of receptors activated by glutamate, including the ionotropic kainate, AMPA, and NMDA receptors as well as a host of metabotropic receptors that do not directly pass Na^{1+} or Ca^{2+} and instead accomplish their function via intracellular second messengers (Fig. 3.2A). We asked whether NMDA receptor stimulation is necessary for MATR3 degradation in addition to being sufficient or if any form of glutamatergic stimulation can clear MATR3. Treatment with AP5, a selective antagonist of NMDARs, had no effect on MATR3 abundance on its own but blocked the effect of not only NMDA—as expected from coadministration of the agonist and the antagonist—but also impaired degradation in response to glutamate (Fig. 3.2B-C). This indicates that the activation of no other glutamatergic receptor is able to reduce MATR3 and that NMDAR stimulation is both necessary and sufficient for this process.

3.3.2 MATR3 reduction after NMDAR activation is Ca^{2+}-dependent

Canonical NMDARs are largely unique among the main classes of glutamatergic receptors in being permeable to both Ca^{2+} or Na^{1+}, and so we wondered whether the dependence of MATR3 clearance on NMDARs stems from this process being dependent on Ca^{2+}. To answer this, we treated neurons with the Ca^{2+} chelator BAPTA before NMDA treatment and found that this chelation blocked NMDA-induced reduction in MATR3, indicating that MATR3 clearance requires Ca^{2+} entry into the cell (Fig. 3.2D-E). If an increase in intracellular Ca^{2+} is the mechanism downstream of NMDAR

activation that drives MATR3 reduction, we would expect non-physiological increase in intracellular Ca^{2+} independent of receptor engagement to mimic this effect. Indeed, treatment with the ionophore ionomycin resulted in MATR3 protein decrease not only in NMDAergically mature DIV14-16 neurons (Fig. 3.2F-G) but also in NMDAergically immature DIV4-5 cells (Fig. 3.2H-I), indicating that increased intracellular Ca^{2+} is both necessary and sufficient for MATR3 reduction and does not require NMDAR machinery. Notably, ionomycin in HEK293T and Neuro2A cell lines did not result in MATR3 decreases, suggesting that the Ca^{2+}-dependent mechanisms responsible may rely on neuron-specific or neuron-enriched factors (Supplemental Fig. 3.2A-B).

3.3.3 NMDA-mediated reduction in MATR3 occurs post-transcriptionally through proteolytic degradation by calpains

Neuronal Ca^{2+} signaling modulates a variety of transcriptional and post-transcriptional pathways that could be responsible for altering protein abundance, and so we wondered whether the reduction in MATR3 we observed upon NMDAR stimulation and downstream Ca^{2+} entry represents a decrease in the production of MATR3 or degradation of existing MATR3. Using RT-PCR, we observed only a weak trend towards reduced *Matr3* transcript with stimulation (Fig. 3.3A), which—along with the rapid timeframe of reduction (Fig. 3.1B)—points to degradation of MATR3 rather than robust transcriptional downregulation as the mechanism for its reduction. In a complementary experiment, we transduced cultures with lentivirus expressing FLAG-tagged MATR3. This construct expressed from exogenous cDNA would be expected to be unaffected by transcriptional or post-transcriptional mRNA control, and thus any

NMDA-induced changes in this protein's abundance would come from post-translational degradation. Indeed, NMDA treatment resulted in the rapid reduction of this protein as determined by probing with a FLAG antibody (Fig. 3.3B), supporting a model in which NMDAR stimulation causes clearance of existing MATR3 protein.

We next asked what Ca^{2+}-dependent proteolytic pathway is responsible for MATR3 clearance, first seeking to determine whether NMDA-triggered degradation occurs through autophagy or through another proteolytic system. Treating neurons with NMDA in the absence or presence of bafilomycin—a inhibitor of the lysosomal acidification necessary for autophagic degradation[41]—or of MG132, which inhibits cysteine proteases as well as the threonine proteases of the proteasome[42] revealed that MATR3 turnover is completely blocked by MG132 but unaffected by bafilomycin (Fig. 3.3B-C). This suggests that MATR3 degradation downstream of a rise in intracellular Ca^{2+} is executed by the ubiquitin-proteasome system (UPS) or by cysteine proteases. Treatment of neurons with bortezomib, a specific inhibitor of the 26S proteasome subunit[43], failed to inhibit MATR3 degradation in response to NMDA, indicating that another MG132-sensitive protease other than those of the UPS is responsible for degrading MATR3 (Fig. 3.3D-E). Further supporting that NMDA-mediated MATR3 degradation is not from the UPS, we saw no accumulation of higher molecular weight, ubiquitinated MATR3 species in neurons treated with MG132 and NMDA from which MATR3 was immunoprecipitated (Supplemental Fig. 2C). Therefore, we asked whether calpains, a group of Ca^{2+}-activated cysteine proteases, may be cleaving MATR3. Treatment with MDL28170, a specific inhibitor of calpains, blocked NMDA-induced degradation (Fig. 3.3F-G), pointing to calpains as the effector proteases of NMDA-

mediated degradation. Notably, we were not able to detect lower molecular weight species of MATR3 produced by calpain cleavage NMDA treatment, even in the context of proteasomal inhibition by bortezomib and using antibodies targeting both N- and C-termini of MATR3 (Supplemental Fig. 3.3A-B). These results are in alignment with previous reports demonstrating that proteolytic fragments produced by calpain cleavage may be extremely unstable and difficult to detect biochemically[44,45].

The two calpains most expressed in the nervous system are calpain 1 (CAPN1) and calpain 2 (CAPN2), with CAPN1 enriched in neurons and CAPN2 enriched in glial cells[46,47]. Although increased Ca^{2+} was not sufficient to drive MATR3 degradation in HEK293T cells (Supplemental Fig. 3.2A), we wondered whether overexpression of CAPN1 or CAPN2 in this cell line could result in MATR3 turnover compared to a control transfection with the fluorescent protein mApple. In previous studies, overexpression of these proteins in HEK293T cells resulted in CAPN1 and CANP1 activation even without the addition of Ca^{2+} due to low expression of the endogenous calpain inhibitor calpastatin, increased basal Ca^{2+} concentration in these cells compared to neurons, or a combination of these and other factors[48,49]. We noted reduced levels of endogenous MATR3 upon CAPN1 but not CAPN2 expression (Fig. 3.4A-B), suggesting that MATR3 is a substrate for CAPN1 but not CAPN2 cleavage.

An online algorithm[50] for identifying putative calpain sites predicted a strong candidate for a CAPN1 cleavage site at residues 82-85 of MATR3 (Fig. 3.4C). Intriguingly, this stretch of amino acids includes S85, a residue altered in the most common pathogenic point mutation in MATR3, S85C. We wondered whether this mutation alters the putative CAPN1 site so as to impair cleavage by CAPN1 and

therefore inhibit degradation. Cotransfection experiments of HEK293T cells with mApple, CAPN1, or CAPN2 and FLAG-tagged MATR3 variants followed by immunoblotting using a FLAG antibody revealed that while exogenous FLAG-MATR3(WT) was degraded by CAPN1 to a comparable degree as endogenous MATR3, FLAG-MATR3(S85C) was completely resistant to CAPN1-mediated cleavage (Fig. 3.4D-E). Taken together, these data present a model in which neuronal depolarization results in MATR3 degradation through an NMDAR-, Ca^{2+}-, and calpain-dependent manner and that this regulatory pathway is impaired by the disease-linked S85C mutation.

3.3.4 Glutamatergic stimulation drives MATR3 clearance in an *ex vivo* system

We wondered whether this activity-dependent degradative pathway identified in primary cortical neurons applies to other neuronal types in other areas of the brain. In particularly, Purkinje cells of the cerebellum intrigued us as a model in that they have been reported to display striking heterogeneity in cell-to-cell MATR3 abundance[51] as well as to exhibit altered MATR3 metabolism and unique degeneration in a model of MATR3-mediated disease[52]. To investigate MATR3 clearance in Purkinje cells, we generated acute cerebellar slices from wild-type C57BL/6J mice that were then treated with vehicle or glutamate before fixation and immunostaining for MATR3 and for the Purkinje cell marker calbindin (Fig. 3.5A). Analysis of these slices revelated that, similar to neurons isolated from cortex (Fig. 3.1C-D), Purkinje neurons treated with glutamate had markedly weaker MATR3 immunoreactivity compared to vehicle-treated slices (Fig. 3.5B-C). These data indicate that mechanisms of degrading MATR3 upon glutamatergic

stimulation apply beyond primary cortical neurons and may explain previous reports of MATR3 in Purkinje neurons.

3.3.5 Ca^{2+} promotes a selective interaction between Ca^{2+}/CaM and MATR3

While our results involving long-term NMDAergic stimulation supports a model in which elevated Ca^{2+} over the course of hours drives MATR3 clearance, we wondered whether stimulation on shorter, more physiologic timescales could also tune MATR3 function. Beyond activation of calpains, Ca^{2+} has numerous rapidly transduced signaling roles in neurons. Many of these are affected through calmodulin (CaM), a ubiquitous and highly conserved protein that, upon binding Ca^{2+} ions, undergoes conformational changes that can greatly alter its binding properties to other proteins, resulting in their activation or inhibition. Notably, previous studies have reported that MATR3 binds selectively to Ca^{2+}/CaM but not free CaM, with the binding region overlapping with RRM2 of MATR3, suggesting an activity-mediated, Ca^{2+}-dependent interaction on a functional domain of MATR3.

We first sought to reproduce these previous results. Using publicly available informatics algorithms to identify CaM-binding sites[53-55], we found a high confidence site predicted in MATR3 overlapping with RRM2 corresponding to a fragment that had previously been shown to be sufficient to bind CaM (Fig. 3.6A)[56]. Repeating these analyses with other RBPs linked to ALS/FTD showed a markedly similar pattern of CaM-binding sites predicted on the RRMs of these proteins, suggesting that CaM-RBP interactions may extend beyond MATR3.

To validate these predicted binding events, we incubated lysates from HEK293T cells with CaM-conjugated sepharose beads in the presence of Ca^{2+}. Following washing, elution was accomplished by incubation with a Ca^{2+} chelator, stripping Ca^{2+} from CaM, returning CaM to its apo conformation, and selectively liberating those proteins that bind to Ca^{2+}/CaM. We found that both MATR3 and TDP-43 bind CaM in a Ca^{2+}-dependent manner, recapitulating previous findings on MATR3 and suggesting that selective CaM binding may extend to other RBPs as well. Focusing our studies on MATR3, we sought to further confirm the selectivity of its interaction with CaM. For this, we incubated lysates with CaM-conjugated beads in the absence or presence of W-7, a small molecule inhibitor that impairs CaM's ability to adopt its activated confirmation even in the presence of Ca^{2+}. Incubation with W-7 resulted in no Ca^{2+}-dependent binding of MATR3, indicating that Ca^{2+} does not promote the CaM-MATR3 interaction through any effects on MATR3 but rather through the Ca^{2+}-triggered conformational changes in CaM (Fig. 3.6C).

3.3.6 Activity rapidly impairs MATR3 binding to target RNAs

What is the functional effect of this binding between Ca^{2+}/CaM and MATR3? We hypothesized that, given the mapping of the CaM-binding site to RRM2, this may represent a mechanism to impair RNA binding by MATR3. CaM is a small protein capable of passing into the nucleus by passive diffusion and thus is found distributed diffusely in the cell. Upon neuronal depolarization, however, CaM has been reported to rapidly become slightly enriched in the nucleus to drive the expression of activity-dependent genes, though the extent of this nuclear shuttling is dependent on

experiment stimulus and cell type. We found that in primary cortical neurons treated with NMDA, CaM becomes modestly more nuclear in a matter of minutes, consistent with previous reports (Fig. 3.7A-B). This enhanced nuclear localization, along with its adoption of the activated Ca^{2+}-bound conformation, would be expected to enhance its association with resident nuclear proteins like MATR3.

Based off the predicated and experimentally confirmed CaM-binding site on MATR3, we hypothesized that depolarization and resulting Ca^{2+} increase impair MATR3's RNA binding by displacing already bound RNAs or preventing new binding events. To test this, we turned to UV CLIP followed by RT-PCR for previously identified MATR3 RNA targets. We irradiated primary neurons after minutes of NMDA or vehicle application to form crosslinks with RNA in a fraction of MATR3 molecules, followed by immunoprecipitation of MATR3 and harsh washing conditions to selectively retain those transcripts that were covalently bound to MATR3 at the time of irradiation (Fig. 3.7C-D). After digesting protein, isolating RNA, and conducting RT-PCR for transcripts MATR3 binds, we found that while levels of these RNAs were not different in input samples, MATR3 pulled down significantly less RNA when crosslinked in the context of NMDA stimulation, indicating that Ca^{2+}/CaM impairs RNA recognition by MATR3 and thus reduces protein function without reducing its abundance.

We wondered what effect CaM activation has on the longer timescale degradation of MATR3. Using W-7 to prevent Ca^{2+}/CaM's adoption of its active conformation and treated neurons with NMDA for 3 hrs, we saw that CaM inhibition blocked degradation (Supplemental Fig. 4A-B). A previous study demonstrated that TDP-43 variants that are deficient in RNA binding are destabilized[57], and so we asked

whether CaM activation might promote MATR3 clearance by inhibiting its RNA binding and, fundamentally, whether MATR3 like TDP-43 is intrinsically unstable when it cannot effectively bind RNA. To answer this, we turned to optical pulse labelling (OPL), a technique in which proteins of interest are fused to the photoconvertible protein Dendra2 and expressed in primary neurons. After illumination with UV light, Dendra2 undergoes an irreversible green-to-red conversion, and so neurons can be imaged over the course of hours or days with the decay in red signal over time used to calculate protein half-life. Using this method, we found that a variant of MATR3 with its key RNA-binding domain deleted (ΔRRM2) had no difference in stability compared to MATR3(WT)-Dendra2, suggesting that impaired RNA binding per se does not destabilize MATR3 and that CaM inhibition may prevent MATR3 degradation through other, Ca^{2+}-dependent mechanisms, as discussed below.

3.4. Discussion

In this work, we aimed to examine physiological regulators of MATR3 function in neurons. Building off previous studies, we first examined the mechanism of MATR3 degradation in response to NMDAergic stimulation. Unlike what has been reported for cerebellar granule neurons, we did not find MATR3 to be a PKA substrate in cortical neurons and observed PKA inhibition to only mildly blunt MATR3 clearance upon NMDA treatment. Rather, we found that in these cells MATR3 reduction is accomplished through a Ca^{2+}- and calpain-dependent degradative mechanism. We confirmed the sufficiency of the neuronally enriched CAPN1 to clear MATR3 in HEK293T cells and, directed by a prediction of the likely CAPN1 cleavage site, found that the most common

pathogenic MATR3 mutant, S85C, alters this site and renders the protein resistant to CAPN1 cleavage.

Extending our findings beyond primary neurons into an *ex vivo* system, we found that cerebellar Purkinje neurons—a cell type previously reported to display altered MATR3 metabolism at baseline and in disease models—likewise clear MATR3 in response to glutamatergic stimulation. Seeking to investigate rapid, non-degradative regulation after neuronal activity, we pursued the binding between Ca^{2+}/CaM and a sequence on MATR3 overlapping its RRM2, experimentally confirming this for MATR3 and TDP-43 but also finding that according to prediction algorithms many disease-associated RBPs have CaM-binding motifs in their RRMs. Functionally, we found that Ca^{2+}/CaM enriches in the nucleus after activation and that this is associated with impaired MATR3 binding to its RNA substrates.

Our results in cortical neurons conflict with those observed in cerebellar granule neurons, in which PKA inhibition by H89 completely blocks MATR3 degradation in response to NMDA and prevents MATR3 phosphorylation as detected using a PKA phospho-substrate antibody[58]. We found H89 to have no effect on the phosphorylation of MATR3, indicating that this is done by another kinase that phosphorylates a residue in a RRXpS/T motif that both forms the consensus PKA substrate motif and is the immunogen against which this antibody is raised[59,60]. The identity of this kinase that phosphorylates MATR3 after NMDA activation remains unknown, as is whether this modification has any functional significance.

While a previous study showed that PKA inhibition by H89 completely blocked MATR3 degradation upon NMDAergic stimulation, we noted only a modest blunting.

This may in turn be due to non-MATR3 targets of PKA that are nevertheless involved in Ca^{2+} dynamics. Namely, PKA—itself activated by Ca^{2+}/CaM through adenylyl cyclase activation[61-63]—phosphorylates key residues on the intracellular portions of NMDARs, thereby rendering them more conductive for Ca^{2+} and so increasing intracellular Ca^{2+} in a feedforward-type mechanism[64,65]. The blunted MATR3 clearance we observe upon PKA (Supplemental Fig. 1C-D) and CaM inhibition (Supplemental Fig. 4A-B) might therefore be not from any selective effects of these molecules on MATR3 but rather on their augmenting of NMDAR Ca^{2+} currents as part of the complex crosstalk between Ca^{2+} and Ca^{2+}-dependent signaling pathways in neurons.

We found instead that the rapid decrease over a matter of hours in MATR3 abundance after NMDA treatment is dependent on Ca^{2+}, and elevated Ca^{2+} is sufficient to drive degradation in both NMDAergically mature DIV14-16 and immature DIV4-5 neurons, indicating the key function of Ca^{2+} in this mechanism even without NMDAR recruitment. Although increases in intracellular Ca^{2+} can activate a number of proteolytic pathways including autophagy[66,67] and the UPS[68,69], we found that neither of these processes were responsible for MATR3 clearance, as specific inhibitors of autophagy and the proteasome did not impair MATR3 reduction. Rather, a selective calpain inhibitor blocked NMDA-triggered degradation, indicating that these are the final effectors of this pathway.

A number of other studies have demonstrated calpain cleavage of RBPs involved in the pathogenesis of ALS/FTD and related disorders. Activated calpains degrade survival motor neuron (SMN)[70] and have been shown *in vitro* and *in vivo* to cleave TDP-43[71], with phosphorylation of TDP-43 impairing this process[72]. MATR3 is abundantly

phosphorylated[73], and whether any post-translational modifications of MATR3 likewise tune its susceptibility to calpain cleavage are unknown. Overexpression of calpastatin, an endogenous negative regulator of calpains, inhibited cleavage of calpain targets while increasing motor function and survival in a transgenic mutant SOD1 mouse model of ALS, though the translation relevance of these findings to human disease are not clear[74].

Although the functional consequences of the degradation of these disease-linked RBPs and of MATR3 are unknown, they may form a feedback mechanism for regulating neuronal activity as is the case for cytoplasmic polyadenylation element binding protein 3 (CPEB3). This RBP negatively regulates glutamatergic synapse strength by translationally repressing mRNAs that encode receptor subunits and synapse scaffolding proteins[75]. In response to NMDAR stimulation, Ca^{2+} activates CAPN2, which cleaves CPEB3, thereby derepressing its targets and presumably resulting in local synaptic strengthening through the expression of plasticity-related proteins[76].

Ca^{2+} and calpains also regulate RBPs beyond simply degrading them, though these mechanisms are less studied. Increases in cellular Ca^{2+} result in the cytoplasmic redistribution of TDP-43 and the ALS-linked RBP FUS[77], while this same stimulus drives the nuclear enrichment of CPEB4[78], indicating that Ca^{2+} can bidirectionally regulate localization depending on the RBP. Calpains may function in this process, as an RNAi screen of calcium signaling proteins in *Drosophila* revealed calpain A to be critical for TDP-43 cytoplasmic localization after Ca^{2+} increase[79], and degradation of nuclear pore complex components by Ca^{2+}-activated calpains resulted in aberrant nucleocytoplasmic transport in mouse CNS[80]. Notably we did not detect any changes in distribution after

NMDA treatment (Fig. 3.1C), suggesting that Ca^{2+}- and calpain-mediated regulation of MATR3 may be purely through altering its abundance and not its localization.

In testing MATR3 susceptibility to the two main calpains present in the CNS, we found that WT protein—but not the pathogenic S85C mutant with an alteration in the predicted CAPN1 cleavage site—is a substrate of CAPN1 (Fig. 4.D-E). This mutation is the most common disease-linked variant in *MATR3*, with a phenotypic spectrum that encompasses both ALS and distal myopathy with vocal cord and pharyngeal weakness (VCPDM)[14,81-83]. In patient tissue[13] as well as cellular[84] and animal[52,85,86] models, this mutation reduces MATR3 solubility through unknown mechanisms. It is possible that inability to be cleaved by CAPN1 is responsible for accumulation and aggregation of this mutant into an insoluble fraction; alternatively, insolubility may be upstream, with localization to an insoluble cellular compartment inaccessible to CAPN1 rendering this variant resistant to cleavage. Like neurons, skeletal muscle cells are excitable and rely not only on Ca^{2+} levels for their function but also on CAPN1 activation as a proteolytic mechanism to control myofiber size and number[87]. Therefore, our finds may offer insight on the unique disease spectrum of the S85C mutation that encompasses motor neuron and skeletal muscle pathology.

In *ex vivo* experiments we observed that, like cortical neurons, Purkinje cells of the mouse cerebellum clear MATR3 upon glutamatergic stimulation. This neuronal subtype has previously been shown to display marked heterogeneity in MATR3 immunostaining on a cell-by-cell basis[51], and our data suggest that differences in Purkinje cell activity may explain disparities in MATR3 abundance. Future experiments might seek to determine what the timeframe is of *in vivo* physiological activation needed

to drive MATR3 clearance, perhaps through motor tasks for vestibular system activaiton[88]. Intriguingly, a knock-in mouse homozygous for the S85C mutation exhibited markedly reduced MATR3 staining in Purkinje cells from an early timepoint followed by age-dependent Purkinje cell death[52]. The mechanism for how this mutation results in aberrant MATR3 metabolism in Purkinje neurons, however, in unclear, as are its implications for human genetics since no *MATR3* mutation identified to date causes cerebellar disease.

In investigating a dynamic, non-degradative regulation of MATR3 by Ca^{2+} we focused on the selective, Ca^{2+}-dependent interaction between CaM and MATR3. Using algorithms for predicting CaM-binding motifs, we found that many other RBPs are also predicted to associate with CaM, and we confirmed this for TDP-43. The Ca^{2+}/CaM binding region for MATR3 has been experimentally demonstrated to overlap with RRM2, and the predicted motifs for other RBPs are also in RNA-binding domains, suggesting a functional effect on nucleic acid binding. To test this for MATR3, we compared its binding to RNA targets between vehicle- and NMDA-treated conditions and found that neuronal activity significantly reduces MATR3's association with substrate RNAs. Despite decades of work on CaM-dependent signal transduction, to our knowledge direct binding of CaM with RBPs to modulate their association with target RNA has only been demonstrated in two instances: for *Arabidopsis* CPSF30[89] and for the CNS-specific mammalian PCP4[90]. Our preliminary results for MATR3 and TDP-43 combined with predictions for other RBPs suggest that this may be a widely applicable Ca^{2+}-dependent mechanism, and the implications of this for neuronal physiology are discussed at length in chapter 4.

In the work presented here, we have shown that glutamatergic stimulation and the resulting increase in Ca^{2+} results in suppression of MATR3 function through two mechanisms. Over the longer timescale, activation of calpains leads to degradation of MATR3 through cleavage, and on a more rapid timeframe, Ca^{2+}/CaM binding to MATR3 impairs its ability to bind RNAs, representing degradative and non-degradative means of inhibiting MATR3, respectively. What consequences these regulatory processes have on MATR3 gene targets, particularly those that encode for activity-related proteins, are currently unclear, as are the implications of this Ca^{2+}-mediated control for neuronal physiology and for RBP-linked neuromuscular disease. It is our hope that continued work in this field will offer insights on both the basic biology of dynamic RNA regulation and on perturbations in this process and that these insights may be leveraged for therapies targeting neurological disorders

3.5 Materials and methods

Plasmids and expression vector delivery:

For lentiviral expression plasmids, the FLAG-MATR3 ORF was isolated using HpaI sites from pGW1 FLAG-MATR3-Dendra2 constructs and cloned into pLV EF1a plasmid containing HpaI sites. CAPN1 (#60941) and CAPN2 (#60942) overexpression constructs were purchased from Addgene. Expression plasmids for pGW1 CMV FLAG-MATR3(WT) and FLAG-MATR3(S85C) were generated by using Q5 Hot Start High-Fidelity DNA Polymerase (New England Biolabs) and flanking primers to delete linker sequences and EGFP from pGW1 CMV FLAG-MATR3-EGFP constructs used from previous studies[84], and this deletion strategy was also used for creating

MATR3(ΔRRM2)-Dendra2. HEK293T cells (ATCC CRL-3216) were transfected in a 6-well plate with 3 µg per well of DNA per well with Lipofectamine 2000 (ThermoFisher) in accordance with the manufacturer's instructions. For lentivirus experiments, viral particles were generated by the University of Michigan Vector Core and neurons transduced at DIV5-6 overnight. The next day, media was removed from cells, after which they were washed once in PBS before being placed in virus-free condition media until experimentation on DIV14-16.

Primary cortical neuron culture and pharmacological treatment:

Primary cortical neurons were isolated from E19-20 rats and plated as previously described[91]. Neurons were treated at DIV14-16 with 100 µM NMDA (Sigma) or L-glutamate (Sigma) for 3 hrs or at the doses and times detailed in Fig. 1. For blocking experiments, cells were cotreated with 100 µM D-AP5 (Tocris), 10 µM MG132 (Sigma), 20 nM bafilomycin (Sigma), 100 nM bortezomib (Sigma), or 20 µM MDL28170 (ThermoFisher). For Ca^{2+} chelation and PKA inhibition experiments, neurons were pretreated for 30 min before NMDA application with 2 mM BAPTA (Cayman Chemical) or 20 µM H89 (Tocris), respectively. In studies increasing Ca^{2+}, ionomycin (ThermoFisher) was applied at 10 µg/mL for 3 hrs. For cerebellar slice experiments, slices were incubated with 500 µM glutamate or vehicle for 3 hrs. All pharmalogical treatments were done at 37°C.

Immunoblot:

For protein immunoblot, cells were washed in PBS and lysed in RIPA buffer (Pierce) supplemented with cOmplete protease inhibitor (Roche) and, for experiments of phospho-MATR3, with PhosSTOP phosphatase inhibitor (Roche) as well. Resuspended cells were sonicated using a Fisherbrand Model 505 Sonic Dismembrenator (ThermoFisher) at 80% amplitude with 5 s on/5 s off cycles for 2 min, and lysates were cleared by centrifugation at 21,000 x g at 4°C for 15 min. 5-20 µg protein were loaded onto 4-20% SDS-PAGE gels (Biorad) and run at 100 V, after which proteins were transferred onto 0.2 µm PVDF membranes (Biorad) at 100 V for 2 hrs at 4°C. Membranes were incubated in blocking buffer (3% BSA in 0.2% tween-20 in Tris-buffered saline (TBST)) and then blotted with the following primary antibodies diluted in blocking buffer: 1:1000 rabbit anti-MATR3 N-terminus (Abcam EPR10634(B)) for all blots except for Supplemental Fig. 2 as noted, 1:1000 mouse anti-GAPDH (MiliporeSigma MAB374), 1:1000 rabbit anti-MATR3 C-terminus (Abcam EPR10635(B)) for Supplemental Fig. 2B, 1:100 mouse anti-ubiquitin (Santa Cruz sc-8017), 1:5000 rabbit anti-TDP-43 (Proteintech 10782-2-AP), 1:1000 rabbit anti-phospho-PKA substrate (Cell Signaling #9624). The following day they were washed 3 x 5 min in TBST and incubated with donkey anti-mouse 800 (LI-COR 925-32213) and donkey anti-rabbit 680 (LICOR 926-68073), both diluted 1:10,000 in blocking buffer, for 1 hr at RT. Membranes were then washed again 3 x 5 min in TBST and imaged on an Odyssey CLx Imaging System (LI-COR).

Immunocytochemistry:

Primary cortical neurons were fixed in 4% PFA in PBS supplemented with 2 mM $CaCl_2$ at RT for 10 min, permeabilized with 0.1% Triton X-100 in PBS, and treated with 10 mM glycine in PBS. They were then placed in ICC blocking solution (0.1% Triton X-100, 2% fetal calf serum, and 3% BSA in PBS) for 1 hr at RT, after which they were probed overnight at 4°C with the following antibodies diluted in ICC blocking solution: 1:1000 rabbit anti-MATR3 (Abcam EPR10635(B)), 1:1000 chicken anti-MAP2 (Novus Biologicals NB300-213), 1:1000 mouse anti-calmodulin (ThermoFisher MA3-917). The next day, samples were washed 3 x 5 min in PBS and then incubated 1 hr at RT with the following secondary antibodies all diluted 1:1000 in ICC blocking solution: donkey anti-rabbit Alexa Fluor 647 (ThermoFisher A-31573), goat anti-mouse Alexa Fluor 568 (ThermoFisher A-11031), goat anti-chicken Alexa Fluor 488 (ThermoFisher A-11039). After 3 x 5 min PBS washes, neurons were imaged for widefield microscopy using an Eclipse Ti inverted microscope (Nikon) with PerfectFocus, Semrock filters, Lambda 421 lamp (Sutter Instruments), and an Andor Zyla 4.2(+) sCMOS camera (Oxford Instruments), with custom BeanShell scripts controlling image acquisition and stage movements via μManager[92]. For confocal microscopy, neurons were mounted in ProLong Gold Antifade Mountant with DAPI (ThermoFisher P36935), and imaging was accomplished with a Nikon A1 inverted point-scanning confocal microscope (Nikon) controlled by NIS-Elements software. For CaM N/C ratio determination, custom scripts were used to create nuclear and cytoplasmic ROIs using DAPI and MAP2 signal, respectively.

Cerebellar slice culture and immunohistochemistry:

Wild-type C57BL/6J mice were anesthetized by isoflurane inhalation. Slices were prepared using a VT1200 vibratome (Leica) at a thickness of 300 μM as before[93,94] and placed in prewarmed aCSF with 5% CO_2 and 95% O_2 for 30 minutes before transferring to Neurobasal Medium (ThermoFisher). They were treated with vehicle or 500 μM glutamate for 3 hrs at 37°C, after which they were processed as before[95]. Briefly, slices were fixed in 4% PBS at 4°C overnight. The following day samples were permeabilized with 1% Triton X-100 in PBS for 1.5 hrs, treated with 20 mM glycine in PBS for 1 hr, blocked in IHC blocking solution (5% normal goat serum in PBS), and probed overnight at 4°C with 1:1000 rabbit anti-MATR3 (Abcam EPR10635(B)) and 1:1000 mouse anti-calbindin (MiliporeSigma C9848). After washing 3 x 5 min in PBS, slices were incubated overnight at 4°C with goat anti-mouse Alexa Fluor 568 and goat anti-rabbit Alexa Fluor 488 (ThermoFisher A-11008), both diluted 1:500 in IHC blocking solution. Stained slices were washed 3 x 5 min PBS and then mounted in ProLong Gold Antifade Mountant with DAPI. Slices were imaged using a 40X objective Nikon A1 inverted point-scanning confocal microscope.

Immunoprecipitation:

DIV14-16 primary neurons treated with 100 μM NMDA, 10 μM MG132, both, or DMSO were collected in PBS, lysed in RIPA buffer supplemented with protease and phosphatase inhibitors and 2 mM of the deubiquitinating enzyme inhibitor N-ethylmaleimide (MiliporeSigma), and sonicated at 80% amplitude with 5 s on/5 s off cycles for 2 min in a Fisherbrand Model 505 Sonic Dismembrenator. Lysates were cleared by centrifugation at 21,000 x g at 4°C for 15 min, and 10x dilution buffer 10x

ChIP dilution buffer (50 mM Tris, 10 mM EDTA, 1.5 M NaCl, 1% Na-deoxycholate, 10% Triton X-100, pH 8.0) was added to a final concentration of 1x before incubation overnight at 4°C with 1 µg rabbit anti-MATR3 antibody per sample (ThermoFisher A300-591A) conjugated to Dynabeads Protein G (ThermoFisher). The following day beads were washed 3 x in wash buffer (20 mM Tris, 1% Triton X-100, 2 mM EDTA, 150 mM NaCl, 0.1% SDS, pH 8.1) before elution by heating in SDS-PAGE sample buffer in RIPA at 95°C for 10 min.

CaM-sepharose pulldown:

HEK293T cells were collected in PBS, resuspended in buffer (10 mM Tris, 5 mM MgCl2, pH 7.4) supplemented with cOmplete EDTA-free protease inhibitor (Roche), and lysed by passing through an 18 G x 1½'' needle and sonication at 80% amplitude with 5 sec on/5 sec off for 2 min in a Fisherbrand Model 505 Sonic Dismembrenator. Cleared lysates were rotated overnight at 4°C with 100 µL per sample of Calmodulin Sepharose 4B resin (Cytiva Life Science) in CaM binding buffer (50 mM Tris HCl, 150 mM NaCl, 2 mM $CaCl_2$, 1 µM DTT, pH 7.5). The next day, beads were washed 3 x in CaM binding buffer and eluted in CaM elution buffer with EGTA (50 mM Tris HCl, 150 mM NaCl, 2 mM EGTA, 1 µM DTT, pH 7.5) or BAPTA (50 mM Tris HCl, 150 mM NaCl, 2 mM BAPTA, 1 µM DTT, pH 7.5). For inactivation of CaM, CaM binding buffer was supplemented with 100 µM W-7 (Tocris).

UV-CLIP and RT-PCR:

Primary neurons at DIV14-16 were treated with vehicle or 100 μM NMDA for 3-5 minutes before crosslinking at 254 nm in a Stratalinker 2400 (Stratagene) at 1500 mJ/cm^2, after which they were lysed in RIPA buffer supplemented with protease inhibitor and RNaisin ribonuclease inhibitor (Promega) and sonicated at 80% amplitude with 5 s on/5 s off cycles for 2 min using a Fisherbrand Model 505 Sonic Dismembrenator. Cleared lysates were incubated overnight at 4°C with 2 μg rabbit anti-MATR3 antibody per sample (ThermoFisher A300-591A) conjugated to Dynabeads Protein G. The following day, beads were washed 1 x in NaCl wash buffer (20 mM Tris, 1% Triton X-100, 2 mM EDTA, 150 mM NaCl, 0.1% SDS, pH 8.1), 1 x in LiCl wash buffer (10 mM Tris, 1% NP-40, 1 mM NP-40, 1 mM EDTA, 0.25% Na-deoxycholate, 250 mM LiCl, pH 8.0), and 2 x in TE buffer (10 mM Tris, 1 mM EDTA, pH 8.0).

Samples were then split for either protein IP validation, for which MATR3 complexes were removed from beads by heating at 95°C for 10 min in SDS-PAGE sample buffer in RIPA for immunoblot, or for RNA analysis. For the latter, beads were resuspended in elution buffer (50 mM Tris, 1 mM EDTA, 150 mM NaCl, 1% SDS, 50 mM $NaHCO_3$, pH 8.1) supplemented with RNasin and incubated with proteinase K (New England Biolabs) for 2 hrs at 50°C. RNA was extracted with TRIzol reagent (ThermoFisher) and chloroform, the suspension centrifuged at 21,000 x g at 4°C for 15 min, the aqueous phase removed, and RNA precipitated overnight at -20°C and resuspended in water by heating at 65°C for 10 min. cDNA was created using iScript Reverse Transcriptase Supermix (Bio-Rad) and qPCR was done with 200 nM each of forward and reverse primers and PowerUp SYBR Green Master Mix (ThermoFisher) according to manufacturer's instructions.

Optical pulse labelling and half-life determination:

Following widefield imaging on a Nikon Eclipse Ti inverted microscope, transfected neurons were identified in an automated matter based upon morphology, size, and fluorescence using custom scripts as previously described[84]. After photoconversion with 405 nm light half-lives were calculated on a per cell basis by fitting log-transformed TRITC intensity over time to a linear equation with a noise tolerance of 5%.

Statistical analysis:

Statistical analyses were performed in Prism 7 (GraphPad). Data were plotted using Prism 7, and significance determined via the two-tailed t-test. One-way ANOVA with Tukey's post-test for more than two comparison or unpaired t-test for comparing two groups were used to assess for significant differences among protein abundances, RNA levels, nuclear/cytoplasmic ratios, and half-lives. Data are shown as mean ± SEM unless otherwise stated.

3.6 Acknowledgements

I would like to thank Haoran Huang and Dr. Vikram Shakkotai for providing samples for as well as advice on *ex vivo* mouse cerebellar slice experiments. I would also like to thank Niki Grotewold, Christie Gillies, and Quinn Doctrove for their work on MATR3-CaM studies. This work was funded by NINDS R01 NS097542 (S.J.B.), NIA

P30 AG053760 (S.J.B.), the Robert Packard Center for ALS Research (S.J.B.), NIGMS T32 GM007863 (A.M.M.), and NINDS F31 NS110119 (A.M.M.).

References

1. Purice, M. D. & Taylor, J. P. Linking hnRNP Function to ALS and FTD Pathology. *Front Neurosci* **12,** 326 (2018).
2. Neumann, M. *et al.* Ubiquitinated TDP-43 in frontotemporal lobar degeneration and amyotrophic lateral sclerosis. *Science* **314,** 130–133 (2006).
3. Arai, T. *et al.* TDP-43 is a component of ubiquitin-positive tau-negative inclusions in frontotemporal lobar degeneration and amyotrophic lateral sclerosis. *Biochemical and Biophysical Research Communications* **351,** 602–611 (2006).
4. Kabashi, E. *et al.* TARDBP mutations in individuals with sporadic and familial amyotrophic lateral sclerosis. *Nat. Genet.* **40,** 572–574 (2008).
5. Vance, C. *et al.* Mutations in FUS, an RNA processing protein, cause familial amyotrophic lateral sclerosis type 6. *Science* **323,** 1208–1211 (2009).
6. Kwiatkowski, T. J. *et al.* Mutations in the FUS/TLS gene on chromosome 16 cause familial amyotrophic lateral sclerosis. *Science* **323,** 1205–1208 (2009).
7. Ticozzi, N. *et al.* Mutational analysis reveals the FUS homolog TAF15 as a candidate gene for familial amyotrophic lateral sclerosis. **156B,** 285–290 (2011).
8. Mackenzie, I. R. *et al.* TIA1 Mutations in Amyotrophic Lateral Sclerosis and Frontotemporal Dementia Promote Phase Separation and Alter Stress Granule Dynamics. *Neuron* **95,** 808–816.e9 (2017).
9. Kim, H. J. *et al.* Mutations in prion-like domains in hnRNPA2B1 and hnRNPA1 cause multisystem proteinopathy and ALS. *Nature* **495,** 467–473 (2013).
10. Belgrader, P., Dey, R. & Berezney, R. Molecular cloning of Matrin 3. A 125-kilodalton protein of the nuclear matrix contains an extensive acidic domain. *The Journal of Biological Chemistry* **266,** 9893–9899 (1991).
11. Hibino, Y., Nakamura, K., Tsukada, S. & Sugano, N. Purification and characterization of nuclear scaffold proteins which bind to a highly repetitive bent DNA from rat liver. *Biochim. Biophys. Acta* **1174,** 162–170 (1993).
12. Hibino, Y. *et al.* Molecular properties and intracellular localization of rat liver nuclear scaffold protein P130. *Biochimica et Biophysica Acta (BBA) - Gene Structure and Expression* **1759,** 195–207 (2006).
13. Senderek, J. *et al.* Autosomal-Dominant Distal Myopathy Associated with a Recurrent Missense Mutation in the Gene Encoding the Nuclear Matrix Protein, Matrin 3. *The American Journal of Human Genetics* **84,** 511–518 (2009).
14. Johnson, J. O. *et al.* Mutations in the Matrin 3 gene cause familial amyotrophic lateral sclerosis. *Nat Neurosci* **17,** 664–666 (2014).
15. Millecamps, S. *et al.* Genetic analysis of matrin 3 gene in French amyotrophic lateral sclerosis patients and frontotemporal lobar degeneration with amyotrophic lateral sclerosis patients. *Neurobiology of Aging* **35,** 2882.e13–2882.e15 (2014).
16. Lin, K.-P. *et al.* Mutational analysis of MATR3 in Taiwanese patients with amyotrophic lateral sclerosis. *Neurobiology of Aging* **36,** 2005.e1–2005.e4 (2015).
17. Origone, P. *et al.* A novel Arg147Trp MATR3 missense mutation in a slowly progressive ALS Italian patient. *Amyotrophic Lateral Sclerosis and Frontotemporal Degeneration* **16,** 530–531 (2015).
18. Leblond, C. S. *et al.* Replication study of MATR3 in familial and sporadic amyotrophic lateral sclerosis. *Neurobiology of Aging* **37,** 209.e17–209.e21 (2016).

19. Xu, L., Li, J., Tang, L., Zhang, N. & Fan, D. MATR3 mutation analysis in a Chinese cohort with sporadic amyotrophic lateral sclerosis. *Neurobiology of Aging* **38,** 218.e3–218.e4 (2016).
20. Marangi, G. *et al.* Matrin 3 variants are frequent in Italian ALS patients. *Neurobiology of Aging* **49,** 218.e1–218.e7 (2017).
21. Narain, P. *et al.* Identification and characterization of novel and rare susceptible variants in Indian amyotrophic lateral sclerosis patients. *Neurogenetics* **20,** 197–208 (2019).
22. Dreser, A. *et al.* The ALS-linked E102Q mutation in Sigma receptor-1 leads to ER stress-mediated defects in protein homeostasis and dysregulation of RNA-binding proteins. 1–17 (2017). doi:10.1038/cdd.2017.88
23. Tada, M. *et al.* Matrin 3 is a component of neuronal cytoplasmic inclusions of motor neurons in sporadic amyotrophic lateral sclerosis. *The American Journal of Pathology* 1–36 (2017). doi:10.1016/j.ajpath.2017.10.007
24. Vucic, S., Nicholson, G. A. & Kiernan, M. C. Cortical hyperexcitability may precede the onset of familial amyotrophic lateral sclerosis. *Brain* **131,** 1540–1550 (2008).
25. Kanai, K. *et al.* Altered axonal excitability properties in amyotrophic lateral sclerosis: impaired potassium channel function related to disease stage. *Brain* **129,** 953–962 (2006).
26. Marchand-Pauvert, V. *et al.* Absence of hyperexcitability of spinal motoneurons in patients with amyotrophic lateral sclerosis. *J Physiol* **597,** 5445–5467 (2019).
27. Pieri, M. *et al.* Altered excitability of motor neurons in a transgenic mouse model of familial amyotrophic lateral sclerosis. *Neurosci Lett* **351,** 153–156 (2003).
28. Wainger, B. J. *et al.* Intrinsic membrane hyperexcitability of amyotrophic lateral sclerosis patient-derived motor neurons. *Cell Rep* **7,** 1–11 (2014).
29. Tremblay, E., Martineau, É. & Robitaille, R. Opposite Synaptic Alterations at the Neuromuscular Junction in an ALS Mouse Model: When Motor Units Matter. *J. Neurosci.* **37,** 8901–8918 (2017).
30. Martínez-Silva, M. de L. *et al.* Hypoexcitability precedes denervation in the large fast-contracting motor units in two unrelated mouse models of ALS. *Elife* **7,** (2018).
31. Devlin, A.-C. *et al.* Human iPSC-derived motoneurons harbouring TARDBP or C9ORF72 ALS mutations are dysfunctional despite maintaining viability. *Nature Communications* **6,** 339 (2015).
32. Tiruchinapalli, D. M. *et al.* Activity-dependent trafficking and dynamic localization of zipcode binding protein 1 and beta-actin mRNA in dendrites and spines of hippocampal neurons. *J. Neurosci.* **23,** 3251–3261 (2003).
33. Ben Fredj, N. *et al.* Depolarization-induced translocation of the RNA-binding protein Sam68 to the dendrites of hippocampal neurons. *J. Cell. Sci.* **117,** 1079–1090 (2004).
34. Nalavadi, V. C., Muddashetty, R. S., Gross, C. & Bassell, G. J. Dephosphorylation-induced ubiquitination and degradation of FMRP in dendrites: a role in immediate early mGluR-stimulated translation. *J. Neurosci.* **32,** 2582–2587 (2012).

35. Weskamp, K. *et al.* Shortened TDP43 isoforms upregulated by neuronal hyperactivity drive TDP43 pathology in ALS. *J. Clin. Invest.* **130,** 1139–1155 (2020).
36. Deisseroth, K., Heist, E. K. & Tsien, R. W. Translocation of calmodulin to the nucleus supports CREB phosphorylation in hippocampal neurons. *Nature* **392,** 198–202 (1998).
37. Mermelstein, P. G., Deisseroth, K., Dasgupta, N., Isaksen, A. L. & Tsien, R. W. Calmodulin priming: nuclear translocation of a calmodulin complex and the memory of prior neuronal activity. *Proc Natl Acad Sci USA* **98,** 15342–15347 (2001).
38. Ma, H. *et al.* γCaMKII shuttles Ca^{2+}/CaM to the nucleus to trigger CREB phosphorylation and gene expression. *Cell* **159,** 281–294 (2014).
39. Cohen, S. M. *et al.* Excitation-Transcription Coupling in Parvalbumin-Positive Interneurons Employs a Novel CaM Kinase-Dependent Pathway Distinct from Excitatory Neurons. *Neuron* **90,** 292–307 (2016).
40. Cohen, S. M. *et al.* Calmodulin shuttling mediates cytonuclear signaling to trigger experience-dependent transcription and memory. *Nature Communications* **9,** 2451–12 (2018).
41. Yamamoto, A. *et al.* Bafilomycin A1 prevents maturation of autophagic vacuoles by inhibiting fusion between autophagosomes and lysosomes in rat hepatoma cell line, H-4-II-E cells. *Cell Struct Funct* **23,** 33–42 (1998).
42. Tsubuki, S., Saito, Y., Tomioka, M., Ito, H. & Kawashima, S. Differential inhibition of calpain and proteasome activities by peptidyl aldehydes of di-leucine and tri-leucine. *J. Biochem.* **119,** 572–576 (1996).
43. Bonvini, P., Zorzi, E., Basso, G. & Rosolen, A. Bortezomib-mediated 26S proteasome inhibition causes cell-cycle arrest and induces apoptosis in CD-30+ anaplastic large cell lymphoma. *Leukemia* **21,** 838–842 (2007).
44. Kobayashi, S. *et al.* Calpain-mediated X-linked inhibitor of apoptosis degradation in neutrophil apoptosis and its impairment in chronic neutrophilic leukemia. *The Journal of Biological Chemistry* **277,** 33968–33977 (2002).
45. Chen, Z., Boor, P. J., Finnerty, C. C., Herndon, D. N. & Albrecht, T. Calpain-mediated cleavage of p53 in human cytomegalovirus-infected lung fibroblasts. *FASEB Bioadv* **1,** 151–166 (2019).
46. Hamakubo, T., Kannagi, R., Murachi, T. & Matus, A. Distribution of calpains I and II in rat brain. *J. Neurosci.* **6,** 3103–3111 (1986).
47. Akashiba, H., Matsuki, N. & Nishiyama, N. Calpain activation is required for glutamate-induced p27 down-regulation in cultured cortical neurons. *Journal of Neurochemistry* **99,** 733–744 (2006).
48. Wang, Y. & Zhang, Y. Regulation of TET protein stability by calpains. *Cell Rep* **6,** 278–284 (2014).
49. Zhang, Y., Li, Q., Youn, J. Y. & Cai, H. Protein Phosphotyrosine Phosphatase 1B (PTP1B) in Calpain-dependent Feedback Regulation of Vascular Endothelial Growth Factor Receptor (VEGFR2) in Endothelial Cells: IMPLICATIONS IN VEGF-DEPENDENT ANGIOGENESIS AND DIABETIC WOUND HEALING. *The Journal of Biological Chemistry* **292,** 407–416 (2017).

50. Liu, Z.-X. *et al.* Precise Prediction of Calpain Cleavage Sites and Their Aberrance Caused by Mutations in Cancer. *Front Genet* **10,** 715 (2019).
51. Rayaprolu, S. *et al.* Heterogeneity of Matrin 3 in the developing and aging murine central nervous system. *Journal of Comparative Neurology* **524,** 2740–2752 (2016).
52. Kao, C. S. *et al.* Selective neuronal degeneration in MATR3 S85C knock-in mouse model of early-stage ALS. *Nature Communications* **11,** 5304–17 (2020).
53. Yap, K. L. *et al.* Calmodulin target database. *J Struct Funct Genomics* **1,** 8–14 (2000).
54. Mruk, K., Farley, B. M., Ritacco, A. W. & Kobertz, W. R. Calmodulation meta-analysis: predicting calmodulin binding via canonical motif clustering. *J Gen Physiol* **144,** 105–114 (2014).
55. Abbasi, W. A., Asif, A., Andleeb, S. & Minhas, F. U. A. A. CaMELS: In silico prediction of calmodulin binding proteins and their binding sites. *Proteins* **85,** 1724–1740 (2017).
56. Alexander Valencia, C., Ju, W. & Liu, R. Matrin 3 is a Ca2+/calmodulin-binding protein cleaved by caspases. *Biochemical and Biophysical Research Communications* **361,** 281–286 (2007).
57. Flores, B. N. *et al.* An Intramolecular Salt Bridge Linking TDP43 RNA Binding, Protein Stability, and TDP43-Dependent Neurodegeneration. *Cell Rep* **27,** 1133–1150.e8 (2019).
58. Giordano, G. *et al.* Activation of NMDA receptors induces protein kinase A-mediated phosphorylation and degradation of matrin 3. Blocking these effects prevents NMDA-induced neuronal death. *Journal of Neurochemistry* **94,** 808–818 (2005).
59. Pearson, R. B. & Kemp, B. E. Protein kinase phosphorylation site sequences and consensus specificity motifs: tabulations. *Methods Enzymol* **200,** 62–81 (1991).
60. Douglass, J. *et al.* Identifying protein kinase target preferences using mass spectrometry. *Am. J. Physiol., Cell Physiol.* **303,** C715–27 (2012).
61. Vorherr, T. *et al.* The calmodulin binding domain of nitric oxide synthase and adenylyl cyclase. *Biochemistry* **32,** 6081–6088 (1993).
62. Gu, C. & Cooper, D. M. Calmodulin-binding sites on adenylyl cyclase type VIII. *The Journal of Biological Chemistry* **274,** 8012–8021 (1999).
63. Masada, N., Ciruela, A., Macdougall, D. A. & Cooper, D. M. F. Distinct mechanisms of regulation by Ca2+/calmodulin of type 1 and 8 adenylyl cyclases support their different physiological roles. *The Journal of Biological Chemistry* **284,** 4451–4463 (2009).
64. Skeberdis, V. A. *et al.* Protein kinase A regulates calcium permeability of NMDA receptors. *Nat Neurosci* **9,** 501–510 (2006).
65. Murphy, J. A. *et al.* Phosphorylation of Ser1166 on GluN2B by PKA is critical to synaptic NMDA receptor function and Ca2+ signaling in spines. *J. Neurosci.* **34,** 869–879 (2014).
66. Knöferle, J. *et al.* Mechanisms of acute axonal degeneration in the optic nerve in vivo. *Proc. Natl. Acad. Sci. U.S.A.* **107,** 6064–6069 (2010).

67. Vingtdeux, V. *et al.* AMP-activated protein kinase signaling activation by resveratrol modulates amyloid-beta peptide metabolism. *The Journal of Biological Chemistry* **285,** 9100–9113 (2010).
68. Djakovic, S. N., Schwarz, L. A., Barylko, B., DeMartino, G. N. & Patrick, G. N. Regulation of the proteasome by neuronal activity and calcium/calmodulin-dependent protein kinase II. *The Journal of Biological Chemistry* **284,** 26655–26665 (2009).
69. Park, J. Y., Jang, S. Y., Shin, Y. K., Suh, D. J. & Park, H. T. Calcium-dependent proteasome activation is required for axonal neurofilament degradation. *Neural Regen Res* **8,** 3401–3409 (2013).
70. Fuentes, J. L., Strayer, M. S. & Matera, A. G. Molecular determinants of survival motor neuron (SMN) protein cleavage by the calcium-activated protease, calpain. *PLoS ONE* **5,** e15769 (2010).
71. Yamashita, T. *et al.* A role for calpain-dependent cleavage of TDP-43 in amyotrophic lateral sclerosis pathology. *Nature Communications* **3,** 1307–13 (2012).
72. Yamashita, T., Teramoto, S. & Kwak, S. Phosphorylated TDP-43 becomes resistant to cleavage by calpain: A regulatory role for phosphorylation in TDP-43 pathology of ALS/FTLD. *Neurosci Res* **107,** 63–69 (2016).
73. Hornbeck, P. V. *et al.* PhosphoSitePlus, 2014: mutations, PTMs and recalibrations. *Nucleic Acids Research* **43,** D512–20 (2015).
74. Rao, M. V., Campbell, J., Palaniappan, A., Kumar, A. & Nixon, R. A. Calpastatin inhibits motor neuron death and increases survival of hSOD1(G93A) mice. *Journal of Neurochemistry* **137,** 253–265 (2016).
75. Chao, H.-W. *et al.* Deletion of CPEB3 enhances hippocampus-dependent memory via increasing expressions of PSD95 and NMDA receptors. *J. Neurosci.* **33,** 17008–17022 (2013).
76. Wang, C.-F. & Huang, Y.-S. Calpain 2 activated through N-methyl-D-aspartic acid receptor signaling cleaves CPEB3 and abrogates CPEB3-repressed translation in neurons. *Mol Cell Biol* **32,** 3321–3332 (2012).
77. Tischbein, M. *et al.* The RNA-binding protein FUS/TLS undergoes calcium-mediated nuclear egress during excitotoxic stress and is required for GRIA2 mRNA processing. *The Journal of Biological Chemistry* **294,** 10194–10210 (2019).
78. Kan, M.-C. *et al.* CPEB4 is a cell survival protein retained in the nucleus upon ischemia or endoplasmic reticulum calcium depletion. *Mol Cell Biol* **30,** 5658–5671 (2010).
79. Park, J. H. *et al.* Cytosolic calcium regulates cytoplasmic accumulation of TDP-43 through Calpain-A and Importin α3. *Elife* **9,** 2436 (2020).
80. Yamashita, T., Aizawa, H., Teramoto, S., Akamatsu, M. & Kwak, S. Calpain-dependent disruption of nucleo-cytoplasmic transport in ALS motor neurons. *Scientific Reports* **7,** 39994–11 (2017).
81. Feit, H. *et al.* Vocal Cord and Pharyngeal Weakness with Autosomal Dominant Distal Myopathy: Clinical Description and Gene Localization to 5q31. *The American Journal of Human Genetics* **63,** 1732–1742 (1998).

82. Kraya, T., Schmidt, B., MüLLER, T. & Hanisch, F. Impairment of respiratory function in late-onset distal myopathy due to MATR3 Mutation. *Muscle & Nerve* **51,** 916–918 (2015).
83. Palmio, J. *et al.* Re-evaluation of the phenotype caused by the common MATR3 p.Ser85Cys mutation in a new family. *J. Neurol. Neurosurg. Psychiatry* **87,** 448–450 (2016).
84. Malik, A. M. *et al.* Matrin 3-dependent neurotoxicity is modified by nucleic acid binding and nucleocytoplasmic localization. *Elife* **7,** 602 (2018).
85. Zhao, M. *et al.* Knockdown of genes involved in axonal transport enhances the toxicity of human neuromuscular disease-linked MATR3 mutations in Drosophila. *FEBS Lett.* **27,** 4103 (2020).
86. Ramesh, N., Kour, S., Anderson, E. N., Rajasundaram, D. & Pandey, U. B. RNA-recognition motif in Matrin-3 mediates neurodegeneration through interaction with hnRNPM. *Acta Neuropathologica Communications* **8,** 138 (2020).
87. Kemp, C. M., Oliver, W. T., Wheeler, T. L., Chishti, A. H. & Koohmaraie, M. The effects of Capn1 gene inactivation on skeletal muscle growth, development, and atrophy, and the compensatory role of other proteolytic systems. *J Anim Sci* **91,** 3155–3167 (2013).
88. Nakamura, T., Sato, A., Kitsukawa, T., Sasaoka, T. & Yamamori, T. Expression pattern of immediate early genes in the cerebellum of D1R KO, D2R KO, and wild type mice under vestibular-controlled activity. *Front Cell Dev Biol* **3,** 38 (2015).
89. Delaney, K. J. *et al.* Calmodulin interacts with and regulates the RNA-binding activity of an Arabidopsis polyadenylation factor subunit. *Plant Physiol* **140,** 1507–1521 (2006).
90. Saladino, P. *et al.* RNA-binding activity of the rat calmodulin-binding PEP-19 protein and of the long PEP-19 isoform. *Int J Mol Med* **29,** 141–145 (2012).
91. Saudou, F., Finkbeiner, S., Devys, D. & Greenberg, M. E. Huntingtin acts in the nucleus to induce apoptosis but death does not correlate with the formation of intranuclear inclusions. *Cell* **95,** 55–66 (1998).
92. Edelstein, A., Amodaj, N., Hoover, K., Vale, R. & Stuurman, N. Computer control of microscopes using μManager. *Curr Protoc Mol Biol* **Chapter 14,** Unit14.20–14.20.17 (2010).
93. Mercer, A. A., Palarz, K. J., Tabatadze, N., Woolley, C. S. & Raman, I. M. Sex differences in cerebellar synaptic transmission and sex-specific responses to autism-linked Gabrb3 mutations in mice. *Elife* **5,** (2016).
94. Ankri, L., Yarom, Y. & Uusisaari, M. Y. Slice it hot: acute adult brain slicing in physiological temperature. *J Vis Exp* e52068 (2014). doi:10.3791/52068
95. Schultz, M. L. *et al.* Synthetic high-density lipoprotein nanoparticles for the treatment of Niemann-Pick diseases. *BMC Med* **17,** 200–18 (2019).

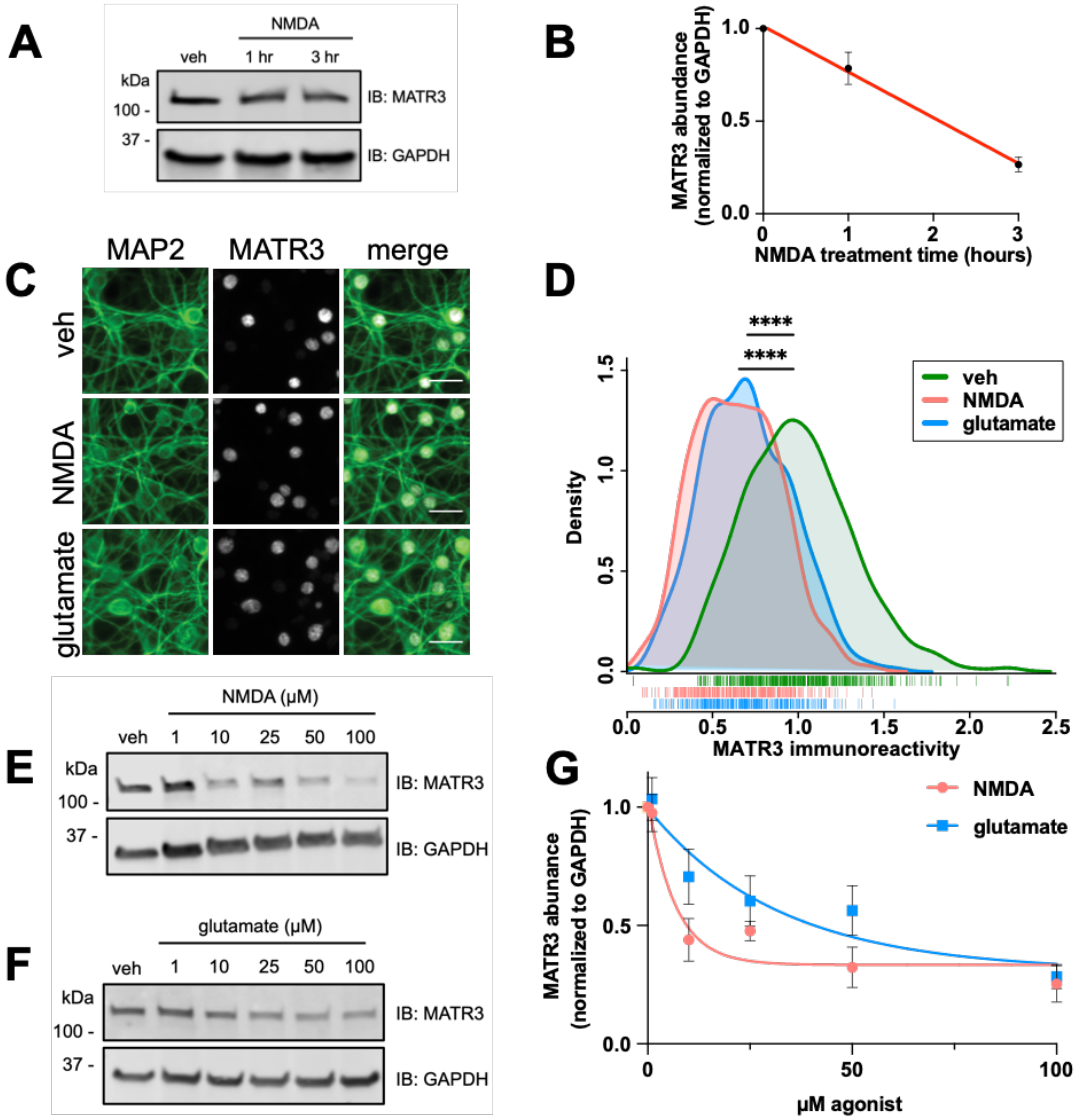

Figure 3.1. Glutamatergic stimulation results in reduced MATR3 in cortical neurons. A-B. Treatment of mature DIV14-16 cortical neuron cultures with 100 μM NMDA results in rapid, time-dependent reduction of MATR3. **C-D**. This reduction is recapitulated with immunostaining but is not accompanied by MATR3 redistribution within neurons (compared to veh, n = 547; NMDA, n = 419, **** $p < 0.0001$; glutamate, n = 337, **** $p < 0.0001$; one-way ANOVA with Tukey's post-hoc test). **E-G.** Both NMDA and the endogenous agonist glutamate are able to produce dose-dependent MATR3 clearance (NMDA, n = 3 per dose, $y = 0.695^{-0.150x} + 0.334$; glutamate, n = 3 per dose, $y = 0.^{687-0.0312x} + 0.307$; nonlinear one phase decay). Scale bars in **(C)**, 20 μm.

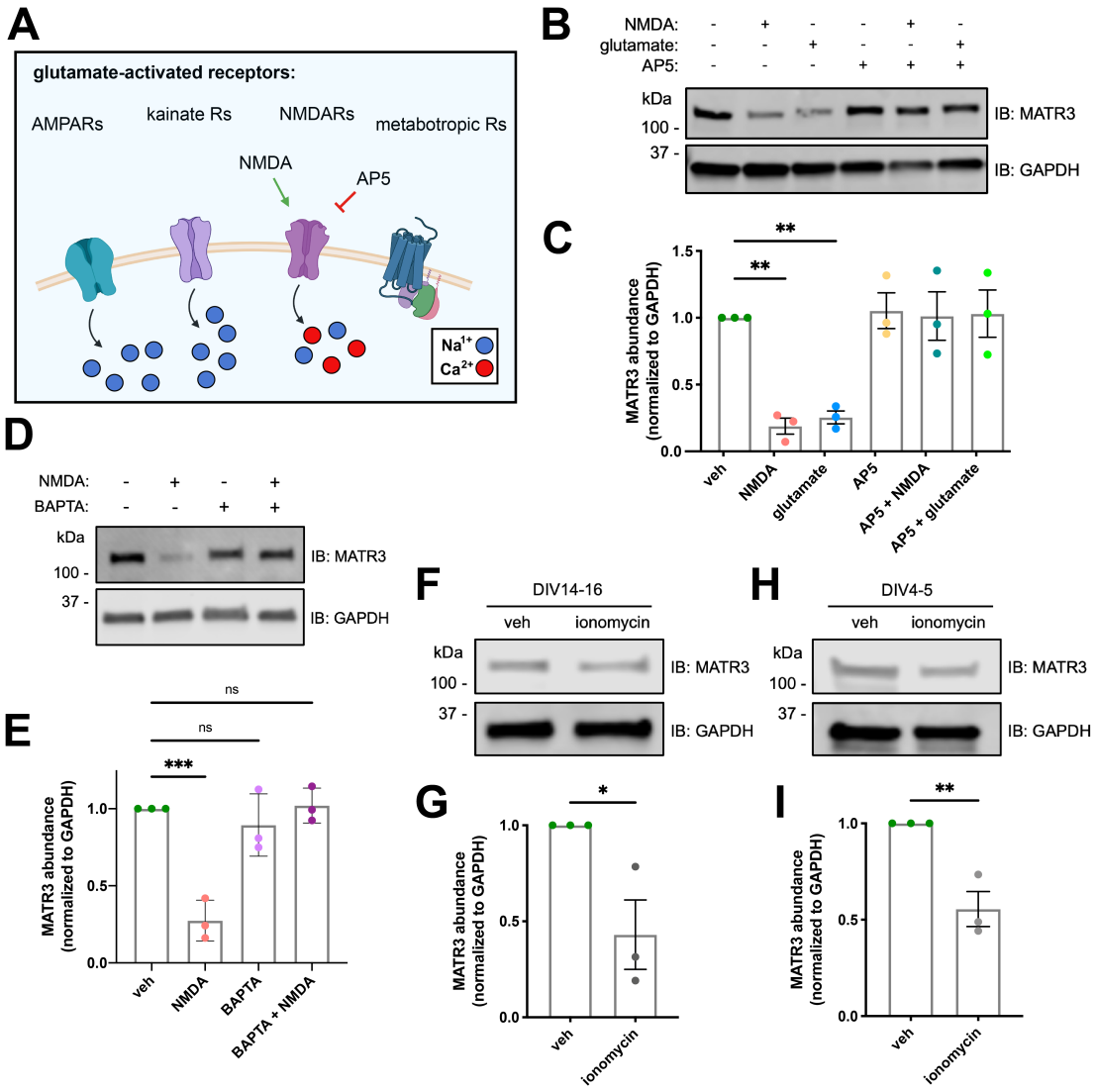

Figure 3.2. MATR3 reduction upon glutamatergic stimulation is NMDAR- and Ca^{2+}-dependent. A. Neurons express a variety of ionotropic and metabotropic receptors activated by glutamate, with NMDA being a selective agonist and AP5 a selective antagonist of NMDARs, which are largely unique in passing Ca^{2+} currents when activated. **B-C.** NMDAR activation is both necessary and sufficient for MATR3 clearance, as activation of all other glutamatergic receptors but with NMDAR blockade is incapable of reducing MATR3 abundance (compared to veh, n = 3; NMDA, n = 3, ** p = 0.0050; glutamate, n = 3, ** p = 0.0094, AP5, n = 3, p > 0.99, AP5 + NMDA, n = 3, p > 0.99, AP5 + glutamate, n = 3, p > 0.99; one-way ANOVA with Tukey's post-hoc test). **D-E.** The Ca^{2+} chelator BAPTA blocks NMDA-mediated MATR3 reduction indicating that Ca^{2+} passage into cells through NMDARs is necessary for this process (compared to veh, n = 3; NMDA, n = 3, *** p = 0.00070; BAPTA, n = 3, p = 0.768; BAPTA + NMDA, n = 3, p > 0.99; one-way ANOVA with Tukey's post-hoc test). **F-I.** Increasing intracellular Ca^{2+} is sufficient for MATR3 reduction, as treatment with the ionophore ionomycin results in MATR3 clearance in NMDAergically mature DIV14-16 (veh, n = 3; ionomycin,

n = 3, * p = 0.034; two-tailed t-test) and immature DIV4-5 (veh, n = 3; ionomycin, n = 3, * p = 0.0080; two-tailed t-test) cultures.

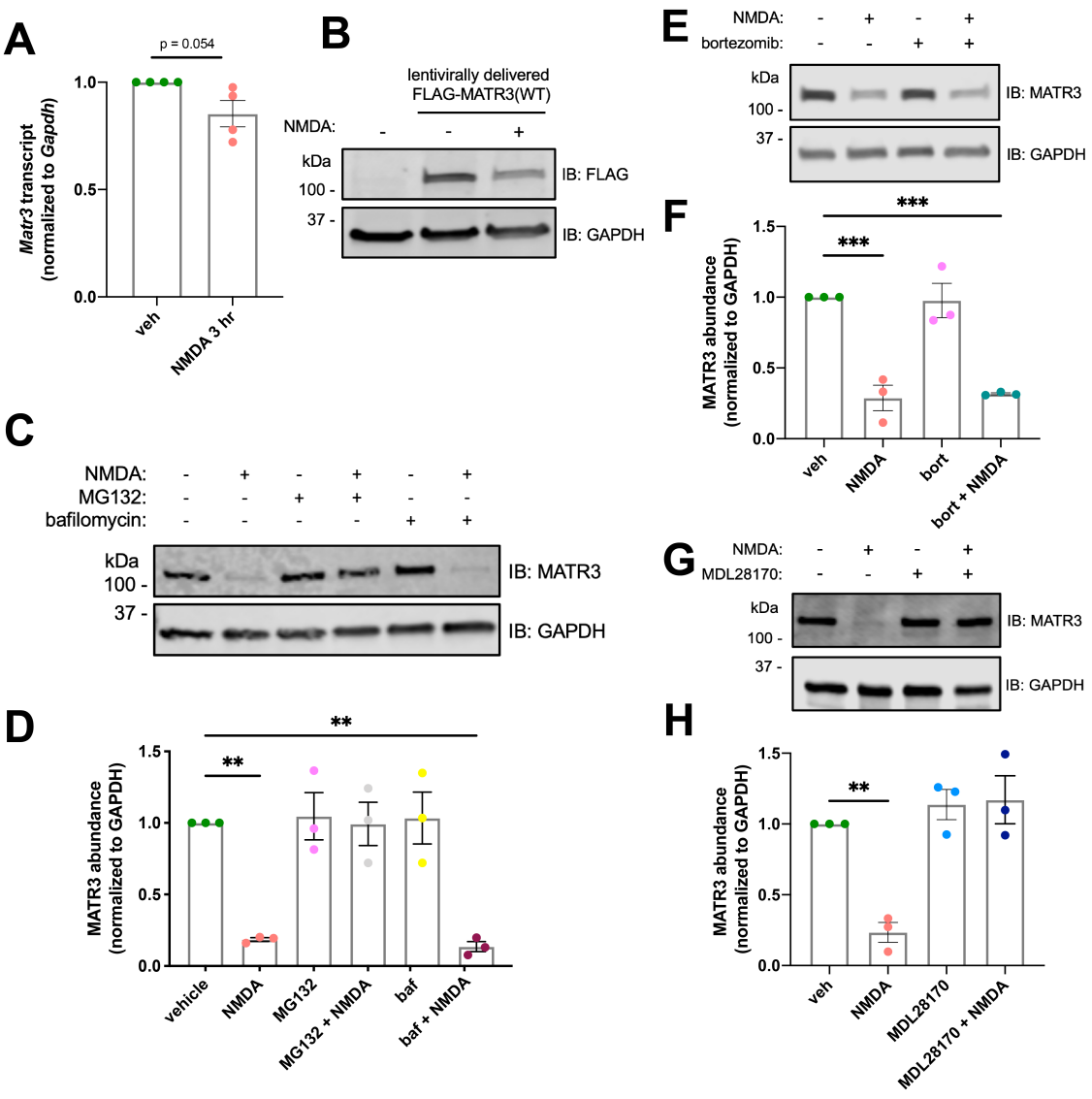

Figure 3.3. NMDA-triggered MATR3 reduction occurs post-translationally through degradation by calpains. A. Treatment with NMDA does not significantly alter *Matr3* transcript abundance, arguing against transcriptional downregulation being responsible for the rapid decrease observed (veh, n = 4; NMDA, n = 4, p = 0.054; two-tailed t-test). **B.** Abundance of exogenous, lentivirally delivered FLAG-MATR3 is reduced similar to endogenous protein, supporting post-translational degradation. **C.** The proteasomal and cysteine protease inhibitor MG132, but not the autophagy inhibitor bafilomycin, is able to block MATR3 clearance (compared to veh, n = 3; NMDA, n = 3, ** p = 0.0041; MG132, n = 3, p = 0.0.999, MG132 + NMDA, n = 3, p > 0.99, bafilomycin, n = 3, p > 0.99, bafilomycin + NMDA, n = 3, p * 0.0025; one-way ANOVA with Tukey's post-hoc test). **E-F.** The selective proteasomal inhibitor bortezomib is unable to block NMDA-triggered MATR3 reduction (compared to veh, n = 3; NMDA, n = 3, *** p = 0.00070; bortezomib, n = 3, p > 0.99; bortezomib + NMDA, n = 3, *** p = 0.0010; one-way ANOVA with Tukey's post-hoc test). **(G-H)** However, MDL28170, an inhibitor of

calpains, is able to effectively impair this process (compared to veh, n = 3; NMDA, n = 3, ** p = 0.0040; MDL28170, n = 3, p = 0.796; MDL28170 + NMDA, n = 3, p = 0.676; one-way ANOVA with Tukey's post-hoc test).

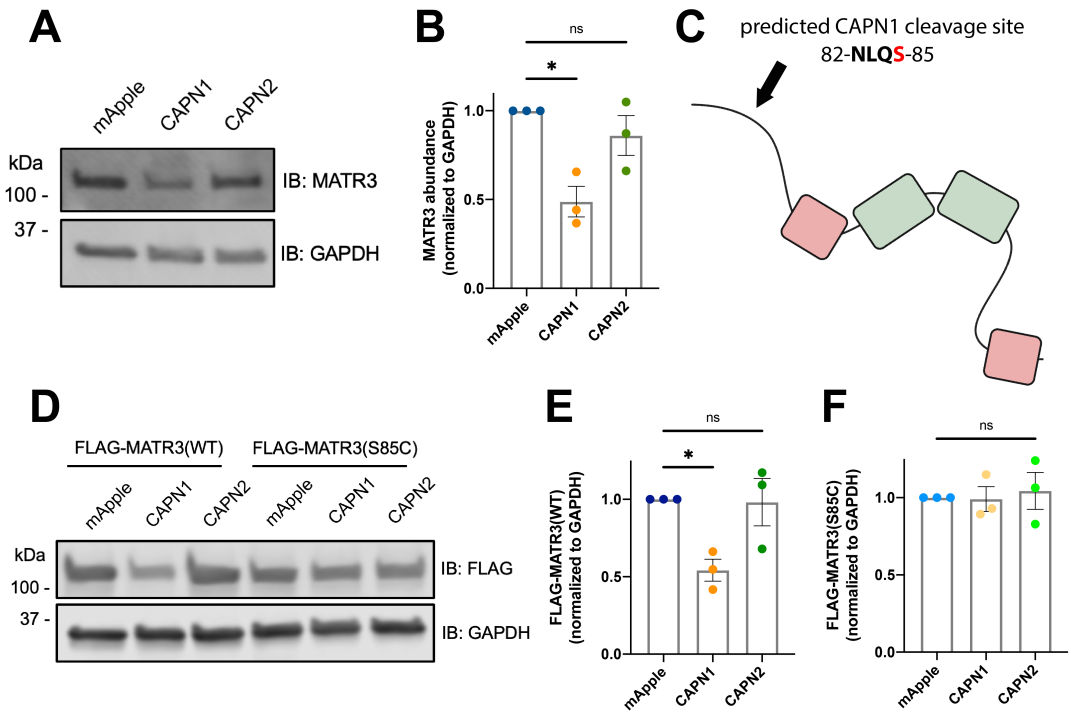

Figure 3.4. MATR3 is a substrate for CAPN1, and the pathogenic S85C mutation renders it resistant to degradation. A-B. Compared to cells transfected with mApple control, HEK293T cells transfected with CAPN1 but not with CAPN2 overexpression plasmids displayed reduced MATR3 (compared to mApple, n = 3; CAPN1, n = 3, * p = 0.10; CAPN2, n = 3, p = 0.49; one-way ANOVA with Tukey's post-hoc test). **C.** The highest confidence CAPN1 cleavage site in MATR3 is predicted to be in amino acids 82-85; notably this includes the S85 residue (red) mutated in familial disease. **D-F.** While exogenous FLAG-MATR3(WT) is comparably susceptibly to cleavage by CAPN1 as the endogenous protein (compared to mApple, n = 3; CAPN1, n = 3, * p = 0.036; CAPN2, n = 3, p > 0.99; one-way ANOVA with Tukey's post-hoc test), the pathogenic S85C mutation is resistance to CAPN1 (compared to mApple, n = 3; CAPN1, n = 3, p > 0.99; CAPN2, n = 3, p = 0.93; one-way ANOVA with Tukey's post-hoc test).

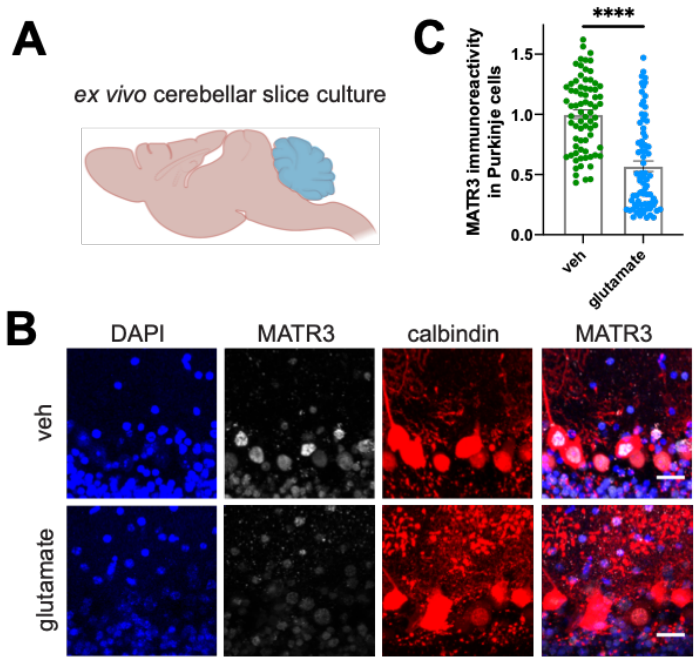

Figure 3.5. Cerebellar Purkinje neurons clear MATR3 in response to glutamatergic activation in an *ex vivo* system. A. Cerebellar slice cultures from wide-type mice were generated and treated with vehicle or glutamate. **B-C.** Calbindin-positive Purkinje neurons displayed markedly reduced MATR3 staining intensity upon glutamate stimulation (veh, n = 73; NMDA, n = 76, **** $p < 0.0001$; two-tailed t-test). Scale bars in **(B)**, 20 μm.

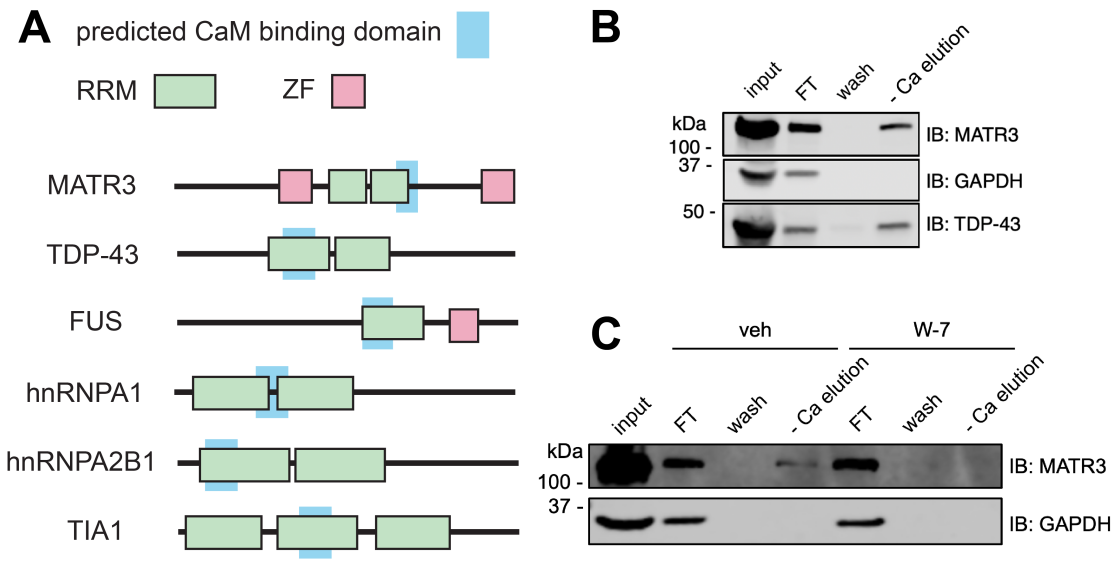

Figure 3.6. CaM binds to RBPs in a selective, Ca^{2+}-dependent manner. A. CaM-binding motif prediction algorithms indicate that CaM interacts with the RNA recognition motifs of many ALS/FTD-linked RBPs. **B.** Ca^{2+}-bound but not free apo-CaM binds to MATR3 and TDP-43, validating *in silico* predictions. **C.** The association between MATR3 and CaM is dependent on CaM adopting its active conformation after Ca^{2+} binding, as the conformational inhibitor W-7 blocks the interaction between Ca^{2+}/CaM and MATR3.

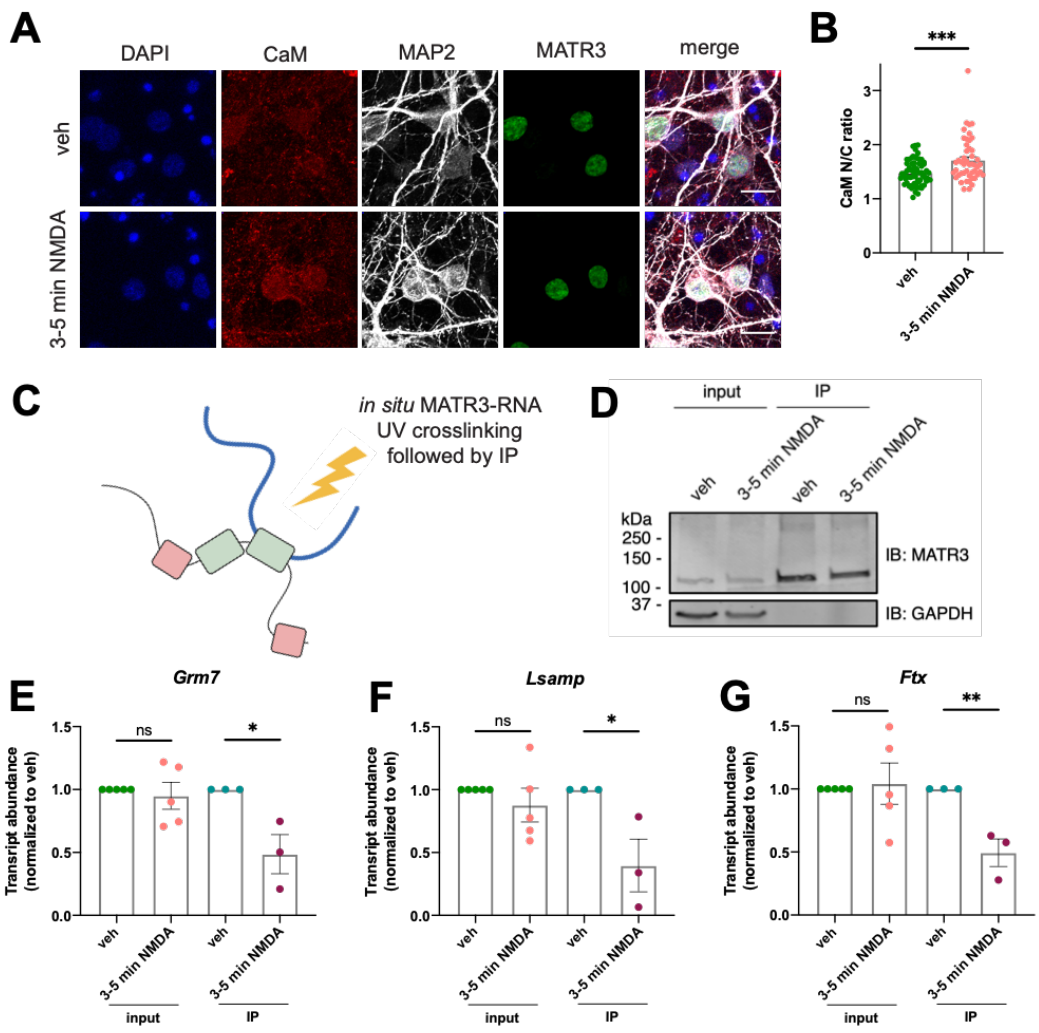

Figure 3.7. NMDA stimulation results in CaM nuclear enrichment and impaired MATR3 binding to RNA. A-B. Minutes after NMDA treatment in cortical neurons, $Ca^{2+/}$CaM enriches in the nucleus (compared to veh, n = 67; NMDA, n = 48; *** p < 0.0001; two-tailed t-test). **C-D**. UV crosslinking followed by IP and harsh washing conditions were used to analyze RNAs bound to MATR3 *in situ* in neurons in basal or stimulated conditions. **E-G.** While NMDA treatment did not alter total levels of tested MATR3 target RNAs (*Grm7*: veh input, n = 5; NMDA input, n = 5; p = 0.65; *Lsamp*: veh input, n = 5; NMDA input, n = 5; p = 0.39; *Ftx*: veh input, n = 5; NMDA input, n = 5; p = 0.80), less RNA was crosslinked to MATR3 in stimulated conditions, indicating impaired RNA binding (*Grm7*: veh IP, n = 3; NMDA IP, n = 3; * p = 0.030; *Lsamp*: veh IP, n = 3; NMDA IP, n = 3; * p = 0.045; *Ftx*: veh IP, n = 3; NMDA IP, n = 3; ** p = 0.0098). Scale bars in **(A)**, 20 μm.

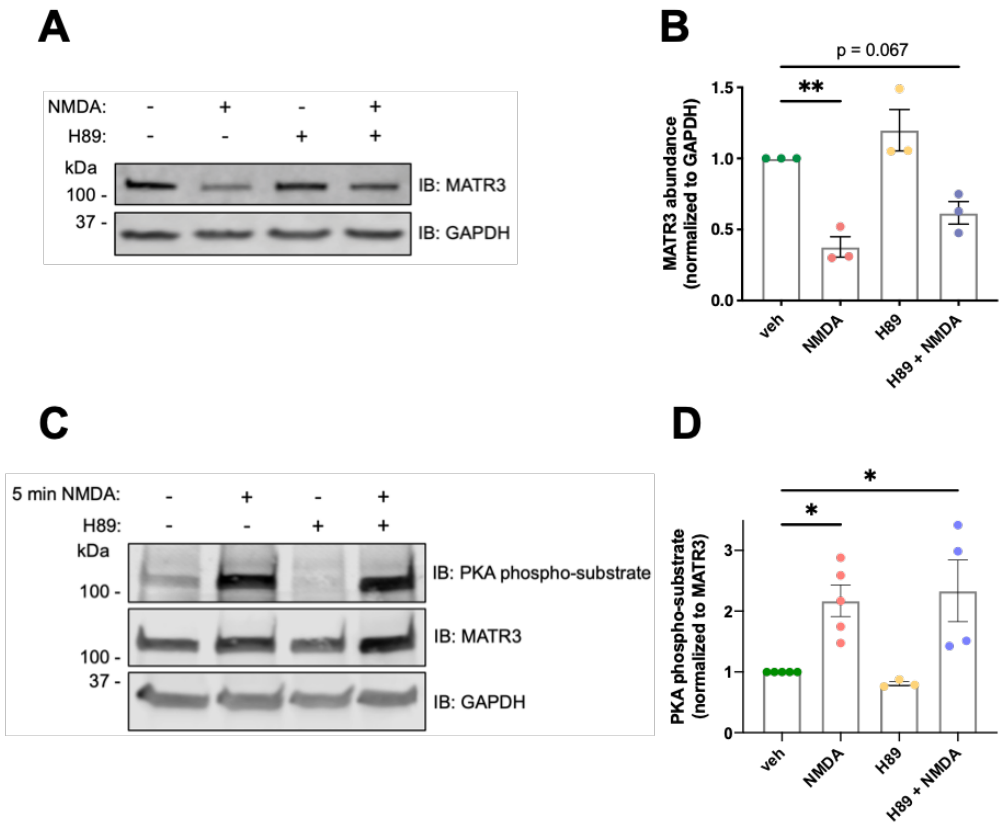

Supplemental Figure 3.1 Inhibition of PKA blunts MATR3 degradation but does not block MATR3 phosphorylation. A-B. Treatment with the PKA inhibitor H89 blunts MATR3 degradation in response to NDMA treatment (compared to veh, n = 4; NMDA, n = 3, ** p = 0.0054; H89, n = 3; p = 0.45; H89 + NMDA, n = 3; p = 0.067). However, the increase in phospho-MATR3 5 min after NMDA stimulation as detected with a general PKA phospho-substrate antibody is not blocked by H89, indicating this phosphorylation is done by another, H89-resistant kinase (compared to veh, n = 5; NMDA, n = 5, * p = 0.033; H89, n = 3, p = 0.97; H89 + NMDA, n = 5, * p = 0.022).

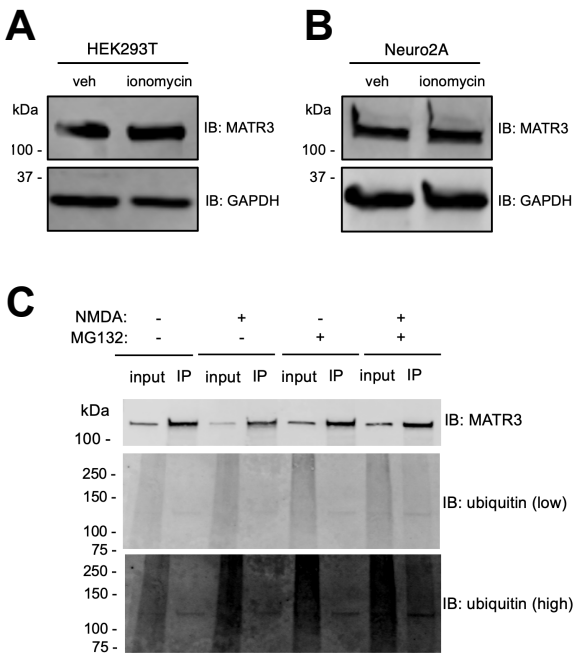

Supplemental Figure 3.2 Neurons clear MATR3 after Ca^{2+} elevation via a selective mechanism not dependent on ubiquitination. A-B. Unlike in cortical neurons, MATR3 in HEK293T cells and Neuro2A cell lines is not degraded with the ionophore ionomycin, pointing to neuron-specific factors in this process. **C.** Proteasomal blockade with MG132 in the context of NMDA stimulation of neurons does not result in the accumulation of ubiquitinated, higher molecular weight MATR3 species, indicating that degradation is not through the UPS.

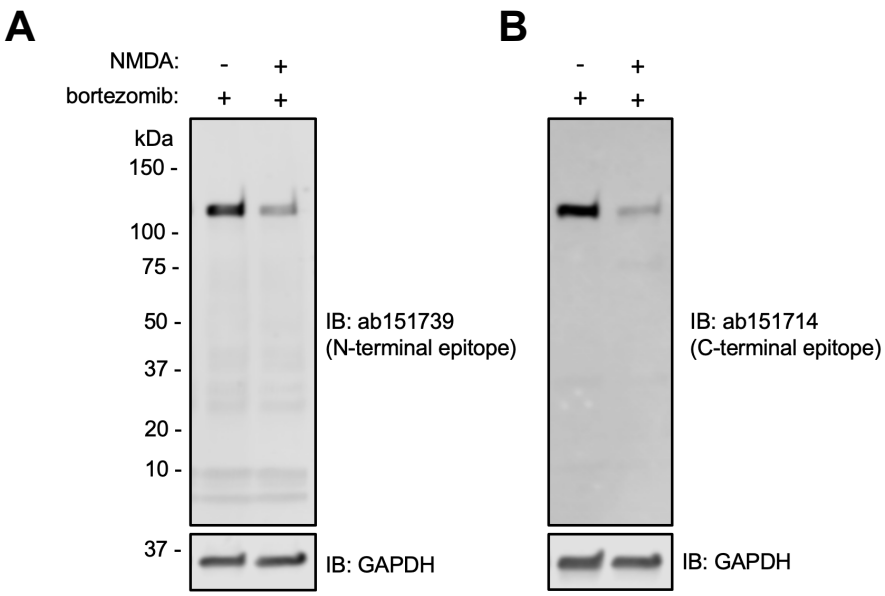

Supplemental Figure 3.3. Lower molecular weight calpain cleavage products are not detected in NMDA-treated neurons. A-B. Antibodies directed towards both the N- and C-termini of MATR3 cannot detect lower molecular weight MATR3 species even in the context of proteasomal block with bortezomib, indicating that MATR3 fragments are highly unstable and that calpain cleavage does not produce functional, shortened MATR3 species.

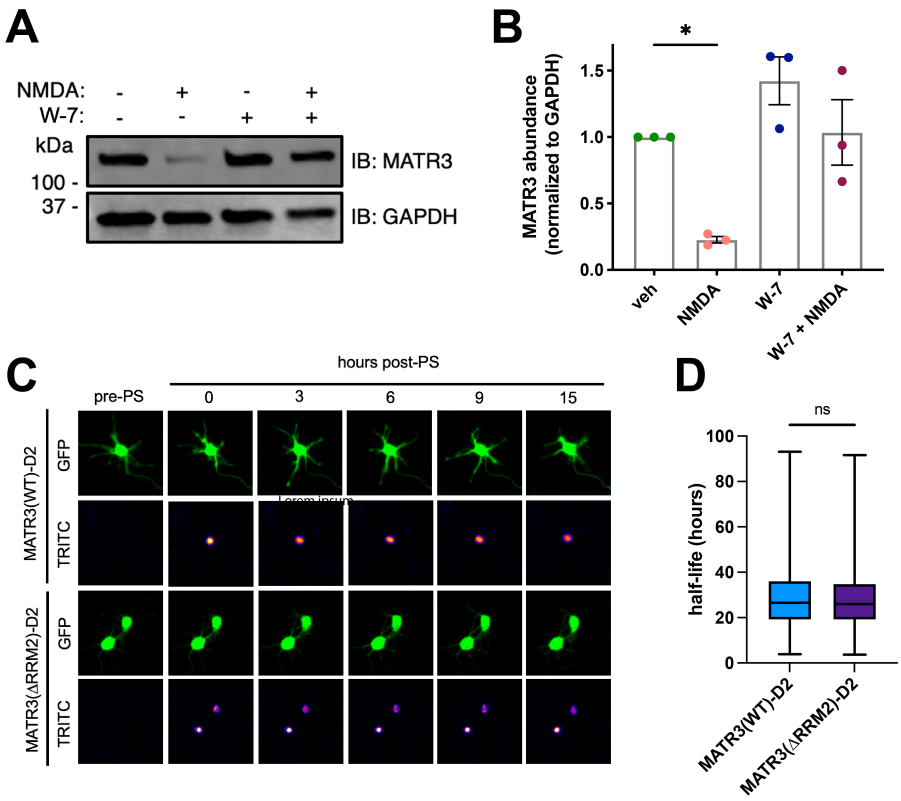

Supplemental Figure 3.4. CaM inhibition blocks NMDA-triggered MATR3 degradation, but RNA binding deficient MATR3 is not destabilized. A-B. Treatment with the CaM inhibitor W-7 blocks MATR3 reduction after NMDA treatment (compared to veh, n = 3; NMDA, n = 3, * p = 0.030; W-&, n = 3, p = 0.28; W-7 + NMDA, n = 3, p > 0.99). **C.** MATR3(WT) and MATR3(ΔRRM2) fused to the green-to-red photoconvertible protein Dendra2 were used in optical pulse labelling (OPL) experiments along with EGFP to fill cell bodies. **D.** Deletion of the main RNA-binding domain of MATR3 did not affect fusion protein half-life, indicating that impaired RNA binding per se is not sufficient to destabilize MATR3 (MATR3(WT)-D2, n = 495; MATR3(ΔRRM2)-D2, n = 701, p = 0.47).

Table 3.1. Primer sequences for RT-PCR targets

Target	Primers	Sequences
Matr3	Forward	5'-GCC ACC TCC TTC ATT TCA TCT-3'
	Reverse	5'-CTG GTT TCC ACT CTG CCT TT-3'
Gapdh	Forward	5'-AAG GTG AAG GTC GGA GTC AA-3'
	Reverse	5'-AAT GAA GGG GTC ATT GAT GG-3'
Tubb3	Forward	5'-GGC ATG GAT GAG ATG GAG TT-3'
	Reverse	5'-CTC CTC GTC GTC ATC TTC ATA C
Lsamp	Forward	5'-CGG GAT GAC ACC AGG ATA AAC-3'
	Reverse	5'-CAC AGG TAT AGT TGC CGT AGT G-3
Grm7	Forward	5'-CAA GGA TCT GTG TGC TGA CTA C-3'
	Reverse	5'-GGT TCC AGC ACT ACC ATT GA-3'
Ftx	Forward	5'-GGC ACT TTG GGT CCC TAT ATC-3'
	Reverse	5'-CAG GTT TGT GCG TAT GTG TAA G-3'

Chapter 4: Discussion and Future Directions[3]

4.1 Overview

Many questions regarding the basic biology of MATR3 and its implication in neuromuscular disorders remain, informed by the data presented in this dissertation. This chapter will discuss promising open questions and possible hypotheses, beginning with molecular functions and moving on to topics immediately relevant to neurological disease.

4.2 Cell-type specific MATR3 DNA- and RNA-binding functions

A pressing question concerns the relevant breadth of MATR3's nucleic acid binding. The work presented in this dissertation as well as other studies have focused largely on the RRMs of MATR3 and its functions in RNA regulation. As a result, there is strong evidence linking it to the splicing of pre-mRNAs and the transport, stabilization, and degradation of mature transcripts[1-4]. This is accomplished largely through its tandem RRM domains, with RRM2 being uniquely critical for binding[5]. As a result, it is unclear what role RRM1 plays. One possibility is that—as for TDP-43—the presence of

[3] Section 4.6 is adapted from the following publication: Malik AM and Barmada SJ. Matrin 3 in neuromuscular disease: physiology and pathophysiology. 2021. *JCI Insight*. 6(1):e143948. doi: 10.1172/jci.insight.143948.

an RRM that does little RNA binding on its own is to tune sequence specificity for RNAs bound by the tandem domains[6-8].

However, the details of MATR3's DNA binding and chromatin-mediated functions *in vivo* remain incompletely understood. As it possesses two C2H2 ZF domains, MATR3 has been annotated since its identification as a DNA-binding protein of the nuclear matrix[9]. Indeed, *in vitro* experiments using EMSA confirmed that MATR3 is capable of recognizing DNA isolated from rat liver and that both ZFs contributed to this activity[5]. Attempts at identifying DNA targets for MATR3 through unbiased genome-wide studies, however, offer a model in which MATR3 interaction with chromatin is indirect and dependent on tissue-specific factors rather than mediated only through its own ZFs.

The first ChIP-seq study for MATR3 was conducted in a rat pituitary cell line and reported that MATR3 significantly overlaps with enhancer sequences[10]. This interaction, however, is dependent on Pit1, a pituitary-specific transcription factor, as knockdown of Pit1 resulted in a marked reduction of MATR3 ChIP-seq signal. A study aimed at developing new chromatin-protein interaction technologies likewise found MATR3 to bind to insulator sequences in a mouse hematopoietic cell line[11]. As before, this interaction was not direct but in this context was dependent on the transcription factor CTCF. Most recently, a report in muscle cells found MATR3 to be largely localized to the relatively insoluble chromatin-associated fraction, with only minor amounts of protein in the nucleoplasm. This chromatin association, in turn, is dependent on the muscle-specific lncRNA *pCharme1*, as knockdown of this transcript causes MATR3 distribution from DNA into the nucleoplasm[12].

Taken together, these data suggest a model in which MATR3 binding to DNA is dependent on tissue- and cell type-specific protein and RNA factors. Neurons express CTCF[13,14], but muscle cells do as well[15,16] despite *pCharme1* disruption alone being sufficient to remove MATR3 from muscle chromatin, arguing that considerations beyond simply the presence or absence of protein/RNA factors may regulate MATR3's DNA association. Therefore, the role of MATR3 in neurons—and its contribution to neurodegenerative disease—remains elusive. It is possible that a complex orchestra of factors work in tandem to regulate MATR3's association with DNA and that neurons lack one or more of these; indeed, data in appendix A support this interpretation. If so, previous work suggests that MATR3's DNA- and RNA-binding functions compete with one another[3], and thus neuronal MATR3 may function exclusively in splicing and RNA control rather than transcriptional regulation. The markedly high neurotoxicity reported in chapter 2 upon expression of MATR3 variants lacking RRM2 that were not sequestered in phase-separated intranuclear droplets (Fig. 2.4) may have been from artificially driving MATR3 to chromatin in a cell type not evolved to have MATR3 in this role.

A lack of neuronal MATR3 association with DNA may arise from unique chromatin demands in post-mitotic cells such as neurons, or it may be a phenomenon present also in other cells lacking certain protein/RNA factors. To this end, it is of great interest to identify what chromatin regions, if any, MATR3 binds in neurons and what function is accomplishes through this interaction. Other proteins that bridge chromatin to the nuclear matrix via binding to matrix/scaffold attachment regions can regulate genes by tuning their accessibility to transcription machinery[17-19]. This appears to be

responsible for the upregulation of genes critical for myocyte differentiation accomplished by MATR3 chromatin association in muscle cells, and indirect *in vitro* data indicate that MATR3 binding is able to drive transcription of reporter constructs[12,20,21]. If MATR3 does have a role in neuronal transcriptional regulation, an interesting line of inquiry might focus on whether those genes overlap with or are distinct from those it regulates on the post-transcriptional level through pre-mRNA splicing and mRNA handling. There may be a set of genes that MATR3 doubly regulates, or its DNA-binding and RNA-binding functions might represent different ontological categories responding to disparate physiological stimuli.

Even RNA binding by MATR3 also could be completely or partially dependent on other factors, with the RBP polypyrimidine tract binding protein 1 (PTBP1) providing a key example. MATR3 directly interacts with PTBP1 via a short PTB-RRM interaction (PRI) motif located between MATR3's ZF1 and RRM1 that allows it to bind to RRM2 and the surrounding repressor domain of PTBP1[22]. MATR3 and PTBP1 have been identified in several independent experiments as direct interactors and have been implicated in similar RNA- and DNA-based functions, with both necessary for the lncRNA *Xist* to seed RBPs onto inactive X chromosomes and for the repression of LINEs[23,24]. Experiments in HeLa cells demonstrated that ~20% of MATR3's splicing targets are co-regulated by PTBP1[3]. Despite this, the PRI motif is necessary for MATR'3 splicing function even of some pre-mRNAs not regulated by PTBP1. Indeed, deletion of the PRI motif ablates MATR3 splicing activity for certain pre-mRNAs to the same extent as deletion of both RRMs. These intriguing data suggest that MATR3's functions in RNA processing might also be cooperative and at least partially indirect.

Conversely, MATR3 may itself act as a factor that promotes RNA binding for PTBP1 and other RBPs, as KD of MATR3 results in less RNA crosslinking to PTBP1 without changes in PTBP1 abundance in HEK293T cells; importantly this relationship does not appear to be bidirectional, as KD of PTBP1 does not diminish RNA crosslinking to MATR3 in this context.

4.3 Post-translational modification in MATR3 regulation

Another explanation for tissue- and cell-specific MATR3 nucleic acid binding lies in post-translational modifications (PTMs) on MATR3. PTMs, particularly phosphorylation, have been shown to enhance MATR3's ability to bind to both DNA[25] and RNA[26], though the location of the phosphoresidues remain unknown, as is whether these two aspects are controlled by the same phosphorylation events or not. It is conceivable that these PTMs alter DNA or RNA binding either directly or by changing MATR3's self-association or its binding to cofactors. Indeed, there are numerous examples of RBPs whose phosphorylation increases[27-29] or decreases[30-32] their affinity towards substrate RNAs. The cell-specific expression of kinases and phosphatases could therefore explain varied functions of MATR3 on nucleic acid regulation.

Even beyond tuning nucleic acid recognition, phosphorylation may control MATR3 function. Proteomics databases curating data from many repositories reveal that MATR3 is heavily phosphorylated[33]. Phosphorylation by protein kinase A (PKA) is implicated in degrading MATR3 in response to NMDAergic activity in cerebellar granule neurons[34], though our data argue against this mechanism in cortical neurons (Supplemental Fig. 3.1). Manipulations of MATR3's phosphorylation state have also

been linked to altered nucleocytoplasmic localization[35,36], although the only specific phosphoresidue functionally identified to date is Ser208[37], whose phosphorylation is tied to enhanced MATR3 nuclear localization and the DNA repair response[38]. Therefore, experiments aimed at identifying how phosphorylation controls MATR3 localization are critical for understanding nucleocytoplasmic shuttling in neurons. A tractable starting point for these studies might involve biochemical separation of nuclear and cytoplasmic lysates from neurons followed by proteomics for phosphoresidues that differentially enriched between nuclear and cytoplasmic compartments.

While no other PTMs besides phosphorylation have been mechanistically studied for MATR3, proteomics databases show abundant PTMs on MATR3 that may also tune its ability to recognize substrate RNA and DNA sequences, with numerous ubiquitination events identified on both of its tandem RRMs[39-43]. While our data blocking the ubiquitin proteasome system (UPS) in primary cortical neurons and probing for ubiquitinated MATR3 did not show such a species (Supplemental Fig. 3.2), the ubiquitination identified via proteomics studies may occur in response to particular physiological stimuli and so may not be involved in basal or NMDA-trigerred turnover of neuronal MATR3. The heavy modification of the RRMs is suggestive of a functional role in inhibition of RNA binding, perhaps in addition to degradation, and this may provide an alternate route for what we propose the Ca^{2+}/CaM system accomplishes in response to depolarization (Fig. 3.7). Moreover, while ZF1 appears to be devoid of PTMs, ZF2 is capable of being acetylated at three independent lysine residues[41,44-46]. Acetylation of key residues in the RRMs of TDP-43 has been shown to impair RNA binding and be

linked to disease pathology[47-49], and the acetylation of MATR3's ZF2 may have a similarly inhibitory function for the recognition of its substrates.

4.4 Ca^{2+}/CaM in RBP regulation and local translation

While we have experimentally validated binding of MATR3 and TDP-43 to Ca^{2+}/CaM but not apo-CaM, prediction algorithms[50-52] identify CaM-binding motifs on other RBPs as well, including many implicated in ALS/FTD spectrum disorders such as FUS, hnRNPA1, hnRNPA2B1, and TIA1 (Fig. 3.5). Notably, the predicted CaM-binding sites on these RBPs are also on their RNA-binding domains, strongly suggesting a functional effect on RNA recognition. Whether these other RBPs bind Ca^{2+}/CaM *in vivo* and what effect this interaction has is unknown but may form the basis of a post-translational, dynamic method for broadly controlling neuronal RBP function.

One particular physiological context this may relate to is that of local translation in neuronal processes. Because of the unique spatiotemporal translation demands faced by neurons, whose neurites may terminate more than a meter away from the soma in humans, these cells have evolved methods of rapidly translating proteins in the appropriate compartment in response to stimuli. This is accomplished through RBPs that transport mRNAs to dendrites and axons and keep them in a translationally repressed state until they are released and able to be translated into protein by resident dendritic and axonal ribosomes[53-55].

Many RBPs, including those implicated in neurological disease, have been linked to local neuronal translation in response to depolarization or other cues. mRNAs are targeted to neuronal processes by transport RBPs that recognize primary or secondary

sequences in their untranslated regions (UTRs), and consistent with neurons' dependence on local translation, neuronal mRNAs possess markedly longer 3' UTRs than non-neuronal transcripts[56,57]. Transporting RBPs traffic their substrate mRNAs via the cytoskeleton from the soma to sites of potential local translation in the form of phase-separated RNA granules[58,59]. At the periphery, these transcripts are held in a translationally repressed state by RBPs until the appropriate signal results in their liberation and exposure to the local translation machinery. Distally located mRNAs are longer lived than their somatically localized counterparts, reflecting the enhanced stability necessary for their unique roles[60].

Depending on the function of the mRNA and the cellular compartment, the nature of stimuli driving translational and their molecular mechanisms can be quite diverse, with some involving the irreversible degradation of RBPs in response to neurotransmitter binding. For example, fragile X mental retardation protein (FMRP), binds to both its substrate transcripts and to ribosomes in dendrites to inhibit translation. Glutamate release from pre-synaptic neurons stimulates metabotropic glutamate receptors on dendrites that in turn activate protein phosphatase 2A, and the resulting dephosphorylation of FMRP drives its rapid ubiquitination and degradation and the translation of its bound mRNAs by ribosomes[61-64]. Other mechanisms respond to trophic factors and are non-degradative instead, involving the dynamic tuning of RNA-RBP interactions. Zipcode binding protein 1 (ZBP1), for instance, traffics β-actin mRNA down axons to growth cones, where it holds this transcript in a repressed state. Binding of extracellular brain derived neurotrophic factor (BDNF) to its receptors on the neuron surface leads to local activation of Src kinase, which phosphorylates ZBP1 on a key

tyrosine residue in its RNA-binding domain, impairing its ability to bind RNA and thereby releasing β-actin transcript for translation and promoting axon growth[31,65,66].

Over the past decade, strong evidence has accumulated tying many RBPs involved in the pathogenesis of ALS/FTD spectrum disorders to local translation in neurites, with much of this work focusing on TDP-43 and FUS. Besides their nuclear role in pre-mRNA splicing, both TDP-43 and FUS function in neuronal cytoplasm in the transport and local translation, and disease-linked mutations impair these processes[67-73]. Based off the predicted CaM binding sites in the nucleic acid-binding domains of these and other proteins, it is of great interest to test whether Ca^{2+} mediates the dynamic release of TDP-43 and FUS target mRNAs for translation in response to depolarization. CaM protein, encoded in mammals by three genes with identical coding sequences but divergent UTRs, is present at sites of local translation, and certain transcripts encoding CaM are not only highly expressed in neuronal tissue but also have 3' UTRs critical for their dendritic targeting and activity-dependent local translation, suggesting this may itself strengthen a Ca^{2+}/CaM RBP regulation system[60,74-76]. Indeed, based off the large number of RBPs we have identified with predicted CaM binding domains, an increase in Ca^{2+} may represent a mechanism of widespread translational disinhibition, particularly in distal compartments. Seeing as how pathogenic mutations have been shown to disrupt local translation in model systems, a change in neuronal excitability may contribute to ALS/FTD pathology through a Ca^{2+}/CaM -dependent pathway.

4.5 MATR3 histopathology in familial and sporadic disease

A key question regarding MATR3's role in human disease centers around patterns of pathology seen in affected tissue. To date, the only spinal cord histology report from a patient with a *MATR3* mutation is from a family harboring the Phe115Cys mutation, which was later categorized as being likely non-pathogenic due to incomplete segregation with disease and the identification of another causative ALS mutation in this family that does completely segregate with ALS[77,78]. Spinal motor neurons from this individual, however, showed a more intense pattern of MATR3 staining, which is in agreement with a later study that reported more intense MATR3 signal as well as more cytoplasmic MATR3 in the motor neurons of sporadic ALS (sALS) cases compared to controls[79]. The most thorough neuropathological investigation of MATR3 by far, however, was unable to replicate the more intense pattern of MATR3 staining in disease tissue, though it reported MATR3-positive cytoplasmic inclusions coupled with relative nuclear clearance in 60% of sALS patients while none were observed in controls[80].

This study raises many critical points for understanding what the precise contribution of MATR3 to human disease is. TDP-43 pathology—consisting of nuclear clearance and cytoplasmic aggregation—is observed in affected tissues in the vast majority of patients with ALS and nearly half of those with FTD[81,82]. In agreement with the prevalence of TDP-43 pathology in ALS, all MATR3-positive inclusions were TDP-43-positive, but the authors were unable to identify a MATR3-positive, TDP-43-negative inclusion. Therefore, TDP-43 and MATR3 may have a complex, temporally linked interplay in the disease context, with TDP-43 possibly exiting the nucleus first, aggregating in the cytoplasm and sequestering MATR3 through an unknown mechanism.

Complicating this model, however, is the finding that sALS cases with MATR3-positive cytoplasmic inclusions on autopsy had a significantly reduced duration of disease, implying more aggressive progression, than those with TDP-43-positive inclusions only. Those with MATR3 pathology may have genetic or environmental modifiers driving disease progression as well as MATR3 deposition in the cytoplasm, or the clearance of MATR3 from the nucleus and its presence in the cytoplasm may itself contribute to neurotoxicity. Our work in a rat neuron model showed, however, that unlike TDP-43 and FUS, whose expression in the cytoplasm is more toxic than expression in the nuclear compartment, MATR3 cytoplasmic redistribution reduced overexpression toxicity (Fig. 2.6). This suggests that cytoplasmic MATR3 is not neurotoxic, though our study was in the context of intact endogenous MATR3 function in the nucleus; the apparent redistribution from nucleus to cytoplasm in disease therefore may represent a very different context combining nuclear loss-of-function with cytoplasmic gain-of-function.

Alternatively, it may be that MATR3 pathology is common, with more ALS patients having MATR3-positive inclusions in motor neurons but in most cases those cells dying well before autopsy. This would leave only those individuals with the most aggressive disease course retaining neurons with MATR3-positive inclusions at the time of death. More detailed analyses of MATR3 neuropathology are desperately needed in both healthy and disease tissue, particularly in regard to its localization, as this is critical in understanding whether ALS pathogenesis is driven by MATR3 clearance from the nucleus, overabundance in the cytoplasm, both, or neither.

4.6 Phenotypic spectrum of MATR3 mutations

Another outstanding question concerns the phenotypic spectrum of MATR3-linked disease and how *MATR3* mutations can cause motor neuron degeneration, cortical neuron loss, and/or myopathy. The Ser85Cys mutation is capable of driving both myogenic and neurogenic disease, suggesting the presence of specific environmental or genetic factors that modify tissue specificity. Moving forward, the continued identification and thorough clinical testing of patients with *MATR3* mutations will be essential if we are to uncover the identity and function of these modifiers. At present, many *MATR3* variants are singletons with only weak evidence to support pathogenicity; therefore, it will be critical to not only verify these mutations in other patients and families but also to confirm their pathogenicity and investigate mutation-specific pathways in model systems.

Cautionary tales for inferring pathogenicity of MATR3 variants based on a paucity of genetic data can already be appreciated. The Phe115Cys MATR3 mutation was originally identified in a family with many members diagnosed with ALS and dementia but was recently reclassified as likely non-pathogenic. This change was due to its incomplete segregation with disease and the identification of a mutation in another ALS-linked gene, *KIF5A*, wholly segregating with ALS/FTD in the original kindred[83]. Additionally, a patient with early onset FTD was found to have a full-length *MATR3* transcript inserted into chromosome 12 via retrotransposition, suggesting disease linked to overabundance of MATR3. Increased MATR3 RNA or protein was not confirmed, however, and at least two unaffected relatives share this retrotransposition, arguing

against its pathogenicity[84]. These results underscore the vital need to critically examine the proposed pathogenicity of variants.

Cellular and animal models have been pivotal for our understanding of MATR3-linked neuromuscular disease, and we expect new models to offer further insights. Induced pluripotent stem cell (iPSC) technology represents a particularly promising approach for understanding MATR3 function, and three patient-derived iPSC lines have already been created[85,86]. iPSCs would be particularly useful in studying tissue-specific functions, as these cells can be differentiated into isogenic motor neurons, cortical neurons, and skeletal muscle cells. In addition to enabling the identification of cell type-specific MATR3 functions and pathogenic pathways triggered by mutant *MATR3* variants, iPSCs may facilitate the identification of elements of MATR3 biology that are unique to human neurons, as has recently been the case for TDP-43[87,88].

4.7 Conclusions

MATR3 was identified nearly three decades ago and has been implicated in a broad spectrum of human disease for many years, but pressing questions still remain about its diverse functions in nucleic acid processing as well as its involvement in sporadic and inherited neuromuscular disorders. It is my hope that continued research in this exciting field will build off the work presented in this dissertation to uncover key elements of MATR3 physiology and pathophysiology and, in doing so, will further our understanding of the neuronal regulation of RBPs and will provide a basis for the rational development of therapies for diseases linked to dysfunction of MATR3 and related proteins.

References

1. Salton, M. *et al.* Matrin 3 Binds and Stabilizes mRNA. *PLoS ONE* **6,** e23882–7 (2011).
2. Rajgor, D., Hanley, J. G. & Shanahan, C. M. Identification of novel nesprin-1 binding partners and cytoplasmic matrin-3 in processing bodies. **27,** 3894–3902 (2016).
3. Coelho, M. B. *et al.* Nuclear matrix protein Matrin3 regulates alternative splicing and forms overlapping regulatory networks with PTB. *The EMBO Journal* **34,** 653–668 (2015).
4. Uemura, Y. *et al.* Matrin3 binds directly to intronic pyrimidine-rich sequences and controls alternative splicing. *Genes Cells* **22,** 785–798 (2017).
5. Hibino, Y. *et al.* Molecular properties and intracellular localization of rat liver nuclear scaffold protein P130. *Biochimica et Biophysica Acta (BBA) - Gene Structure and Expression* **1759,** 195–207 (2006).
6. Ayala, Y. M. *et al.* Human, Drosophila, and C.elegans TDP43: nucleic acid binding properties and splicing regulatory function. *J. Mol. Biol.* **348,** 575–588 (2005).
7. Kuo, P.-H., Doudeva, L. G., Wang, Y.-T., Shen, C.-K. J. & Yuan, H. S. Structural insights into TDP-43 in nucleic-acid binding and domain interactions. *Nucleic Acids Research* **37,** 1799–1808 (2009).
8. Buratti, E. & Baralle, F. E. Characterization and functional implications of the RNA binding properties of nuclear factor TDP-43, a novel splicing regulator of CFTR exon 9. *The Journal of Biological Chemistry* **276,** 36337–36343 (2001).
9. Nakayasu, H. & Berezney, R. Nuclear matrins: identification of the major nuclear matrix proteins. *Proc Natl Acad Sci USA* **88,** 10312–10316 (1991).
10. Skowronska-Krawczyk, D. *et al.* Required enhancer–matrin-3 network interactions for a homeodomain transcription program. *Nature* 1–13 (2014). doi:10.1038/nature13573
11. Fujita, T. & Fujii, H. Direct identification of insulator components by insertional chromatin immunoprecipitation. *PLoS ONE* **6,** e26109 (2011).
12. Desideri, F. *et al.* Intronic Determinants Coordinate Charme lncRNA Nuclear Activity through the Interaction with MATR3 and PTBP1. *Cell Rep* **33,** 108548 (2020).
13. Brito, D. V. C. & Gulmez Karaca, K. Neuronal Chromatin Architecture Regulator CTCF Dictates Remote Memory. *J. Neurosci.* **38,** 10239–10240 (2018).
14. López Soto, E. J. & Lipscombe, D. Cell-specific exon methylation and CTCF binding in neurons regulate calcium ion channel splicing and function. *Elife* **9,** 483 (2020).
15. Abbadi, D., Yang, M., Chenette, D. M., Andrews, J. J. & Schneider, R. J. Muscle development and regeneration controlled by AUF1-mediated stage-specific degradation of fate-determining checkpoint mRNAs. *Proc. Natl. Acad. Sci. U.S.A.* **116,** 11285–11290 (2019).
16. Delgado-Olguín, P. *et al.* CTCF promotes muscle differentiation by modulating the activity of myogenic regulatory factors. *The Journal of Biological Chemistry* **286,** 12483–12494 (2011).

17. Craig, J. M., Boyle, S., Perry, P. & Bickmore, W. A. Scaffold attachments within the human genome. *J. Cell. Sci.* **110 (Pt 21),** 2673–2682 (1997).
18. Poljak, L. & Käs, E. Resolving the role of topoisomerase II in chromatin structure and function. *Trends Cell Biol.* **5,** 348–354 (1995).
19. Gerdes, M. G., Carter, K. C., Moen, P. T. & Lawrence, J. B. Dynamic changes in the higher-level chromatin organization of specific sequences revealed by in situ hybridization to nuclear halos. *J. Cell Biol.* **126,** 289–304 (1994).
20. Hibino, Y., Ohzeki, H., Sugano, N. & Hiraga, K. Transcription Modulation by a Rat Nuclear Scaffold Protein, P130, and a Rat Highly Repetitive DNA Component or Various Types of Animal and Plant Matrix or Scaffold Attachment Regions. *Biochemical and Biophysical Research Communications* **279,** 282–287 (2000).
21. Banerjee, A., Vest, K. E., Pavlath, G. K. & Corbett, A. H. Nuclear poly(A) binding protein 1 (PABPN1) and Matrin3 interact in muscle cells and regulate RNA processing. *Nucleic Acids Research* **45,** 10706–10725 (2017).
22. Joshi, A. *et al.* Crystallographic analysis of polypyrimidine tract-binding protein-Raver1 interactions involved in regulation of alternative splicing. *Structure* **19,** 1816–1825 (2011).
23. Pandya-Jones, A. *et al.* A protein assembly mediates Xist localization and gene silencing. *Nature* **587,** 145–151 (2020).
24. Attig, J. *et al.* Heteromeric RNP Assembly at LINEs Controls Lineage-Specific RNA Processing. *Cell* **174,** 1067–1081.e17 (2018).
25. Hibino, Y., Ohzeki, H., Hirose, N. & Sugano, N. Involvement of phosphorylation in binding of nuclear scaffold proteins from rat liver to a highly repetitive DNA component. *Biochimica et Biophysica Acta (BBA) - Gene Structure and Expression* **1396,** 88–96 (1998).
26. Yamazaki, F. *et al.* pY RNA1-s2: a highly retina-enriched small RNA that selectively binds to Matrin 3 (Matr3). *PLoS ONE* **9,** e88217 (2014).
27. Zhang, M., Lam, T. T., Tonelli, M., Marzluff, W. F. & Thapar, R. Interaction of the histone mRNA hairpin with stem-loop binding protein (SLBP) and regulation of the SLBP-RNA complex by phosphorylation and proline isomerization. *Biochemistry* **51,** 3215–3231 (2012).
28. Borchers, C. H. *et al.* Combined top-down and bottom-up proteomics identifies a phosphorylation site in stem-loop-binding proteins that contributes to high-affinity RNA binding. *Proc Natl Acad Sci USA* **103,** 3094–3099 (2006).
29. Prischi, F., Nowak, P. R., Carrara, M. & Ali, M. M. U. Phosphoregulation of Ire1 RNase splicing activity. *Nature Communications* **5,** 3554–11 (2014).
30. Cho, S. *et al.* Interaction between the RNA binding domains of Ser-Arg splicing factor 1 and U1-70K snRNP protein determines early spliceosome assembly. *Proc. Natl. Acad. Sci. U.S.A.* **108,** 8233–8238 (2011).
31. Hüttelmaier, S. *et al.* Spatial regulation of beta-actin translation by Src-dependent phosphorylation of ZBP1. *Nature* **438,** 512–515 (2005).
32. Perycz, M., Urbanska, A. S., Krawczyk, P. S., Parobczak, K. & Jaworski, J. Zipcode binding protein 1 regulates the development of dendritic arbors in hippocampal neurons. *J. Neurosci.* **31,** 5271–5285 (2011).
33. Hornbeck, P. V. *et al.* PhosphoSitePlus, 2014: mutations, PTMs and recalibrations. *Nucleic Acids Research* **43,** D512–20 (2015).

34. Giordano, G. *et al.* Activation of NMDA receptors induces protein kinase A-mediated phosphorylation and degradation of matrin 3. Blocking these effects prevents NMDA-induced neuronal death. *Journal of Neurochemistry* **94,** 808–818 (2005).
35. Erazo, A., Yee, M. B., Banfield, B. W. & Kinchington, P. R. The Alphaherpesvirus US3/ORF66 Protein Kinases Direct Phosphorylation of the Nuclear Matrix Protein Matrin 3. *Journal of Virology* **85,** 568–581 (2010).
36. Hisada-Ishii, S., Ebihara, M., Kobayashi, N. & KITAGAWA, Y. Bipartite nuclear localization signal of matrin 3 is essential for vertebrate cells. *Biochemical and Biophysical Research Communications* **354,** 72–76 (2007).
37. Niimori-Kita, K., Tamamaki, N., Koizumi, D. & Niimori, D. Matrin-3 is essential for fibroblast growth factor 2-dependent maintenance of neural stem cells. *Scientific Reports* **8,** 13412 (2018).
38. Salton, M., Lerenthal, Y., Wang, S.-Y., Chen, D. J. & Shiloh, Y. Involvement of Matrin 3 and SFPQ/NONO in the DNA damage response. *Cell Cycle* **9,** 1568–1576 (2014).
39. Akimov, V. *et al.* UbiSite approach for comprehensive mapping of lysine and N-terminal ubiquitination sites. *Nat. Struct. Mol. Biol.* **25,** 631–640 (2018).
40. Udeshi, N. D. *et al.* Refined preparation and use of anti-diglycine remnant (K-ε-GG) antibody enables routine quantification of 10,000s of ubiquitination sites in single proteomics experiments. *Mol Cell Proteomics* **12,** 825–831 (2013).
41. Mertins, P. *et al.* Integrated proteomic analysis of post-translational modifications by serial enrichment. *Nat. Methods* **10,** 634–637 (2013).
42. Kim, W. *et al.* Systematic and quantitative assessment of the ubiquitin-modified proteome. *Mol. Cell* **44,** 325–340 (2011).
43. Lumpkin, R. J. *et al.* Site-specific identification and quantitation of endogenous SUMO modifications under native conditions. *Nature Communications* **8,** 1171–11 (2017).
44. Wu, Q. *et al.* Suberoylanilide hydroxamic acid treatment reveals crosstalks among proteome, ubiquitylome and acetylome in non-small cell lung cancer A549 cell line. *Scientific Reports* **5,** 9520–11 (2015).
45. Beli, P. *et al.* Proteomic investigations reveal a role for RNA processing factor THRAP3 in the DNA damage response. *Mol. Cell* **46,** 212–225 (2012).
46. Choudhary, C. *et al.* Lysine acetylation targets protein complexes and co-regulates major cellular functions. *Science* **325,** 834–840 (2009).
47. Cohen, T. J. *et al.* An acetylation switch controls TDP-43 function and aggregation propensity. *Nature Communications* **6,** 5845–13 (2015).
48. Wang, P., Wander, C. M., Yuan, C.-X., Bereman, M. S. & Cohen, T. J. Acetylation-induced TDP-43 pathology is suppressed by an HSF1-dependent chaperone program. *Nature Communications* **8,** 82–15 (2017).
49. Yu, H. *et al.* HSP70 chaperones RNA-free TDP-43 into anisotropic intranuclear liquid spherical shells. *Science* **371,** eabb4309 (2021).
50. Yap, K. L. *et al.* Calmodulin target database. *J Struct Funct Genomics* **1,** 8–14 (2000).

51. Mruk, K., Farley, B. M., Ritacco, A. W. & Kobertz, W. R. Calmodulation meta-analysis: predicting calmodulin binding via canonical motif clustering. *J Gen Physiol* **144,** 105–114 (2014).
52. Abbasi, W. A., Asif, A., Andleeb, S. & Minhas, F. U. A. A. CaMELS: In silico prediction of calmodulin binding proteins and their binding sites. *Proteins* **85,** 1724–1740 (2017).
53. Hafner, A.-S., Donlin-Asp, P. G., Leitch, B., Herzog, E. & Schuman, E. M. Local protein synthesis is a ubiquitous feature of neuronal pre- and postsynaptic compartments. *Science* **364,** eaau3644 (2019).
54. Shigeoka, T. *et al.* Dynamic Axonal Translation in Developing and Mature Visual Circuits. *Cell* **166,** 181–192 (2016).
55. Ostroff, L. E., Fiala, J. C., Allwardt, B. & Harris, K. M. Polyribosomes redistribute from dendritic shafts into spines with enlarged synapses during LTP in developing rat hippocampal slices. *Neuron* **35,** 535–545 (2002).
56. Miura, P., Shenker, S., Andreu-Agullo, C., Westholm, J. O. & Lai, E. C. Widespread and extensive lengthening of 3' UTRs in the mammalian brain. *Genome Res* **23,** 812–825 (2013).
57. Taliaferro, J. M. *et al.* Distal Alternative Last Exons Localize mRNAs to Neural Projections. *Mol. Cell* **61,** 821–833 (2016).
58. Knowles, R. B. *et al.* Translocation of RNA granules in living neurons. *J. Neurosci.* **16,** 7812–7820 (1996).
59. Liao, Y.-C. *et al.* RNA Granules Hitchhike on Lysosomes for Long-Distance Transport, Using Annexin A11 as a Molecular Tether. *Cell* **179,** 147–164.e20 (2019).
60. Tushev, G. *et al.* Alternative 3' UTRs Modify the Localization, Regulatory Potential, Stability, and Plasticity of mRNAs in Neuronal Compartments. *Neuron* **98,** 495–511.e6 (2018).
61. Antar, L. N., Afroz, R., Dictenberg, J. B., Carroll, R. C. & Bassell, G. J. Metabotropic glutamate receptor activation regulates fragile x mental retardation protein and FMR1 mRNA localization differentially in dendrites and at synapses. *J. Neurosci.* **24,** 2648–2655 (2004).
62. Darnell, J. C. *et al.* FMRP stalls ribosomal translocation on mRNAs linked to synaptic function and autism. *Cell* **146,** 247–261 (2011).
63. Ascano, M. *et al.* FMRP targets distinct mRNA sequence elements to regulate protein expression. *Nature* **492,** 382–386 (2012).
64. Nalavadi, V. C., Muddashetty, R. S., Gross, C. & Bassell, G. J. Dephosphorylation-induced ubiquitination and degradation of FMRP in dendrites: a role in immediate early mGluR-stimulated translation. *J. Neurosci.* **32,** 2582–2587 (2012).
65. Sasaki, Y. *et al.* Phosphorylation of zipcode binding protein 1 is required for brain-derived neurotrophic factor signaling of local beta-actin synthesis and growth cone turning. *J. Neurosci.* **30,** 9349–9358 (2010).
66. Nicastro, G. *et al.* Mechanism of β-actin mRNA Recognition by ZBP1. *Cell Rep* **18,** 1187–1199 (2017).

67. Gopal, P. P., Nirschl, J. J., Klinman, E. & Holzbaur, E. L. F. Amyotrophic lateral sclerosis-linked mutations increase the viscosity of liquid-like TDP-43 RNP granules in neurons. *Proc Natl Acad Sci USA* **114,** E2466–E2475 (2017).
68. Alami, N. H. *et al.* Axonal transport of TDP-43 mRNA granules is impaired by ALS-causing mutations. *Neuron* **81,** 536–543 (2014).
69. Rotem, N. *et al.* ALS Along the Axons - Expression of Coding and Noncoding RNA Differs in Axons of ALS models. *Scientific Reports* **7,** 44500–17 (2017).
70. Nagano, S. *et al.* TDP-43 transports ribosomal protein mRNA to regulate axonal local translation in neuronal axons. *Acta Neuropathol* **140,** 695–713 (2020).
71. Chu, J.-F., Majumder, P., Chatterjee, B., Huang, S.-L. & Shen, C.-K. J. TDP-43 Regulates Coupled Dendritic mRNA Transport-Translation Processes in Co-operation with FMRP and Staufen1. *Cell Rep* **29,** 3118–3133.e6 (2019).
72. López-Erauskin, J. *et al.* ALS/FTD-Linked Mutation in FUS Suppresses Intra-axonal Protein Synthesis and Drives Disease Without Nuclear Loss-of-Function of FUS. *Neuron* **106,** 354 (2020).
73. Kamelgarn, M. *et al.* ALS mutations of FUS suppress protein translation and disrupt the regulation of nonsense-mediated decay. *Proc. Natl. Acad. Sci. U.S.A.* **115,** E11904–E11913 (2018).
74. Jones, K. J. *et al.* Rapid, experience-dependent translation of neurogranin enables memory encoding. *Proc. Natl. Acad. Sci. U.S.A.* **115,** E5805–E5814 (2018).
75. Bae, B. *et al.* Elimination of Calm1 long 3'-UTR mRNA isoform by CRISPR-Cas9 gene editing impairs dorsal root ganglion development and hippocampal neuron activation in mice. *RNA* **26,** 1414–1430 (2020).
76. Sharangdhar, T. *et al.* A retained intron in the 3'-UTR of Calm3 mRNA mediates its Staufen2- and activity-dependent localization to neuronal dendrites. *EMBO Rep.* **18,** 1762–1774 (2017).
77. Johnson, J. O. *et al.* Mutations in the Matrin 3 gene cause familial amyotrophic lateral sclerosis supplemental. *Nat Neurosci* **17,** 664–666 (2014).
78. Saez-Atienzar, S. *et al.* Identification of a pathogenic intronic KIF5A mutation in an ALS-FTD kindred. *Neurology* 10.1212/WNL.0000000000011064 (2020). doi:10.1212/WNL.0000000000011064
79. Dreser, A. *et al.* The ALS-linked E102Q mutation in Sigma receptor-1 leads to ER stress-mediated defects in protein homeostasis and dysregulation of RNA-binding proteins. 1–17 (2017). doi:10.1038/cdd.2017.88
80. Tada, M. *et al.* Matrin 3 is a component of neuronal cytoplasmic inclusions of motor neurons in sporadic amyotrophic lateral sclerosis. *The American Journal of Pathology* 1–36 (2017). doi:10.1016/j.ajpath.2017.10.007
81. Neumann, M. *et al.* Ubiquitinated TDP-43 in frontotemporal lobar degeneration and amyotrophic lateral sclerosis. *Science* **314,** 130–133 (2006).
82. Arai, T. *et al.* TDP-43 is a component of ubiquitin-positive tau-negative inclusions in frontotemporal lobar degeneration and amyotrophic lateral sclerosis. *Biochemical and Biophysical Research Communications* **351,** 602–611 (2006).
83. Saez-Atienzar, S. *et al.* Identification of a pathogenic intronic KIF5A mutation in an ALS-FTD kindred. *Neurology* 10.1212/WNL.0000000000011064 (2020). doi:10.1212/WNL.0000000000011064

84. Castro, M. *et al.* Case Report: Early-Onset Behavioral Variant Frontotemporal Dementia in Patient With Retrotransposed Full-Length Transcript of Matrin-3 Variant 5. *Front Neurol* **11,** 600468 (2020).
85. Pollini, D. *et al.* Generation and characterization of a human iPSC line from an ALS patient carrying the Q66K-MATR3 mutation. *Stem Cell Res* **33,** 146–150 (2018).
86. Medina, D. X. *et al.* Generation of two induced pluripotent stem cell (iPSC) lines from an ALS patient with simultaneous mutations in KIF5A and MATR3 genes. *Stem Cell Res* **50,** 102141 (2020).
87. Klim, J. R. *et al.* ALS-implicated protein TDP-43 sustains levels of STMN2, a mediator of motor neuron growth and repair. *Nat Neurosci* **22,** 167–179 (2019).
88. Melamed, Z. *et al.* Premature polyadenylation-mediated loss of stathmin-2 is a hallmark of TDP-43-dependent neurodegeneration. *Nat Neurosci* **22,** 180–190 (2019).

Appendix A: MATR3 ChIP-seq in Neurons

A.1 Introduction:

MATR3 was first identified as a major component of the nuclear matrix[1,2], and its ability to bind DNA has since been confirmed through *in vitro* and in situ experiments. The two ZF domains of MATR3 have been shown to both contribute to its binding to at least one DNA fragment[3], though since RRMs can also exhibit DNA-binding capacity it cannot be ruled out that it uses its tandem RRMs to interact with other DNA sequences. With the exception of a report from muscle cells[4], studies *in situ* have been conducted in pituitary[5] and hematopoietic[6] cell types not known to be involved in the spectrum of MATR3-mediated disease, leaving it unclear whether DNA-mediated functions of MATR3 are involved in neurological disease. Experiments in neurons, including those presented in chapters 2 and 3 of this dissertation, and neuron-like cells[7] have rather focused on the importance of RRMs and RNA binding in MATR3's neuronal toxicity and localization. Therefore, it is unclear what chromatin sequences, in any, MATR3 binds in neurons and what functions it affects through this interaction.

Chromatin immunoprecipitation followed by sequencing (ChIP-seq) is a technique for identifying binding between a protein of interest and DNA in a genome-wide, unbiased fashion[8,9]. In this process, covalent protein-DNA complexes are created

through chemical fixation, after which mechanical or enzymatic fragmentation is used to shear chromatin to fragment sizes that allow unambiguous, localized mapping of reads to the target genome followed by peak calling. A number of analyses are then made possible, including sequence motif discovery[10] and the identification of overlap with genomic elements such as enhancer and promoters[11].

In this appendix, I will detail attempted chromatin-immunoprecipitation followed by sequencing (ChIP-seq) studies in primary cortical neurons. Although I was unable to observe enrichment of DNA sequences co-immunoprecipitated with MATR3 despite technically validating fixation, immunoprecipitation, and chromatin shearing protocols, these negative results still offer potential insight into the tissue-specific functions of MATR3, pointing to a more RNA-centric role for MATR3 in neurons and implicating RNA dyshomeostasis in MATR3-linked neurodegenerative disease.

A.2 Results:

A.2.1 Primary cortical neuron ChIP optimization

DNA-protein complexes in DIV14-16 rat cortical neurons were fixed in 1% formaldehyde for 10 or 30 min, after which chromatin was sheared and samples were incubated with either MATR3 antibody to pull down MATR3-DNA complexes or IgG control. Western blot analysis after IP confirmed crosslinked high molecular weight MATR3 species robustly formed in a fixation time-dependent manner that were effectively immunoprecipitated along with uncrosslinked, free protein running at approximately 120 kDa (Fig. A.1A). As 10 minutes of fixation was sufficient for crosslinking, this timepoint was used for generating sequencing data.

Efficiency of chromatin shearing via sonication in lysates was assessed by purifying DNA from input and subjecting it to agarose electrophoresis. As desired, the vast majority of DNA signal from the sheared chromatin represented fragments approximately 200 bp in size (Fig. A.1B), which is in the optimal range for downstream sequencing analysis.

A.2.2 ChIP-seq analyses revealed no enrichment across the genome in MATR3 IgG samples

Despite technical validation of this ChIP protocol, sequencing results after read processing and mapping showed no appreciable chromatin signal immunoprecipitated with MATR3 antibody, either when compared to input or to IgG control. Across the genome, relatively few peaks were called for both types of analyses, even when stringency was reduced by allowing peak calling not in narrow peak, transcription factor-like mode but rather in broad and shallow peak mode (Fig. A.2A). When visualized through a genome viewer, however, even these few peaks, most of which barely achieved significance, were not impressively distinct and represented areas where there were only slightly more reads for the MATR3 antibody sample than input or IgG control (Fig. A.2B).

Fingerprint analysis can be used in ChIP-seq studies to validate the extent of enrichment across the genome. In a successful ChIP-seq experiment, comparatively small regions of the genome account for a disproportionally large fraction of reads, resulting in a sharply upward curving fingerprint plot of coverage against genomic enrichment rank. For example, in an effective experiment the lower 95% of ranked

genome segments account for far less than 95% of mapped reads, and the remaining 5% of highest rank will account for the vast majority of reads[12]. While theoretically an unenriched sample would form a linear plot, differential openness of chromatin results in even unenriched input samples displaying an upward curve as genomic rank increases. Sequencing samples from DNA coimmunoprecipitated from MATR3 antibody and from input DNA were analyzed using fingerprint analysis. Whether analyzed as mapped single-end reads or as mapped paired-end reads, MATR3 ChIP samples showed no deviation from the input curves (Fig. A.2C-D), indicating an unsuccessful ChIP-seq experiment, with no genomic regions preferentially associating with MATR3.

A.3 Discussion

Although MATR3 has been shown to bind DNA through *in vitro* electromobility shift studies and through ChIP-seq experiments, we were unable to observe any binding to DNA. While technical obstacles cannot be disregarded as an explanation, the validation of IP and shearing procedures leaves open a biological mechanism for the lack of chromatin signal observed. Namely, all *in situ* MATR3-DNA associations reported thus far have been shown to be dependent on protein or RNA cofactors necessary for MATR3 binding to chromatin. As discussed in chapter 4, it is possible that neurons lack cell- or tissue-specific cofactors and thus MATR3 has little to no neuronal DNA binding capacity despite its two ZFs that are necessary for DNA binding *in vitro*.

The higher molecular weight MATR3 species observed after fixation (Fig. A.1A) may rather represent covalent bonds to RNA or to other proteins, as formaldehyde is non-specific in its fixation of biomolecules. Incubation of immunoprecipitated samples

with RNase before SDS-PAGE might effectively resolve the nature of these larger complexes, since it would be expected that if they are composed of RNA instead of DNA then this would result in the liberation of free, monomeric MATR3. Incubation with DNase would also be insightful, as no difference in MATR3 complex migration would be expected if the protein truly is not binding DNA. Another somewhat straightforward experiment to determine if MATR3 associates with chromatin in neurons would involve biochemical fractionation of cytoplasm, nucleoplasm, and relatively insoluble chromatin as proposed in chapter 4 to test whether the latter contains MATR3. It should be noted that the ChIP-seq detailed here was attempted in DIV14-16 primary rat cortical neurons in basal conditions. Similar fractionation experiments could be attempted in cultures silenced with TTX or activated with glutamatergic agonists, as MATR3 association with DNA may rely on physiological stimuli such as activity status.

A.4 Materials and methods

Cortical neuron culture and ChIP-seq:

Primary cortical neurons were isolated from embryonic day (E)19-20 Long-Evans rat embryos as previously described[13], and 6 x 10^6 cells were plated for ChIP. ChIP-seq procedures were adapted from previous studies on primary neurons[14]. Briefly, neurons were washed in PBS and fixed for 10 or 30 min at RT in HBSS with 1% methanol-free formaldehyde (Pierce). Fixation was quenched with the addition of 125 mM glycine in PBS for 5 min, after which cells were collected and plasma membranes lysed in cell lysis buffer (50 mM, 1% Triton X-100, 0.1% Na-deoxycholate, 5 mM EDTA, 150 mM NaCl, 1% SDS, pH 8.1) supplemented with cOmplete protease and PhosSTOP

phosphatase inhibitor tablets (Roche), with occasional inversion on ice for 15 min. Nuclei were pelleted at 6000 x g at 4°C for 5 min, washed twice in TE buffer (10 mM Tris, 1 mM EDTA, pH 8.0), and lysed in nuclei lysis buffer (50 mM Tris, 10 mM EDTA, 0.1% SDS, pH 8.0) supplemented with protease and phosphatase inhibitor tablets (Roche). Chromatin was mechanically sheared in a QSonica water bath sonicator at 4°C and 70% amplitude in 15 s on/20 s off cycles for a total sonication time of 30 min. Lysates were cleared by centrifuging at 21,000 x g and 10x ChIP dilution buffer (50 mM Tris, 10 mM EDTA, 1.5 M NaCl, 1% Na-deoxycholate, 10% Triton X-100, pH 8.0) was added to a final concentration of 1x. Lysates were incubated with either 5 µg anti-MATR3 antibody (Abcam ab70336) or 5 µg IgG control (Santa Cruz sc-2025) conjugated to Dynabeads Protein G (ThermoFisher) overnight at 4°C.

The following day, beads were washed 3 x in low salt wash buffer (20 mM Tris, 1% Triton X-100, 2 mM EDTA, 150 mM NaCl, 0.1% SDS, pH 8.1), 2 x in high salt wash buffer (20 mM Tris, 1% Triton X-100, 2 mM EDTA, 500 mM NaCl, 0.1% SDS, pH 8.1), 1 x in LiCl immune complexes wash buffer (10 mM Tris, 1% NP-40, 1 mM NP-40, 1 mM EDTA, 0.25% Na-deoxycholate, 250 mM LiCl, pH 8.0), and 2 x in TE buffer, all of which were at 4°C. Protein-chromatin complexes were eluted in by incubating in elution buffer (50 mM Tris, 1 mM EDTA, 150 mM NaCl, 1% SDS, 50 mM $NaHCO_3$, pH 8.1) at RT with agitation twice, and both eluates were pooled. Uncrosslinking was accomplished by the addition of NaCl to a final concentration of 350 mM NaCl and incubation at 65°C overnight. RNA was removed by digestion with PureLink RNase A (ThermoFisher) for 30 min at 37°C, and protein was degraded with Proteinase K (New England Biolabs) for 1 hour at 50°C. Immunoprecipitated DNA was washed twice in neutral

phenol:chloroform and purified using the Zymo Clean-up and Concertation kit according to the manufacturer's instructions and eluted in 3 x 20 µL of water warmed to 37°C.

Bioinformatics analyses:

DNA libraries were prepared from input and from immunoprecipitated samples by University of Michigan Advanced Genomics Core and libraries were sequenced using paired-end 151 x 151 bp runs on a NovaSeq 6000 (Illumina). Quality control and trimming was performed via Trimgalore default parameters, after which reads were mapped to the rat genome (rn6) using HISAT2 in both single- or paired-end mode for comparative analysis[15]. Peaks were called based off the aligned reads using MACS2 in both narrow peak or broad peak settings with an effective genome size of 2.2×10^9 bp[16,17]. Genomic enrichment plots were created using the plotFingerprint package as adapted from the ChIP-seq ANalytics and Confidence Estimation (CHANCE) protocol[12].

A.5 Acknowledgements

I would like to thank Dr. Dhananjay Yellajoshyula for technical advice on fixation and immunoprecipitation in cultured neurons and Drs. Patricia Garay and Shigeki Iwase for insightful conversations on sequencing parameters and informatics analysis.

References

1. Nakayasu, H. & Berezney, R. Nuclear matrins: identification of the major nuclear matrix proteins. *Proc Natl Acad Sci USA* **88,** 10312–10316 (1991).

2. Belgrader, P., Dey, R. & Berezney, R. Molecular cloning of Matrin 3. A 125-kilodalton protein of the nuclear matrix contains an extensive acidic domain. *The Journal of Biological Chemistry* **266,** 9893–9899 (1991).
3. Hibino, Y. *et al.* Molecular properties and intracellular localization of rat liver nuclear scaffold protein P130. *Biochimica et Biophysica Acta (BBA) - Gene Structure and Expression* **1759,** 195–207 (2006).
4. Desideri, F. *et al.* Intronic Determinants Coordinate Charme lncRNA Nuclear Activity through the Interaction with MATR3 and PTBP1. *Cell Rep* **33,** 108548 (2020).
5. Skowronska-Krawczyk, D. *et al.* Required enhancer–matrin-3 network interactions for a homeodomain transcription program. *Nature* 1–13 (2014). doi:10.1038/nature13573
6. Fujita, T. & Fujii, H. Direct identification of insulator components by insertional chromatin immunoprecipitation. *PLoS ONE* **6,** e26109 (2011).
7. Uemura, Y. *et al.* Matrin3 binds directly to intronic pyrimidine-rich sequences and controls alternative splicing. *Genes Cells* **22,** 785–798 (2017).
8. Ren, B. *et al.* Genome-wide location and function of DNA binding proteins. *Science* **290,** 2306–2309 (2000).
9. Johnson, D. S., Mortazavi, A., Myers, R. M. & Wold, B. Genome-wide mapping of in vivo protein-DNA interactions. *Science* **316,** 1497–1502 (2007).
10. McLeay, R. C. & Bailey, T. L. Motif Enrichment Analysis: a unified framework and an evaluation on ChIP data. *BMC Bioinformatics* **11,** 165–11 (2010).
11. Kim, D. *et al.* A principled strategy for mapping enhancers to genes. *Scientific Reports* **9,** 11043–14 (2019).
12. Diaz, A., Nellore, A. & Song, J. S. CHANCE: comprehensive software for quality control and validation of ChIP-seq data. *Genome Biol.* **13,** R98–15 (2012).
13. Saudou, F., Finkbeiner, S., Devys, D. & Greenberg, M. E. Huntingtin acts in the nucleus to induce apoptosis but death does not correlate with the formation of intranuclear inclusions. *Cell* **95,** 55–66 (1998).
14. Yellajoshyula, D. *et al.* The DYT6 Dystonia Protein THAP1 Regulates Myelination within the Oligodendrocyte Lineage. *Dev. Cell* **42,** 52–67.e4 (2017).
15. Kim, D., Paggi, J. M., Park, C., Bennett, C. & Salzberg, S. L. Graph-based genome alignment and genotyping with HISAT2 and HISAT-genotype. *Nat. Biotechnol.* **37,** 907–915 (2019).
16. Zhang, Y. *et al.* Model-based analysis of ChIP-Seq (MACS). *Genome Biol.* **9,** R137–9 (2008).
17. Feng, J., Liu, T., Qin, B., Zhang, Y. & Liu, X. S. Identifying ChIP-seq enrichment using MACS. *Nat Protoc* **7,** 1728–1740 (2012).

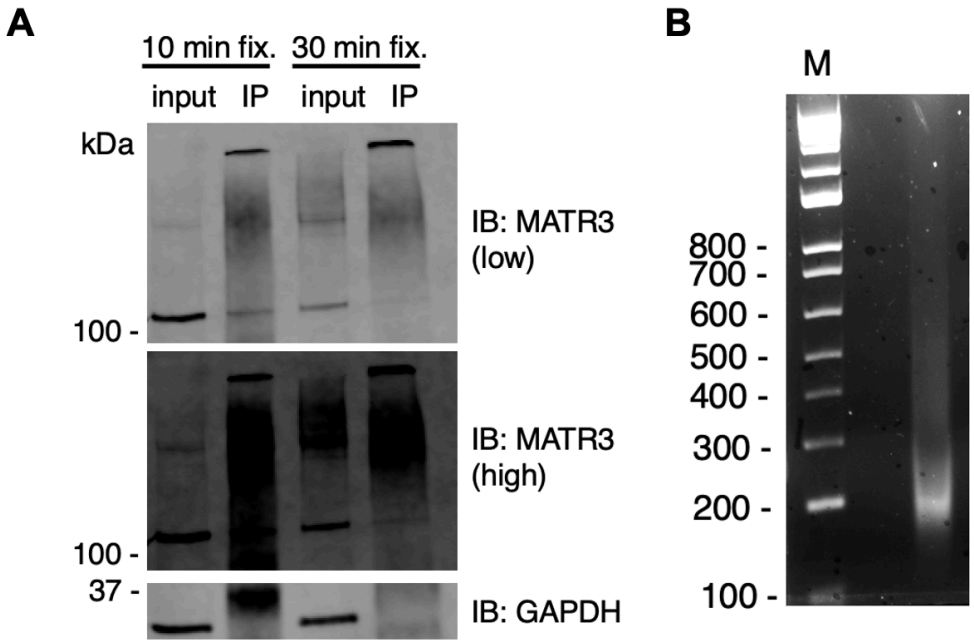

Figure A.1. Effective fixation and immunoprecipitation of MATR3 complexes and optimal chromatin shearing in neurons. High molecular weight crosslinked MATR3 complexes were formed with 10 and 30 min of formaldehyde fixation in primary cortical neurons and were effectively immunoprecipitated with anti-MATR3 antibody (A). DNA from neuron lysates was mechanically sheared to an optimal 200 bp average fragment length (B).

A

	Narrow peak analysis	Broad peak analysis
MATR3-to-input	664	1129
MATR3-to-IgG control	221	431

B

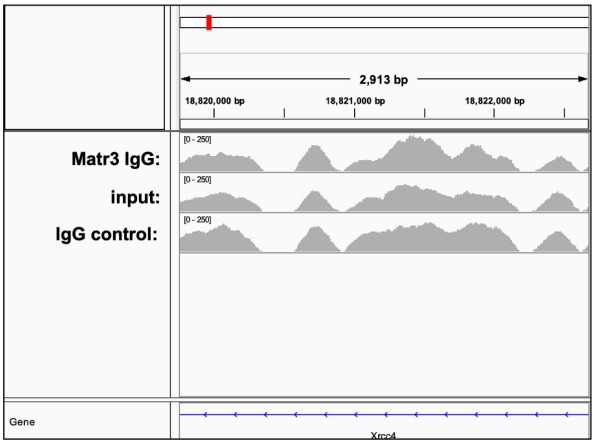

C

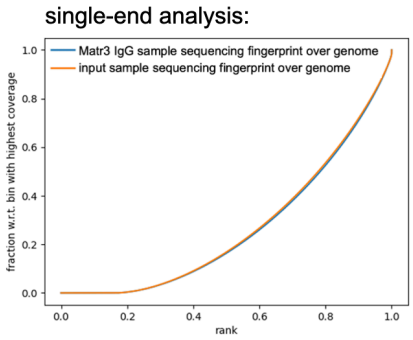

D

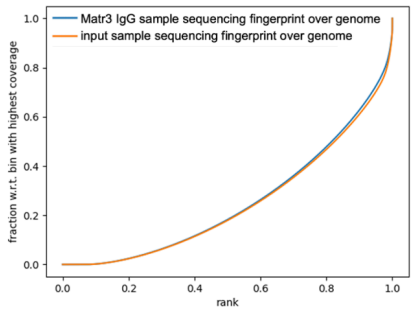

Figure A.2. anti-MATR3 antibody failed to efficiently co-immunoprecipitate DNA for ChIP-seq analysis or enrich over input. Peak calling of aligned DNA copurified with anti-MATR3 antibody gave few peaks—both when compared to input and to IgG control antibody—in narrow, transcription factor-like mode and broad, methylation mark-like mode (A). Those peaks that were called represented only minor enrichment about input or IgG control samples (B). Fingerprint analysis across the genome produced no enrichment of genomic areas for MATR3 ChIP samples compared to input control (C-D).